An update to PR12-09-014: Target Single Spin Asymmetry in Semi-Inclusive Deep-Inelastic $(e, e'\pi^{\pm})$ Reaction on a Transversely Polarized ^{3}He Target at 8.8 and 11 GeV

December 14, 2009

B.-Q. Ma, Y.J. Mao
School of Physics, Beijing University, P. R. China

A. Kolarkar
Boston University, Boston, MA

K. Aniol, D. J. Margaziotis
California State University-Los Angles, Los Angles, CA

X.M. Li, J. Yuan, S. Zhou
China Institute of Atomic Energy, Beijing, P. R. China

D. Armstrong, T. Averett, P. Bradshaw, J. Katich, B. Zhao
College of William & Mary, Williamburg, VA

W. Chen, H. Gao (Co-spokesperson/Contact), M. Huang, G. Laskaris, X. Qian (Co-spokesperson), Y. Qiang, Q. Ye, Q.J. Ye
Duke University and the Triangle Universities Nuclear Laboratory, Durham, NC

P. Markowitz
Florida International University, Miami, FL

Y. Li, L.Y. Zhu
Hampton University, Hampton, VA

H.P. Cheng, R.C. Liu, H.J. Lu, Y. Shi
Huangshan University, Huangshan, P. R. China

U. D'Alesio, F. Murgia
Cagliari University and INFN, Cagliari Torino, Italy

R. De Leo, L. Lagamba, S. Marrone, G. Simonetti, I. Vilardi
INFN-Bari and University of Bari, Bari, Italy

E. De Sanctis, M. Mirazita, S. A. Pereira, P. Rossi
INFN Laboratori Nazionali di Frascati, Frascati, Italy

B. Pasquini
INFN, Sezione di Pavia, Pavia, Italy

S. Scopetta
University degi Studi di Perguria, INFN, Perugia, Italy

E. Pace
Rome-Tor Vergata University, Rome, Italy

E. Cisbani, F. Cusanno, S. Frullani, F. Garibaldi, G. Salme', G. M. Urciuoli
INFN-Roma and gruppo collegato Sanitá, Rome, Italy

M. Anselmino, M. Boglione, A. Prokudin
Torino University and INFN, Torino, Italy

A. Afanasev, A. Bacchetta, A. Camsonne, J.-P. Chen (Co-spokesperson), E. Chudakov, A. Deur, J. Gomez, D. W. Higinbotham, J. O. Hansen, C. W. de Jager, M. Jones, J. LeRose, R. Michaels, S. Nanda, A. Saha, M. Schlegel, B. Sawatzky, B. Wojtsekhowski
Jefferson Lab, Newport News, VA

M. Mihovilovič, M. Potokar, S. Širca
Jožef Stefan Institute, Liubljana, Slovenia

B.T. Hu, Y.W. Zhang, Y. Zhang
Lanzhou University, Lanzhou, P. R. China

B. Xiao, F. Yuan
Lawrence Berkeley National Laboratory, Berkeley, CA

T. Holmstrom
Longwood University, Farmville, VA

L. Guo, X. Jiang (Co-spokersperson), M.X. Liu, A. Puckett
Los Alamos National Laboratory, Los Alamos, NM

W. Bertozzi, S. Gilad, J. Huang, V. Sulkosky, X. Zhan
Massachusetts Institute of Technology, Cambridge, MA

J. Dunne and D. Dutta
Mississippi State University, Starkville, MS

M. Burkardt
New Mexico State University, Las Cruces, NM

L. Weinstein
Old Dominion University, Norfolk, VA

L. Gamberg
Pennsylvania State University at Berks, Reading, PA

L. El Fassi, R. Gilman, G. Kumbartzki, R. Ransome, E. Schulte
Rutgers University, Piscataway, NJ

Seonho Choi, Hoyoung Kang, Hyekoo Kang, Byungwuek Lee, Yoomin Oh
Seoul National University, Seoul, Korea

A. J. Sarty
St. Mary's University, Halifax, Nova Scotia, Canada

P. Souder and R. Holmes
Syracuse University, Syracuse, NY

E. Piasetzky
Tel aviv University, Tel Aviv, Israel

W. Armstrong, Z.-E. Meziani, H. Yao
Temple University, Philadelphia, PA

W.-C. Ding, J.-B. Wang, Y. Wang, Z.G. Xiao
Tsinghua University, Beijing, P. R. China

P. Schweitzer
University of Connecticut, Storrs, CT

J. Annand, D. Hamilton, D. Ireland, K. Livingston, R. Kaiser,
D. Protopopescu, G. Rosner, B. Seitz
University of Glasgow, Glasgow, Scotland

A. Nathan, N. Makins, J.-C. Peng (Co-spokesperson), Y. Wang
University of Illinois, Urbana-Champaign, IL

K. Allada, C. Dutta, W. Korsch
University of Kentucky, Lexington, KY

E.J. Beise
University of Maryland, College Park, MD

K. Kumar
University of Massachusetts, Amherst, MA

S. Phillips, K. Slifer
University of New Hampshire, Durham, NH

X. Yan, Y. Ye, P.J. Zhu
University of Science and Technology of China, Hefei, P. R. China

G. Cates, M. Dalton, R. Lindgren, N. Liyanage, V. Nelyubin,
B. Norum, K. Paschke, M. H. Shabestari, R. Subedi, W. A. Tobias,
K. Wang, X.C. Zheng
University of Virginia, Charlottesville, VA

and the HallA Collaboration

Abstract

We propose to carry out precision measurements of Single target Spin Asymmetries (SSA) from semi-inclusive electroproduction of charged pions from a 40-cm long transversely polarized ^{3}He target in Deep-Inelastic-Scattering kinematics using 11 and 8.8 GeV electron beams. We propose to carry out this coincidence experiment in Hall A with a newly proposed solenoid spectrometer (SoLID) and the Hall A polarized ^{3}He target. The full 2π azimuthal angular coverage on the ϕ_S angle and large azimuthal angular coverage on the ϕ_h angle are essential in controlling the systematic uncertainties in extracting different asymmetries. The proposed experiment will provide precise 4-D (x, z, P_T and Q^2) data on the Collins, Sivers and Pretzelosity asymmetries for the neutron through the azimuthal angular dependence. The results from this experiment, when combined with the future proton Collins asymmetry measurement and the Collins fragmentation function determined from the e^+e^- collision data, will allow for a flavor separation of the quark tensor charge, and achieve a determination of the tensor charge of d quark to 10% in a model independent way. The extracted Sivers and Pretzelosity asymmetry will provide important information to understand the correlation between the quark orbital angular momentum and the nucleon spin. We request a total of 90 days of beam time (polarized) at incident beam energies of 11 and 8.8 GeV and at a beam current of 15 μA.

Contents

1 Overview

We present an update to Proposal PR12-09-014, *Target Single Spin Asymmetry in Semi-Inclusive Deep-Inelastic* $(e, e'\pi^{\pm})$ *Reaction on a Transversely Polarized* ^{3}*He Target at 11 GeV*. This proposal was deferred with regret by PAC34 and the original proposal can be found in Ref. [1]. In the PAC34 report, a list of general questions to all Semi-Inclusive-Deep-Inelastic Scattering (SIDIS) proposals as well as specific questions to PR12-09-014 were raised. In this update, we present firstly our response to the general SIDIS questions as well as PR12-09-014 specific questions, followed by a brief introduction of the physics we are pursuing and an updated section on the existing Single-Spin-Asymmetry (SSA) data from SIDIS. We then present new studies following the submission of the PAC34 proposal to address the PAC34 concerns and present our case with a second option of solenoid magnet, the CDF magnet. The CDF solenoid magnet (see Table.1 in Ref. [1]) is 5 m long. In comparison, the original proposal is based on the BaBar magnet, which is 3.5 m long. The diameter of the CDF (BaBar) magnet is 2.9 (2.8) m. The conceptual designs of detection system for the two options are very similar. The background levels in tracking detectors and calorimeters are shown at the same level. The major difference is the length of the magnet, which leads to a slightly different kinematic coverage. (The CDF option will favor slightly forward angles.) The CDF option will provide a better resolution in the reconstructed momenta and angles, because the integrated magnetic field over distance is larger. Nevertheless, many studies are inter-changeable between the two options. We are working closely with the PVDIS collaboration in finalizing the design. In this update, we also request to take additional data at an incident beam energy of 8.8 GeV to increases the Q^2 coverage and provide precision data for radiative corrections. In total, we request 90 days of beam time to carry out the complete measurements at 11 GeV and 8.8 GeV.

Below we listed all the major changes/updates from PR12-09-014 [1]:

- Detailed responses to PAC comments (Sec. 2)
- Studies and updates using CDF magnet as an option.
- Additional request with 8.8 GeV beam (Sec. 11.1)
- Target collimator design (Sec. 5.4)
- Tracking Monte-Carlo simulation (Sec. 5.2)
- Reconfiguration plan of GEM detectors from PVDIS Setup (Sec. 5.2)
- Updated information in PID detectors (Sec. 6 and 7)
- Detailed information about trigger and DAQ design (Sec. 8)
- Projected results with CDF magnet in 4-D format requested by PAC (Sec. 12)

2 PAC Report and Response

2.1 Response to PAC report on PR12-09-014

Motivation: This collaboration proposes to measure target single spin 0azimuthal asymmetries (SSA) of semi-inclusive charged pion electroproduction from transversely polarized ^3He in deep inelastic kinematics, in particular the Collins, Sivers, and Pretzelosity asymmetries. Combined with knowledge of the Collins fragmentation functions from other experiments, the Collins asymmetry can be used to extract the quark transversity distribution of the neutron, and ultimately integrated over x to determine the tensor charge of the d quarks in the nucleon.

Measurement and Feasibility: The collaboration proposes to use the same solenoid as the PVDIS (PR12-09-012) experiment (SoLID) but with the detectors deployed to different locations and augmented with Čerenkov detectors, and with the polarized target located upstream of SoLID. The open geometry spectrometer allows significant study of the dependence of the asymmetries on p_T, z, x, Q^2 and ϕ^*. (the azimuthal angle of the pion about the virtual photon direction). The 2π azimuthal coverage of the spectrometer around the beam direction will allow the collection of a larger event sample than that of small acceptance spectrometers, for a given luminosity. Clearly this is at the cost of requiring efficient and strong identification of both electrons and pions over the full acceptance. Furthermore, it is expected that the full azimuthal coverage will allow significant cancellation of systematic uncertainties arising from acceptance/efficiency variations across the spectrometer acceptance using a minimal number of target spin orientation. The proposed polarized target is already operating with adequate performance. Raw rates in the planned GEM appear to be acceptable, however, the rates in the Čerenkov detectors were of concern, especially given the large photon backgrounds. The overall factor of 100 increase in luminosity compared to CLAS12 and the effects of Moller scattering from the target raised significant concerns about the feasibility of the measurement with the spectrometer as described.

A: The Geant Monte-Carlo simulation including a realistic magnetic field model shows that the Moller scattering from the target will be constrained into a cone very close to the beam pipe, and will not reach the tracking and PID detectors. The low energy charged-particles will be bent by the fringe field of the SoLID magnet. The description of the GEANT3 simulation and the discussion on the Moller scattering can be found in Sec. 18. With the designed target window collimator, the overall (unpolarized) luminosity is about 2×10^{36} $cm^{-2}s^{-1}$, which is about factor of 20 increase compared to CLAS12. The current designed goal of luminosity in PVDIS with SoLID is 5.4×10^{38} $cm^{-2}s^{-1}$ with baffles [2]. Some of our collaboration members have extensive experience in working with Čerenkov detectors in open geometry spectrometer (BigBite) at 6 GeV. Simulations of SoLID suggest that the Čerenkov detectors will work at the proposed luminosity to achieve the design goal. The detailed discussion can be found in Sec. 6.2.

The spectrometer is claimed to be able to identify the events of interest both in the fast

time required for a readout trigger as well as in the offline analysis, while operating with close to 10^{37} $cm^{-2}s^{-1}$ *luminosity. Particular technical concerns that should be addressed are:*

A: With target collimator, the unpolarized luminosity is about 2×10^{36} $cm^{-2}s^{-1}$**.**

1) Which specific processes and background reactions are included in the studies?

A: We include all processes and background reactions in the small angle scattering processes, such as Moller, Mott, etc in GEANT3.

2) For the case of Moller scattering, what low energy cuts are applied to electrons and photons included in the simulations?

A: The standard cut in GEANT for EM processes is 1 MeV. No additional low energy cut was applied in estimating the background.

3) How will collimation around the target be implemented; how was the efficacy determined?

A: We provide a design in Sec. 5.4. The effects of the collimator are included in the projections and all simulation studies. Target collimator were implemented successfully in the recently completed 6 GeV neutron transversity experiment E06-010 at 30 degrees [1] (electron scattering angle) and small angle GDH experiment (E97-110) at 6 degrees in Hall A.

4) In addition to average rates in a given (entire) detector, what are the locally highest rates in particular sections of the detectors?

A: Generally, detectors closer to beam pipe will have higher rates. For example, with 11 GeV beam energy, the highest rate on GEM detectors is about 5 kHz/mm^2 **at the second chamber. The background rates in the GEM tracker are shown in Fig. 12. The highest rate on the calorimeter at 11 GeV is about** 2.5×10^5 $GeV/10cm^2/s$**. The background rate in the calorimeter is shown in Fig. 17. For the MRPC detectors, the background will be less than 0.1** kHz/mm^2 **(Fig. 22). The Čerenkov detectors are divided into 30 units in the azimuthal angle (beam momentum direction is the z-axis.), and no segment will be made in the polar direction. Thus, rates on different units are similar due to symmetry in the azimuthal angle. For the light gas Čerenkov, the total background rate, including both the low energy background and secondary background from high energy particles is about 40 MHz. The total background rate for heavy gas Čerenkov is about 60 MHz. The singles rate for physics particles in the calorimeter is shown in Fig. 39 for the trigger study.**

[1] See Halog `http://www.jlab.org/~adaq/halog/html/0810_archive/081030075719.html`

5) For the granularity of detectors proposed, what are the occupancies, again both peak and average, especially in those regions of the detectors where the bulk of the SIDIS yield is detected?

A: The occupancies in the GEM trackers are shown in Fig. 13. The average occupancies on the whole GEM tracking planes are less than 30. The study of tracking MC demonstrates that the tracking will not be a problem at the proposed luminosity through the entire acceptance. For calorimeter, only the ADC around the electron-like hit will be recorded. Since electron-like event will deposit large energies in the calorimeter, the energy readout will not be sensitive to low energy backgrounds. In addition, The single-rate dependence on radial distance in the calorimeter is shown in Fig. 39 for different particle. For Čerenkov detectors, we plan to divide the entire 2π azimuthal angle into 30 sectors. No segment will be made in the polar angle direction. With a 20 ns coincidence window, the probability of having a fake signal due to random background hits on Čerenkov is $40\ MHz \times 20\ ns/30\ =\ 2.6\%$ (40:1 pion rejection on-line, 80:1 pion rejection offline by increasing the threshold and reducing the coincidence window). For heavy gas Čerenkov, this factor will be $60 MHz \times 20\ ns/30\ =\ 6.67\%$ (25:1 kaon rejection online, 50:1 kaon rejection offline by increasing the threshold and reducing the coincidence window). For MRPC, assuming a 100 cm^2 pad and 2 ns window, the probability to have a fake timing signal is 0.2% for a background rate of 0.1 kHz/mm^2. The scintillator will primarily be used in forming the hadron trigger.

6) Tracking studies should be performed to demonstrate that the proposed tracking and PID detectors provide sufficient information and redundancy in the high rate environment to efficiently and correctly identify real SIDIS events out of the accidental coincidences/ghost tracks from charged and neutral background. Do the Čerenkov detectors have sufficient granularity/position resolution to allow adequate PID for each track? A detailed description of the tracking chambers positions, readout strip pitch and orientation should be included.

A: A Tracking Monte-Carlo is performed. Out results shows that the tracking would not be a problem at the proposed luminosity with proposed setup. More details can be found in Sec. 5.2. We provide the detailed description of the tracking chamber positions, orientation and reconfiguration from PVDIS GEM chambers in Sec. 5.2 and Table. 1. The Čerenkov detectors/MRPC will have sufficient granularity/position resolution to allow adequate PID for each track. The detailed answer can be found in answers to item 5).

7) A plan should be developed which describes in detail how the change from the PVDIS setup to the ^3He setup would be accomplished, and what special constraints on the PVDIS detector designs are required. For example, how will the GEM planes be constructed so that the PVDIS GEMS can be redeployed in the upstream part of the solenoid?

A: We present the reconfiguration plan of GEM tracking from PVDIS to this experiment in Sec. 5.2. A new GEM tracking plane is needed for

this experiment (the first layer). A new gas tank and some new mirrors are needed to convert the light gas Čerenkov detector from PVDIS configuration to this configuration. We will need more calorimeter blocks in this experiment (Sec 5.3).

8) A more detailed description of the trigger/DAQ including trigger definition and rate, at level 1, 2 (3?), data rates to the DAQ and data volume written to storage for analysis. Is the granularity sufficient to suppress accidental triggers?

A: We discussed the current design of trigger and DAQ setup in Sec. 8. The single electron trigger (L1) rates will be about 200 kHz. With coincidence with the single hadron trigger, we expect to reduce the coincidence trigger (L2) to about 50 kHz, which is corresponding to 200 MB/s DAQ rates. With on-line farm (L3), we expect to reduce another factor of 5-10 for the data rates to storage.

9) What are the impacts of a solenoid this large being installed and instrumented in Hall A? What interference with other Hall A experiments is foreseen (not just the Moller PV experiment)?

A: In the current design of SoLID, we assume Moller/PVDIS/SIDIS will run continuously. The BigBite/Super BigBite program will finish before the running period for these three experiments. The switch-over time from PVDIS to SIDIS or vice verse, is estimated as 3-6 months. The changes include installation/de-commissioning of the target and reconfiguration of the detectors. With current design, the switch-over to an experiment using HRS or BigBite/Super-BigBite will be around half to one year [2]. We are working closely with the PVDIS collaboration on the design of SoLID to reduce the switch over time and costs. The current design is under development by engineers at the Argonne National Laboratory.

10) A more detailed demonstration of how much the full azimuthal coverage reduces the systematic uncertainties, with simulation studies using realistic variations in efficiency/acceptance of the spectrometer, would be very useful.

A: We address this point in Sec. 13 . With the symmetry in our acceptance, most of the systematic uncertainties will be canceled in the raw asymmetry. The incomplete coverage of the azimuthal angle ϕ_S and ϕ_h will lead to an increase in the uncertainties in separated asymmetries. We list the formula for estimating the statistical uncertainties in Sec. 16. For the SoLID setup, we have a full azimuthal coverage in ϕ_S. The effects of the incomplete coverage of ϕ_h on the projections are included in all the projections. In addition, the recent progress in reducing the average time between flipping the ^3He spin [3] can further reduce the random systematic uncertainties.

[2] There is one possibly to install wheels on SoLID, which can significantly reduce the switch-over time.

[3] In E06010, the time is 20 mins. It has been shown that this time can be reduced to 10 mins

11) Finally, what is the justification for the particular statistical accuracy which is the goal of the experiment; if a significantly lower luminosity was used, would the impact the measurement be significantly degraded relative to any other proposed experiments?

A: We discussed this point in Appendix II of the previous proposal. With collaboration's extensive experience with the open-geometry detectors and detailed MC simulations, we believe that we will reach the proposed luminosity with the current design. In addition, several R&D programs are planned in the next couple years to carefully optimize the design of various detectors. Our collaboration will work closely with the PVDIS collaboration to minimize the cost. The only competing experiment is the Hall A conditionally approved transversity experiment using BigBite/Super-BigBite (E09-12-018). The requirement on the detector system for both BigBite/Super-BigBite and SoLID are similar [4]. In this proposal, we assume the achieved target luminosity, while R&D is needed to achieve the proposed luminosity in the BigBite/Super-BigBite proposal. From the kinematics point of view, this proposal will perform a precise SSA measurements in 4-D (x, Q^2, z and P_T) within a wide kinematic coverage, while the Super-BigBite proposal is focusing on the high Q^2 measurement, where the cross section is usually small. In addition, the 2π ϕ_S azimuthal angular coverage, the large ϕ_h azimuthal angular coverage, and the symmetry in the acceptance in this proposal will strongly suppress different sources of systematic uncertainties.

Issues: First, see "Comments to All SIDIS Proposals" in the overall report. As described in the above comments, it is important to understand the systematic uncertainties arising from gaps in the multidimensional space of SIDIS measurements. In this experiment, there are concerns that loss in ϕ^* acceptance at very small forward angles leads to larger systematic uncertainty in the azimuthal asymmetries than presently estimated. Future proposals should show the acceptance in p_T vs ϕ^* for each Q^2-x bin separately, rather than just p_T vs x or p_T vs z (though this was very much appreciated).

A: We generated the requested plots. They can be found in Sec. 17.

In order to extract the SSA, corrections for intrinsic backgrounds will need to be applied. In particular, will data at lower beam energies (cross sections and asymmetries) be needed to adequately model the radiative tails from exclusive and resonance region ($\Delta(1232)$ in particular) pion production? Also, will the contributions from diffractive ρ^0 production be known well enough (not relying on Lund M.C., which doesn't model the SSA of a single pion from ρ^0 decay properly)? Is there a plan to measure this with π^+/π^- coincidences, and if so, if the acceptance big enough (i.e., is better coverage at small angles needed)?

A: The acceptance for ρ^0 meson has been studied in Sec. 13.6. Since the SoLID is designed for the DIS program (PVDIS and SIDIS), the capability

[4]The SoLID detectors are located at more forward angle, while the luminosity proposed with BigBite/Super-BigBite is much higher.

in detecting multi-particles from exclusive channels is rather limited. CLAS will provide better data on the ρ^0 diffractive production at 12 GeV.

The PAC is also concerned that nuclear corrections, beyond the usual impulse approximations typically used to correct neutron structure from ^3He measurements, may play a larger role in azimuthal observables than in inclusive or semi-inclusive (yield) asymmetries. The collaboration is aware of these issues and the PAC endorses the theoretical efforts to investigate these nuclear effects.

A: Due to the fact that a free neutron does not live long enough to allow for a scattering experiment, a polarized deuteron or polarized ^{3}He target needs to be employed to access information related to the neutron spin structure. To understand QCD in the confinement region, flavor separation to the structure of nucleon is essential. Therefore, experiments on proton and "neutron" (deuteron or ^{3}He) are equally important. A lot progress has been made in understanding the nuclear corrections to the extraction of the neutron information using a deuteron or ^{3}He target ranging from neutron electromagnetic form factor to the longitudinal spin structure function.

The proponents of this proposal are very much aware of nuclear effects using a polarized ^{3}He target to extract information on neutron SSA. We have been communicating with a number of theoreticians about these issues and the list includes Jianwei Qiu, Misak Sargsians, Gianni Salme, Sergio Scopetta and Emanuele Pace. All these theorists appreciate the issues and expressed interest in addressing them. Further, as suggested by Salme and Scopetta, we can investigate and determine the final state interaction effect in SSA using our proposed data by looking at SSA at fixed values of Q^2 and x, but with different values of z to see if there is an approaching to a scaling behavior. The proposed large kinematic coverage in Q^2, x and z, and the high statistics of the proposed measurement will allow for such a study. We are confident that the nuclear effect using a polarized ^{3}He target will be under good control by the time we have data from this experiment both from the theoretical developments and by taking advantage of the data.

Another complicating factor for the PAC was the coupling of this proposal to the PVDIS proposal (PR12-09-012). It was not felt that the ^3He measurement alone could justify the expense of the SoLID spectrometer; however, a broad program of high priority physics measurements beyond that of the PVDIS program certainly strengthens the case to invest in SoLID.

Despite the questions of feasibility raised above, the PAC strongly endorses the physics goals of the experiment and the collaboration is encouraged to submit a new proposal that addresses the technical concerns in some detail, as the ambitious experimental setup and high luminosity requires a more thorough justification than more modest proposals. These necessary simulation studies will be required by any subsequent technical review in any case.

Recommendation: Defer with Regret

2.2 Response to PAC report on all SIDIS proposals

Semi-inclusive deep inelastic scattering (SIDIS) provides a powerful way to access the structure of the nucleon and the intricacies of the hadron formation process. The 12 GeV era at JLab can move this field to a new level of sophistication, thanks to the extraordinary statistical accuracy achievable and the extended kinematic reach provided by the 11 GeV beam. A new level of statistical accuracy must however be accompanied by a commensurate level of systematic precision, both experimental and theoretical. The multi-dimensional phase space of SIDIS is complex, with interesting and unknown physics reflected in each kinematic dependence. Fully differential analysis of SIDIS observables will be essential if one hopes to develop an understanding of the SIDIS mechanism at a level commensurate with the projected statistical accuracy. Examples of issues that must be addressed are the level of current/target separation, the applicability of x-z factorization to $p_{h\perp}$-integrated distributions, the $p_{h\perp}$-dependence of identified hadrons, and the size of higher-twist contributions. A strong SIDIS program at 12 GeV will be able to address these questions. It is the clear opinion of the PAC that model-dependent approaches to SIDIS analysis should be avoided, and that instead the proposals concentrate on a systematic, coherent approach to the field. We ask that SIDIS proposals focus on their kinematic coverage, experimental limitations, and complementarity with the rest of the laboratory program, rather than pursuing variegated model-dependent extractions based on uncontrolled assumptions. We also believe that a broad phenomenological effort is needed in which theory and experiment work together to explore the SIDIS reaction mechanism at JLab kinematics. We strongly encourage the involvement of experienced global-fitting groups such as the DSS, LSS, Torino, MRST, and CTEQ groups.

The SIDIS proposals fall naturally into two groups: large-acceptance detectors (such as CLAS), and small-acceptance spectrometers (such as the HMS and SHMS). In developing a coherent program, both of these must be represented, but they must coordinate their efforts and concentrate on what they can uniquely contribute.

A: In this proposal, we plan to spend dedicated beam time to study the naive x-z factorization using unpolarized hydrogen and deuterium targets. In addition, our wide kinematic coverage allows us to do a mapping of precise SSA in 4-D (x, z, P_T and Q^2). This experiment is complimentary to the Hall C program in measuring the longitudinal to transverse cross section ratio R in SIDIS. Point spectrometers can measure the cross section very precisely with high luminosity at large Q^2 and high P_T, where cross sections are generally small. Those data can provide important information on the higher twist contributions. Our data in combination with proton results in CLAS can be used to extract the tensor charge of quarks. Furthermore, the large acceptance in CLAS for multi-particle detection is perfect for measuring/constraining the diffractive ρ meson production, which is one of the major physics background channels for SIDIS process. In addition, our collaboration has a very strong theoretical support. Dr. Feng Yuan (DSS) and the Torino group joined our collaboration. They have extensive experience in global fitting of (Transverse) Parton Distribution Functions (PDFs).

Specifically:

(a) Large-acceptance experiments will form the core of the program, as they are uniquely capable of providing complete differential binnings of observables. Without this, the program cannot succeed. In addition, multi-purpose detectors such as CLAS, with the ability to measure many different channels in a given run period, allow one to explore unknown territory at "low cost" to the total JLab program, e.g. kinematic regions and observables which may or may not be dominated by higher twist effects or target fragmentation.

(b) Small-acceptance spectrometers provide other unique capabilities: L/T separations, precise measurement of unpolarized cross sections with percent-level control over absolute normalization and charge-dependent cross section ratios, and the abilities to access kinematic corners as needed where the cross section is low or where the resolution of the large-acceptance devices is inadequate.

All the 12 GeV proposals will have to re-present their case to a future PAC for beam-time allocation. In order to build the best possible program, it is vital to know what the large-acceptance experiments can do, and where they need support from more focused spectrometer experiments. The PAC asks that all the SIDIS experiments clearly show their capabilities in the following areas:

(1) Multi-dimensional binnings of projected observables. For example, azimuthal moments such as $< cos(2\phi) >_{UU}$ should be shown in a fully-differential (x,Q^2,z,$p_{h\perp}$) binning. (This can be easily accomplished in one figure with a grid of panels, e.g. Fig. 37 of PR12-06-117.) At the statistical precision of the 12 GeV experiments, it is useless to show one-dimensional projections of these observables with minute but irrelevant statistical errors. It is also vital that the large-acceptance proposals clearly present their fully correlated kinematic coverage so that other proposals may be developed to fill in important "holes".

(2) Resolution. All proposals should evaluate their experimental resolution carefully; kinematic bin widths should be chosen accordingly, and regions of degrading resolution should be identified.

A: Resolutions for different reconstructed kinematic variables are presented in Fig. 14. The discussion about the azimuthal angular ϕ_h resolution with respect to the transverse momentum p_T can be found in Sec. 5.2.

(3) Specific dependence's. It is well known that the dependence of SIDIS observables on certain kinematic variables is of particular importance. The PAC requests that proposals address with their projections, if possible:

(a) the ability to determine the Q^2 dependence of observables (such as $p_{h\perp}$-integrated azimuthal moments) at some fixed x and z, to see how well higher twist effects and scaling behavior can be constrained.

A: Our kinematic coverage is shown in Fig. 23 and Fig. 24. The wide Q^2 coverage will allow us to test the Q^2 dependence of the $p_{h\perp}$-integrated azimuthal moments at fixed x and z bins.

(b) the ability to vary x and z independently to test factorization and the separation of the target/current factorization regions.

A: We propose to have dedicated beam time to test factorization.

(c) the ability to measure the differential $p_{h\perp}$ distribution at fixed x and z, explore its change with Q^2, and ascertain possible non-Gaussian behavior.

A: We plan to map the azimuthal asymmetry precisely in a 4-D manner (x, Q^2, z, $p_{h\perp}$).

(d) the ability to measure $p_{h\perp}$-weighted integrals of azimuthal moments. Here, in addition to the fully-differential coverage plots requested above (which will include $p_{h\perp}$), we suggest that the experiments estimate the fraction of the full $p_{h\perp}$ integral they can measure without extrapolation; this fraction can be estimated using a current model of the Transverse Momentum Distributions.

A: Our average P_T coverage is about 0.8 GeV/c, while the largest P_T coverage is 1.2 GeV/c at small x value. In this proposal, we plan to study the P_T dependence of the SSA.

(e) the ability to integrate over ϕ and/or ϕ_S: experiments measuring azimuthal moments must show that they have enough coverage and resolution to fit the spectra up to third-order Fourier terms; experiments seeking to integrate over "unwanted" ϕ dependence must demonstrate that their azimuthal coverage is complete.

A: We have a full 2π coverage in the ϕ_S and a large ϕ_h coverage for each of our kinematic bin. The resolution of ϕ_h is shown in Fig. 15 and Fig. 16. We have a good ϕ_h resolution for the entire kinematic coverage. The effect of incomplete coverage of ϕ_h and the acceptance effect on the statistical uncertainties in separating different azimuthal angular dependent terms are discussed in Sec. 16. Our projections are obtained by fitting all three leading twist contributions (Collins, Sivers and Pretzelosity) simultaneously. The P_T vs ϕ_h coverage plots are shown for each of kinematic bin in Sec. 17.

It is essential that results from the broad-based studies of SIDIS with CLAS will be made available in a timely fashion, to provide guidance for future high precision experiments with small-acceptance spectrometers. Past experience indicates however that experiments with small-acceptance spectrometers can provide important results on a much faster timescale, even without guidance from broad-based studies. Thus, it is highly desirable to have a parallel, dedicated and well-motivated program with small-acceptance spectrometers.

3 Introduction

At leading twist if we integrate over the transverse momenta of quarks, there are three quark distribution functions: the unpolarized parton distribution f_1, the longitudinal polarized parton distribution g_1, and the quark transversity distribution h_1. The unpolarized parton distribution functions (PDF) have been extracted with excellent precision over a large range of x and Q^2 from DIS, Drell-Yan and other processes after several decades of experimental and theoretical efforts. The comparison of the structure functions in the large Q^2 range with QCD evolution equations has provided one of the best tests of QCD.

Spin is an intrinsic quantum-mechanical and relativistic property of the constituents of matter which plays a fundamental role in physical processes and in theories of fundamental interactions. Motivated by the original "spin crisis" from the European Muon Collaboration experiment in the 1980s, the longitudinal polarized parton distribution functions have been determined with significantly improved precision over a large region of x and Q^2 from polarized DIS experiments carried out at CERN, SLAC, DESY in the last two decades, and more recently at JLab and at RHIC from polarized proton-proton scattering. The intensive experimental and theoretical investigation has resulted in a great deal of knowledge on the partonic origin of the nucleon longitudinal spin structure. We have also learned that precise knowledge of the transverse structure is an essential part of the partonic spin and momentum substructure of the nucleon.

The transversity function, a chirally odd quark distribution function, is the least known among the three leading twist parton distribution functions. It was discussed for the first time by Hidaka, Monsay and Sivers [3] in 1978, by Ralston and Soper [4] in 1979, and later by Jaffe and Ji in early 1990s [5]. In the quark-parton models, the nucleon transversity distribution, $h_1(x, Q^2)$ [5] describes the net quark transverse polarization in a transversely polarized nucleon. In the non-relativistic limit, the transversity distribution function is the same as the longitudinal quark polarization distribution function, $g_1(x, Q^2)$. Therefore, the transversity distribution functions probe the relativistic nature of the quarks inside the nucleon. There are several interesting features about quark transversity distributions. First, they do not mix with gluons, therefore follow simpler evolution and have valence-like behavior [6]. Second, it is predicted that there exists the Soffer's inequality [7], $|h_1^q| \leq \frac{1}{2}(f_1^q + g_1^q)$, for the transversity based on unitarity and parity conservation. However, doubts have been casted [8] recently on this inequality and therefore it is interesting to test the Soffer's inequality experimentally. Lastly, the lowest moment of h_1^q measures the "tensor charge", which is a fundamental property of the nucleon, analogous to the axial charge, and has been calculated from lattice QCD [9] and various models [10, 11, 12, 13]. Due to the valence-like nature of the transversity distribution, probing transversity in the high-x region (JLab kinematics) is crucial to determine tensor charge of quarks.
The experimental determination of the transversity function is challenging - it is not accessible in polarized inclusive DIS measurements because of its chiral-odd nature. To probe the quark transversity functions, an additional chiral-odd distribution or function is needed, for example, double polarized Drell-Yan processes (two transversity distributions), single target spin azimuthal asymmetry from semi-inclusive DIS pion electroproduction (transversity and Collins fragmentation function).

Besides the aforementioned f_1, g_1 and h_1, which survive the integration over the quark

transverse momentum there are five more transverse momentum dependent distribution functions (TMDs) at leading twist [14, 15]. TMDs give the description of the parton distributions beyond the collinear approximation. They depend not only on the longitudinal momentum fraction x, but also on the transverse momentum (k_T). An intuitive interpretation of the transversity distribution, h_1, is that it gives the probability of finding a transversely polarized parton inside a transversely polarized nucleon with certain longitudinal momentum fraction x and certain transverse momentum k_T. Both the Sivers function $f_{1T}^{\perp}$ and the Boer Mulders function $h_1^{\perp}$ require wave function components with nonzero orbital angular momentum and thus provide information about the correlation between the quark orbital angular momentum (OAM) and the nucleon/quark spin, respectively. Furthermore, they are T-odd functions which rely on the final state interactions (FSI) experienced by the active quark in a SIDIS experiment as both functions vanish without FSI. Although FSIs are usually unwelcome phenomena because they tend to be inextricably intertwined with the structure information one is interested in, they also provide important information of QCD. The Sivers and Boer-Mulders function provide a clean probe of the QCD FSI. In contrast to $f_{1T}^{\perp}$ and $h_1^{\perp}$, the functions g_{1T} and $h_{1L}^{\perp}$ are (naive) T-even, and thus do not require FSI to be nonzero. Nevertheless, they also require interference between wave function components that differ by one unit of OAM and thus require OAM to be nonzero. Finally, the 'pretzelosity' $h_{1T}^{\perp}$ requires interference between wave function components that differ by two units of OAM (e.g. p-p or s-d interference). Combining the wealth of information from all these functions could thus be invaluable for disentangling the spin orbit correlations in the nucleon wave function, thus providing important information about the quark orbital angular momentum.

Complementary to Generalized Parton distributions (or Impact Parameter Dependent distributions), which describe the probability of finding a parton with certain longitudinal momentum fraction and at certain transverse position b (1-D momentum space and 2-D coordinate space), TMDs give a description of the nucleon structure in 3-D momentum space. Furthermore, by including the transverse momentum of the quark, the TMDs reveal important information about the nucleon/parton spin-orbital angular momentum correlations.

All eight leading twist TMDs can be accessed in SIDIS. Four of them (transversity, sivers, pretzelosity and g_{1T}) can be accessed through a transversely polarized target. There are three mechanisms which can lead to the single (transversely polarized target) spin azimuthal asymmetry for semi-inclusive DIS electroproduction of pions. They are the so-called Collins asymmetry, the Sivers asymmetry and the Pretzelosity asymmetry. The quark transversity function in combination with the chiral-odd Collins fragmentation function [16] gives rise to an azimuthal (Collins) asymmetry in $sin(\phi_h + \phi_S)$, where azimuthal angles of both the hadron (pion) (ϕ_h) and the target spin (ϕ_S) are about the virtual photon axis and relative to the lepton scattering plane. The Sivers asymmetry [17, 18, 19] refers to the azimuthal asymmetry in $sin(\phi_h - \phi_S)$ due to the correlation between the transverse target polarization of the nucleon and the transverse momentum of the quarks, which involves the orbital angular momentum of the unpolarized quarks [20, 21]. The Pretzelosity asymmetry is similar to Collins asymmetry except the polarization is due to quarks polarized perpendicularly to the nucleon spin direction in the transverse plane inside a transversely polarized nucleon. It has an azimuthal angular dependence of $sin(3\phi_h - \phi_S)$.

One can disentangle these angular distributions by taking the azimuthal moments of the asymmetries as has been done by the HERMES Collaboration [22] and the COMPASS Collaboration [23]. In this proposal, the main focus is to measure the Collins, Sivers and Pretzelosity SSAs with an unpolarized beam and a transversely polarized ^{3}He (an effective polarized neutron) target.

4 Existing data from SIDIS

Single spin asymmetries (SSA) in inclusive charged pion production from a tranversely polarized anti-proton beam of 200 GeV/c ($\bar{p}^{\uparrow} + p$) was observed by the Fermilab Experiment E704 [24]. The observation of non-zero values of SSAs at such high energies can be explained by the role of transverse momentum dependent (TMD) partonic effects such as the Sivers mechanism [18] and the Collins mechanism [16], as well as higher twist effects arising from quark-gluon correlations [25, 26]. The observation of E704 has been confirmed recently by the BRAHMS Collaboration at RHIC [27] at a much higher energy, a center-of-mass energy of 62.4 GeV from $p^{\uparrow} + p$ collision. In this section, we review the experimental status on SIDIS, which is another way to access transverse-momentum-dependent parton distributions. For the complete formalism for SSA from SIDIS and the associated angular convention, we refer to our original PAC 34 proposal [1], Sec 2.1 and 2.2.

The HERMES Collaboration [22] and the COMPASS Collaboration [23] reported first results on single-spin asymmetries from a transversely polarized proton target and deuteron target, respective, from semi-inclusive electroproduction of hadrons in DIS kinematics. The HERMES Collaboration reported from SIDIS pion production a non-zero moment of the Collins asymmetry $< \sin(\phi_h + \phi_S) >$ which is a product of the previously unmeasured quark transversity distribution and the unknown Collins fragmentation function. While the HERMES π^+ data show positive Collins moments, the π^- data show rather larger negative values. This surprising feature might be explained by the possibility that the disfavored Collins fragmentation function could be of an unexpected importance, and it is of the same magnitude as that of the favored Collins fragmentation function, but with an opposite sign. Furthermore, HERMES Kaon Collins moments show interesting features. The K^+ moments are consistent with zero, and the K^- moments slightly favor positive values. The Sivers asymmetry due to the correlation between the target transverse polarization and quark transverse momentum was also extracted for the first time from a transversely polarized proton target from the moment of the Sivers asymmetry $< \sin(\phi_h - \phi_S) >$. A very interesting observation from the HERMES data is that the Sivers moments extracted from π^+ and π^0 are positive over the entire x and z range of the experiment, while the Sivers moment from the π^- seems to be consistent with zero. Recently, the HERMES Collaboration published data [28] on Sivers moments from charged kaon semi-inclusive DIS production in addition to pion production. The HERMES data provide evidence (See Fig. 1) for a naive-T-odd, transverse-momentum-dependent parton distribution function from non-vanishing Sivers effects for π^+, π^0, and $K^{\pm}$.

The COMPASS collaboration reported first measurements [23, 29] of the Collins and

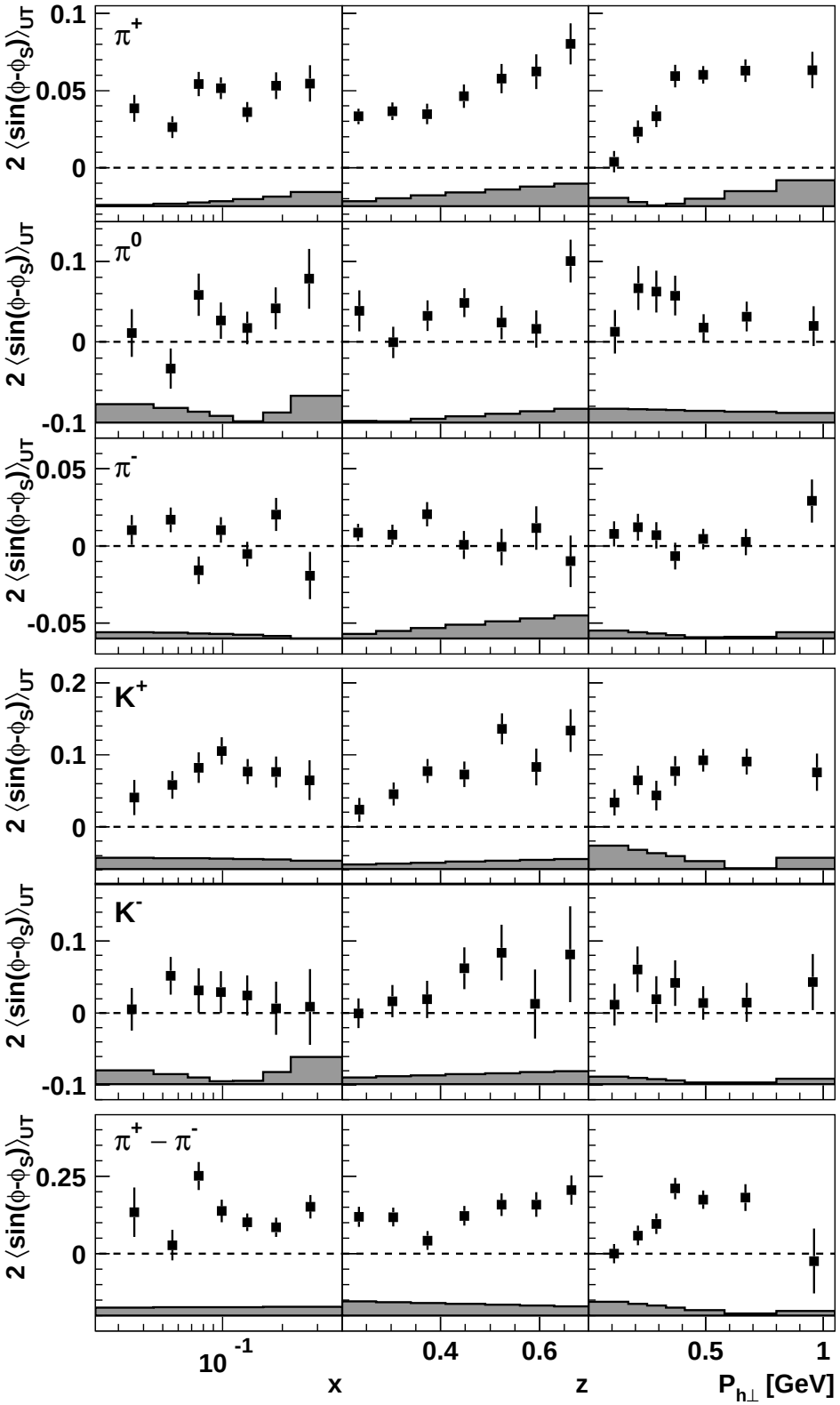

Figure 1: Sivers amplitude for pions, charge kaons and the pion-difference asymmetry as functions of x, z and $P_{h\perp}$. Figure is from Ref. [28].

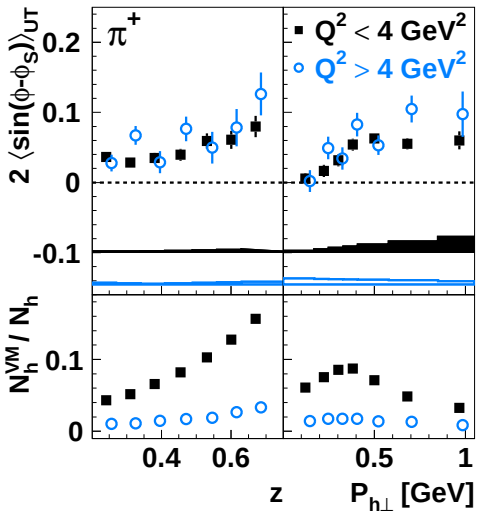

Figure 2: Sivers amplitude for π^+. The results at different Q^2 range are shown in different colors. The contamination's from vector meson diffractive scattering are shown at bottom panel. The Figure is from Ref. [28].

Sivers asymmetries of charged hadrons production from deuteron from semi-inclusive scattering of muons from a transversely polarized ^{6}LiD target in DIS kinematics. Both the Collins asymmetry and the Sivers asymmetry are consistent with zero within experimental uncertainties. One explanation is that the transversity of u quark and d quark have opposite signs so some cancellations in SSAs exist in measurements using a transversely polarized deuteron target. This may explain the smallness of both the COMPASS Collins asymmetry and the Sivers asymmetry. Recently, the COMPASS Collaboration published final results [30] for the Collins and Sivers asymmetries for charged pions and charged kaons, and neutral kaons on the deuteron target. All the measured asymmetries are small, a trend that was observed by COMPASS previously in the published, unidentified hadron data samples [23, 29].

In 2008 the COMPASS collaboration [31] released the preliminary results on both the Collins and the Sivers asymmetry from a polarized proton target. Fig. 3 shows the preliminary COMPASS proton results on the Collins asymmetry (top panel) and the Sivers asymmetry (bottom panel). Also shown are the predictions from Anselmino *et al.* [32] based on the global analysis of the HERMES proton data, the COMPASS deuteron data, and the BELLE e^+e^- collision data for the Collins asymmetry. In addition, the latest predictions from Anselmino *et al.* [33] for the Sivers asymmetry based on the global analysis of the HERMES proton data and the COMPASS deuteron data are also shown. The agreement between the prediction from the global analysis and the COMPASS preliminary proton data is good for the Collins asymmetry. The preliminary COMPASS proton data show that the Sivers asymmetries are statistically consistent with zero for both the positively charged hadrons and the negatively charged hadrons. While they are described quite well by Anselmino *et al.* [33] for the negatively charged hadrons, the results from the positively charged hadrons show possible deviations from the predictions which are based on the HERMES proton data and the COMPASS deuteron data.

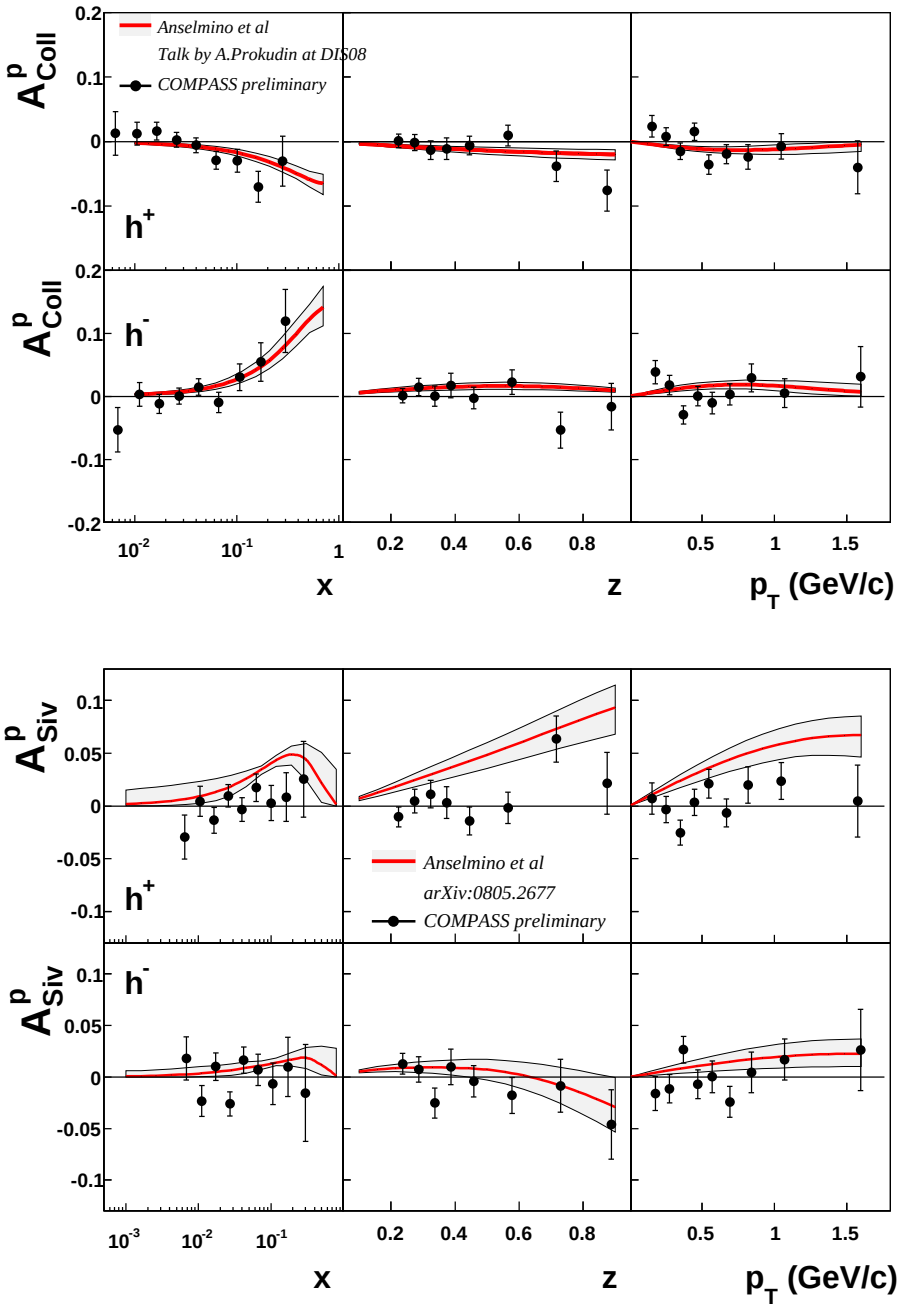

Figure 3: The preliminary COMPASS proton results [31] on the Collins asymmetry (top panel) and the Sivers asymmetry (bottom panel) as a function of x, z, and p_T for charged hadrons. Also shown are the predictions from Anselmino *et al.* [32] based on the global analysis of the HERMES proton data, the COMPASS deuteron data as well as the BELLE e^+e^- collision data for the Collins asymmetry, and for the Sivers asymmetry from Anselmino *et al.* [33]. The shaded areas represent the theoretical uncertainties in the predictions.

At Jefferson Lab, the Hall B CLAS collaboration reported [34] the first evidence for a non-zero beam-spin azimuthal asymmetry in the semi-inclusive production of positive pions in the deep inelastic scattering region. At Hall A, the 6 GeV neutron transversity experiment [35] (E06-010: $n^{\uparrow}(e, e'\pi^{\pm})$ reaction) employing a high-pressure polarized ^{3}He target was completed successfully in February of 2009. Experiment E06-010 will provide first data for the Collins and Sivers asymmetries on ^{3}He, and neutron. The preliminary results will be released in the very near future. Fig. 4 and Fig. 5 show the projected 6 GeV measurements on the Collins moment and the Sivers moment from the $n^{\uparrow}(e, e'\pi^{-})$ and $n^{\uparrow}(e, e'\pi^{+})$ reaction, respectively. Also shown are the theoretical predictions from Vogelsang and Yuan [36], and Ma, Schmidt and Yang [37] in the case of the Collins moment; Anselmino *et al.* [38] and Vogelsang and Yuan [39] for the Sivers moment. Both models fit the HERMES transverse proton data [22] very well. While the π^- Collins asymmetry for the neutron is predicted to be small, the π^+ Collins asymmetry can be as large as 5-10% depending on models. On the other hand, the predicted Sivers asymmetries for the π^+ in the case of the neutron can be as large as 40-50%. And the recent preliminary COMPASS proton (see the lower panel of Fig. 3) results show possible deviations from the predictions. One possible explanation for the possible inconsistency between the HERMES proton results and the COMPASS preliminary proton results might be due to a rapid Q^2 evolution of the Sivers function. Our proposed measurements will have excellent statistics over a Q^2 range of 1 - 4 (GeV/c)^2 and a large range of x, z values. As such it has very good overlap with the HERMES kinematics and will provide independent measurement of the Sivers asymmetry from neutron at 11 GeV. The 11 GeV neutron data together with future proton measurements at similar kinematics from CLAS12 will resolve the experimental situation with Sivers asymmetries. For theoretical parametrization of TMD and SSA, we refer to our original PAC34 proposal: PR12-09-014, Section 2.4. For the importance of precision measurement of SSAs over a large kinematic range and additional observables other than SSAs which will be measured parasitically from the proposed experiment, we refer to Sections 2.4 and 2.5 of PR12-09-014.

Jefferson Lab is in a unique place to make important contributions to the study of the quark transversity and other transverse momentum dependent distribution functions. The measurement in the high x region is essential in determining the nucleon and the quark tensor charge. The polarized inclusive DIS program at Jefferson Lab has made important, well-recognized contributions already in the field, particularly in the study of the nucleon longitudinal polarization distributions in the large x region. With the upcoming 12 GeV upgrade, JLab will play a leading role in the study of the transverse spin with high luminosity. The separate determination of the Collins, Sivers and pretzelosity asymmetries from a transversely polarized "neutron" target employing a high pressure polarized ^{3}He target is very important to test theoretical predictions of TMDs and to improve our understanding of TMDs ultimately from the first principles of QCD.

5 Experimental Setup

The layout of the experiment is shown in Fig. 6 (Fig. 10 in [1]). The entire detector system consists of two parts: forward-angle detectors and large-angle detectors.

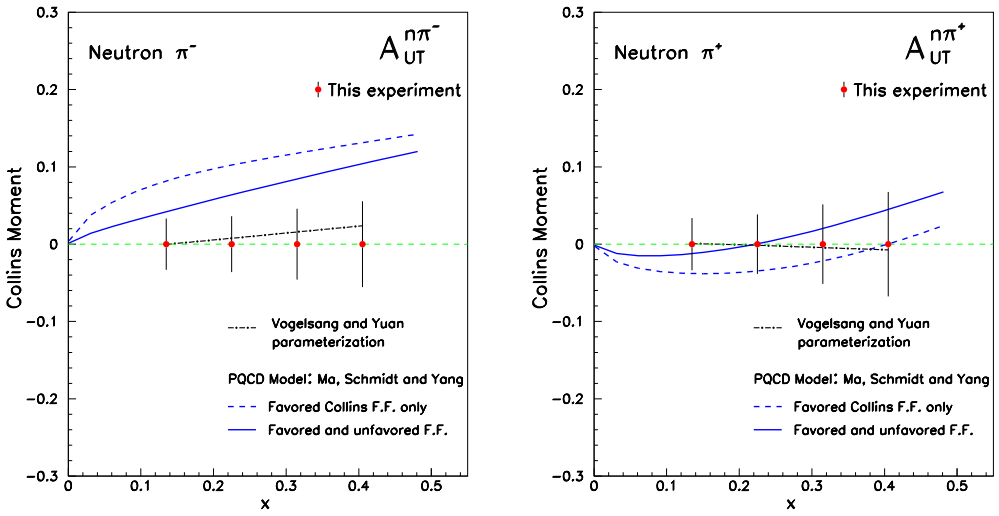

Figure 4: The projected 6 GeV JLab measurements on Collins moment from the $n^{\uparrow}(e, e'\pi^-)$ and $n^{\uparrow}(e, e'\pi^+)$ reaction together with theoretical predictions.

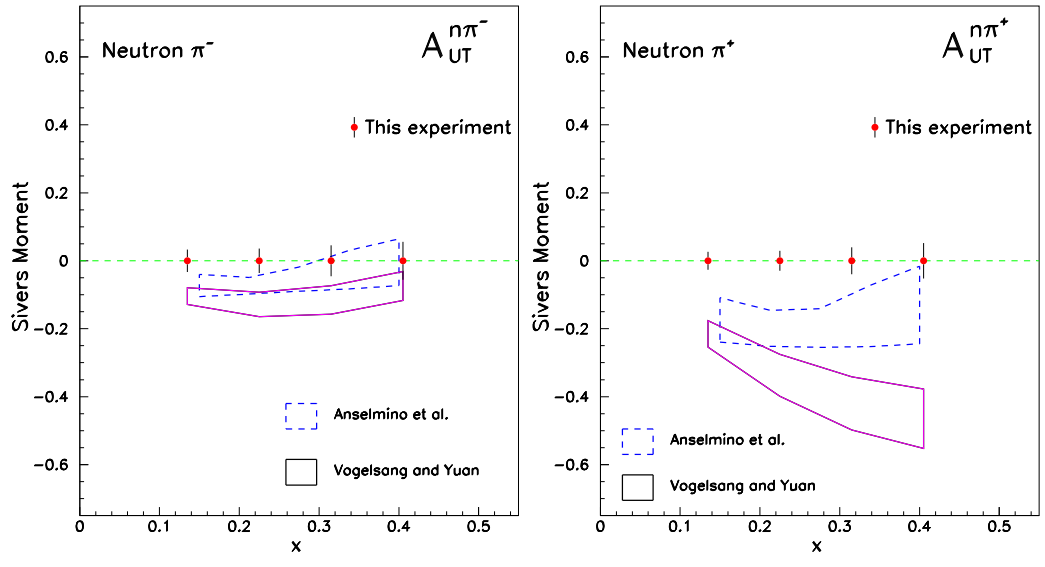

Figure 5: The projected 6 GeV JLab measurements on Sivers moment from the $n^{\uparrow}(e, e'\pi^-)$ and $n^{\uparrow}(e, e'\pi^+)$ reaction together with theoretical predictions.

The polar angular coverage for the forward-angle detectors is from 6.6° to 12° and the momentum coverage is from 0.9 GeV/c to 7.0 GeV/c. The total solid angle is about 57 msr for this momentum coverage. GEM detectors will be used as tracking detectors (Six layers of the GEM detectors are placed inside the coils. Five of them will be used in tracking for the forward-angle detection). A combination of an electromagnetic calorimeter, gas Čerenkov counters, a layer of Multi-gap Resistive Plate Chamber (MRPC) and a thin layer of scintillator will be used for particle identifications.

The polar angular coverage for the large-angle detectors is from 14.5° to 22°. They are mainly used for electron detections for momentum range of 3.5-6.0 GeV/c. The expected π^-/e ratio is smaller than 1.5. The "shashlyk"-type calorimeter will be sufficient to provide the pion rejection (200:1). Four layers of GEM detectors will be used as tracking detectors. The total solid angle is about 231 msr for this momentum range. The acceptance is shown in Fig. 7 (Fig. 17 in [1]).

5.1 Solenoid Magnet

A new yoke will be added to the CDF solenoid magnet for our spectrometer. The upstream endcap plate will keep the magnetic field and field gradients low in the target region. The conceptual design is shown in Fig. 8 (Fig. 11 in [1]) [5]. The field strength is simulated using the 2-dimensional code Poisson Superfish [44]. In this design, the absolute magnetic field strength in the target region is about a few Gauss with the field gradient < 50 mG/cm. Correction coils around the target will further reduce the field gradient to the desired level (~ 30 mG/cm). The magnetic field in the central line (x = 0 and y = 0) is shown in Fig. 9 [6].

5.2 GEM Tracker and Tracking

The GEM detectors will be used as tracking device. A total of six layers of GEM tracking detectors will be used to provide the momentum, angle and interaction vertex of the particles detected. They will all be placed uniformly inside the magnet. For the forward-angle detectors, five layers (except for the first layer) of GEM detectors will be used. Usually, 3 points are needed for reconstructing kinematic variables. The 4/5 points that we have will provide enough redundancies to compensate for the inefficiency of the GEM tracking detector. For the large-angle detector, the first four layers of GEM detectors will be used to provide the momentum, angle and vertex reconstruction. In this case, four layers of GEM detectors are enough since the background level in the large-angle kinematics are expected to be smaller.

The required active area is shown in Table. 1. The total required surface area including all six layers for this experiment is less than 18 m^2, which is smaller than that in the

[5] In the new design of yoke, we will use part of the original CDF yoke. The conceptual design is still under development with the PVDIS collaboration. In this proposal, we assume that the yoke structure outside the coil is similar to the one in the original proposal which is based on BABAR solenoidal magnet. We updated the geometry slightly to match the CDF magnet for the coil positions and extend the length of coils to 5 m. The differences in terms of acceptance and magnetic field properties are expected to be small between the current design and future design with CDF yoke.

[6] Depending on the running current in the coils, the magnetic field can be slightly different.

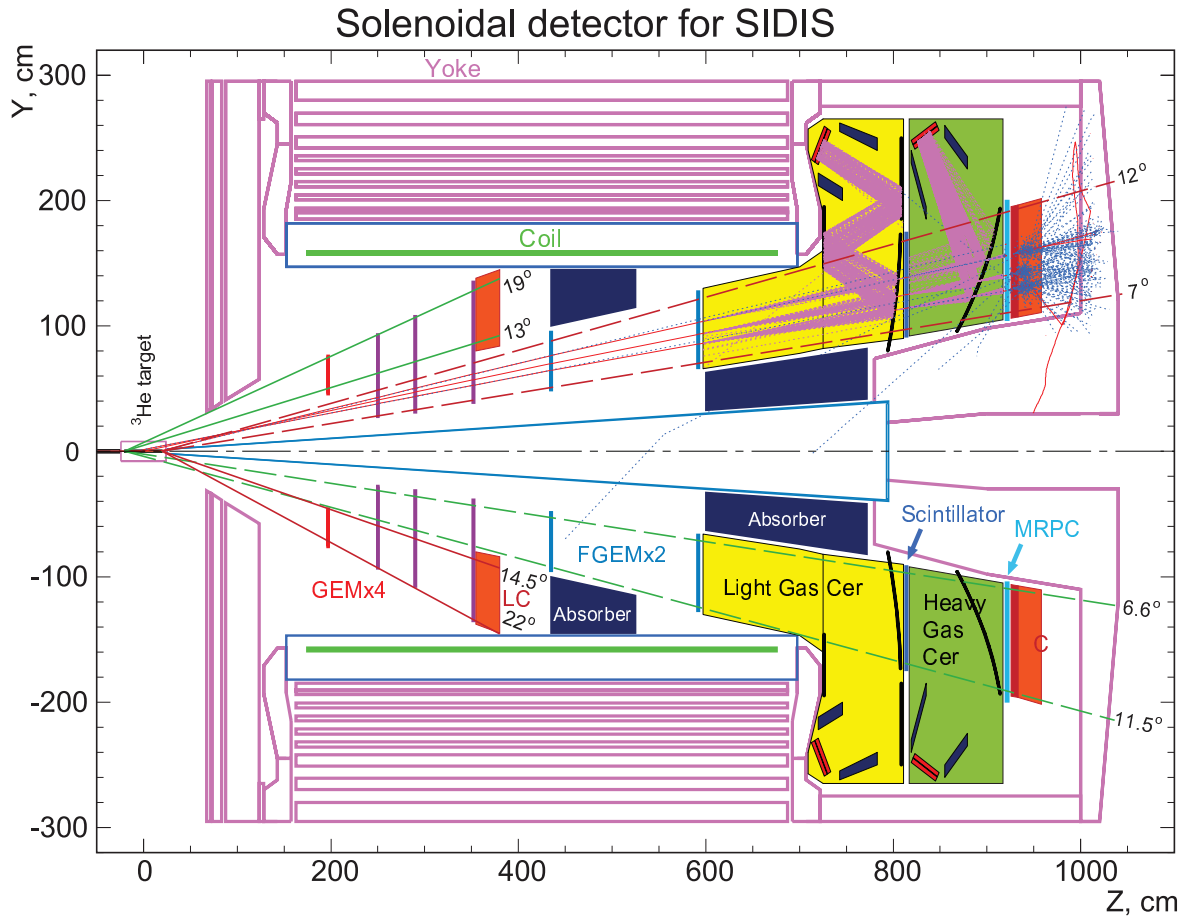

Figure 6: The experimental layout of the SoLID based on the option of CDF magnet. At forward angle, there are five layers of GEM detectors (The first three, in purple color, are shared with the large-angle detectors. The rest two layers are in blue color.) inside the coils in the upstream of the Gas Čerenkov. A 2.1 m long light Gas Čerenkov, (yellow) is used to separate the electrons and pions. One layer of scintillator (dark blue) will be placed after the light gas Čerenkov. It will primarily be used in forming the hadron trigger. A 1 m long heavy gas Čerenkov, in green color, is placed after the light gas Čerenkov to exclude the kaons and the protons from the pions at high momentum. One layer of Multi-gap Resistive Plate Chamber (MRPC), in light blue, is placed after the heavy gas Čerenkov to provide timing information to form coincidence. The calorimeter detectors, in orange color, will be used for electron/pion separation, especially at high momentum. For the large-angle detector, four layers of the GEM detectors (The last three layers are shared with the forward-angle detection) are placed inside the coils. A "shashlyk"-type calorimeter will be placed inside the coils. Then an absorber will be placed after the large-angle calorimeter to absorb the low energy background. Another absorber will be placed close to the beam line to prevent the forward detectors from the low energy backgrounds.

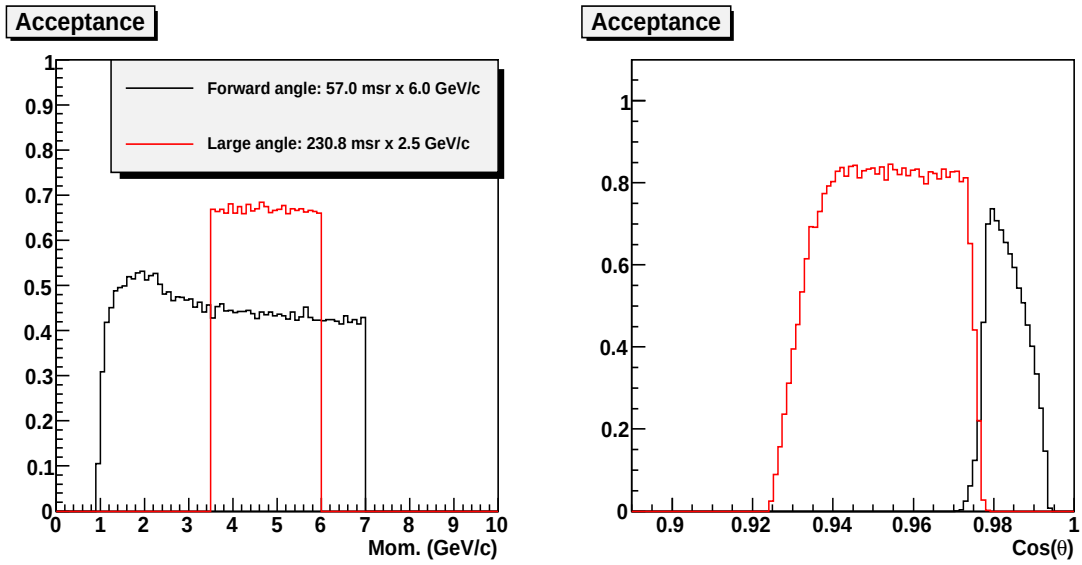

Figure 7: The momentum-dependent acceptance is shown in the left panel, while the polar-angle-dependent acceptance is shown in the right panel.

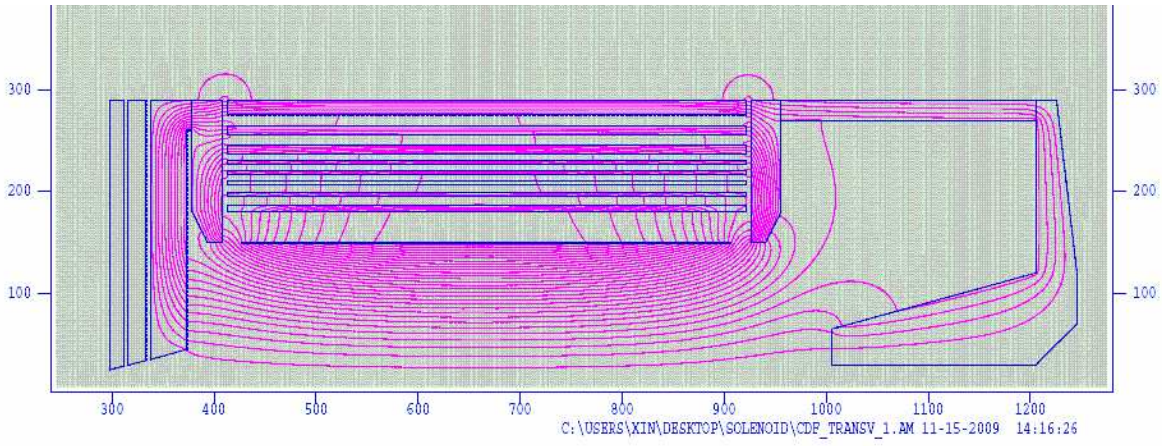

Figure 8: The magnetic field simulation with the current design of the yoke.

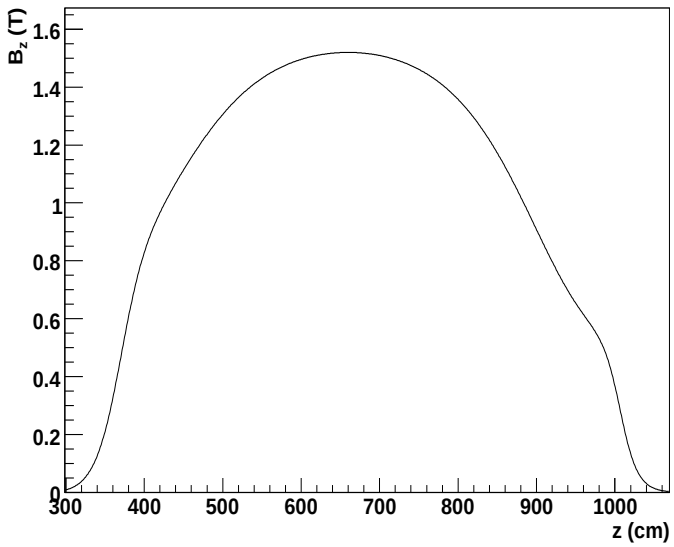

Figure 9: The simulated magnetic field in the line of x=0 and y=0, which is along the beam line direction.

PVDIS [2] (23 m^2) experiment. The 2nd to 6th chamber will be reconfigured from the PVDIS GEM detectors. The first chamber needs to be built for this experiment. The PVDIS configuration is also shown in Table. 1.

In the PVDIS configuration, there are in total four layers of GEM detectors. Each layer consists of 30 pieces, which will cover in total 300 degrees. In the reconfiguration process, we will move each piece of GEM detectors closer to the beam line. In this case, we do not need 30 pieces anymore. We will need 28, 27, 24 and 22 pieces from PVDIS first to fourth chambers, respectively. The original PVDIS layout is shown in Fig. 10. The coverage after the reconfiguration can be found in Fig. 11. This design would require the PVDIS chamber-4 to be reconfigured as two smaller chambers.

Each of our GEM layer will cover 360 degrees. The fist chamber is divided into 36 small pieces, each covers 10 degrees. The GEM detectors are used with 2-D readouts. The induction electrode contains two sets of stripes or pads, insulated from each other. The angle between the two readout directions depends on the width of one sector, which may be selected in a range of $9^\circ - 12^\circ$ depending on the plane. The amplitude correlation of the signals from the two planes allows for a suppression of the false U-V combination by a factor of $\sim$3-5 in reducing fake hit. Although the first chamber will be a new chamber to be built, we can reuse the electronics for the PVDIS chamber. There are in total 19 pieces (1/30 for each layer) of PVDIS chamber that are not used in the reconfiguration. The number of channels for the new chamber-1 is 24k, assuming the pitch is 0.4 mm. The number of channels which can be reused from the PVDIS is about 20 k.

The background rates from the GEM detectors have been studied using GEANT3 with all physics processes turned on (Moller/Mott ... etc). The studies in Hall A show that the wire chamber background rates can be predicted by GEANT3 within 50% level.

	R_{min} (cm)	R_{max} (cm)	z (cm)	Status	PVDIS configuration (cm)
Chamber1	46	76	197	New	N/A
Chamber2	28	93	250	PVDIS C1	50-115
Chamber3	31.5	107.5	290	PVDIS C2	64-140
Chamber4	39	135	352	PVDIS C3	104-200
Chamber5	49	95	435	PVDIS C4	109-215
Chamber6	67	127	592	PVDIS C4	109-215

Table 1: In this table, we present the required active area for the GEM detectors. For z position, we assume the zero point is at the center of the polarized ^3He target. The fifth column shows the status of current design. Five layers of GEM detectors will be reconfigured from the four PVDIS chambers. The first chamber will be built for this experiment. The last column shows the original configuration in terms of the radial coverage in the PVDIS design.

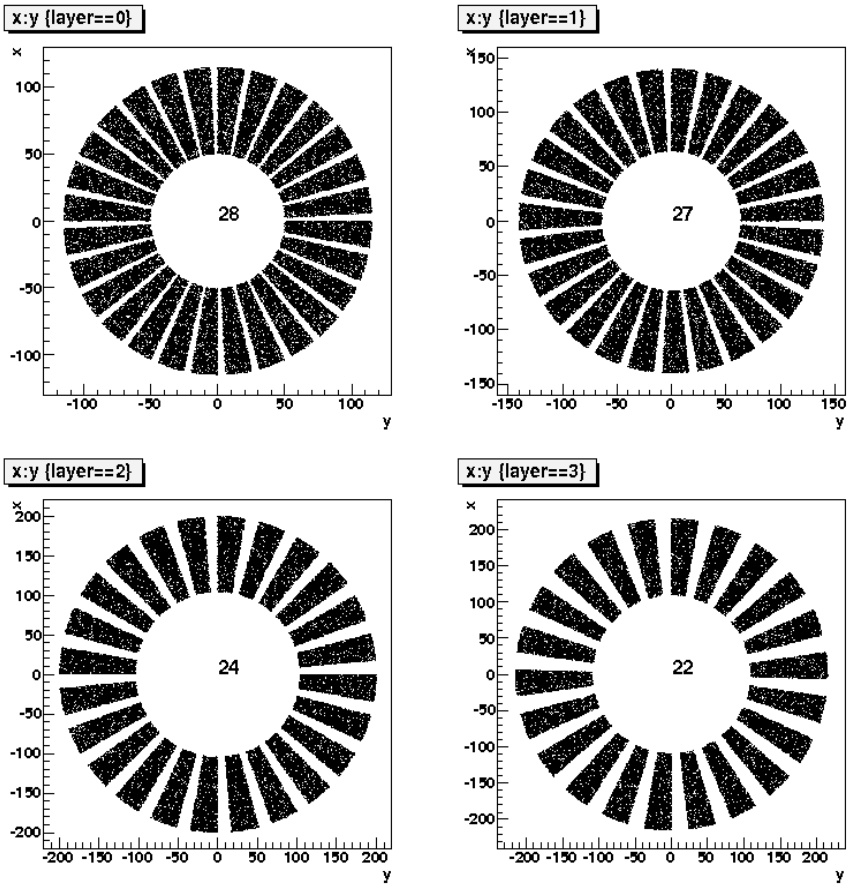

Figure 10: The GEM configuration in the PVDIS layout. We only show the needed pieces for the reconfiguration

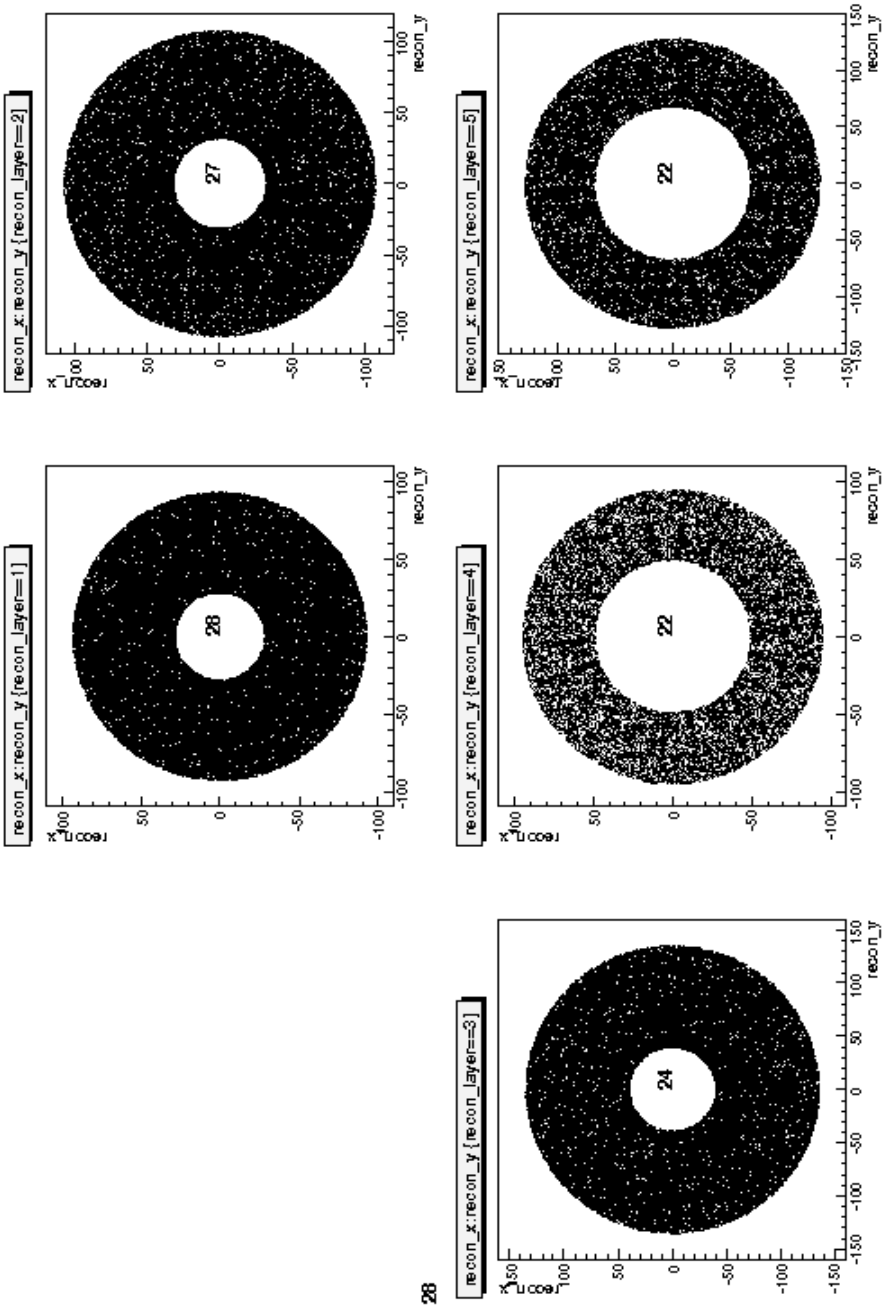

Figure 11: The coverage after reconfiguration.

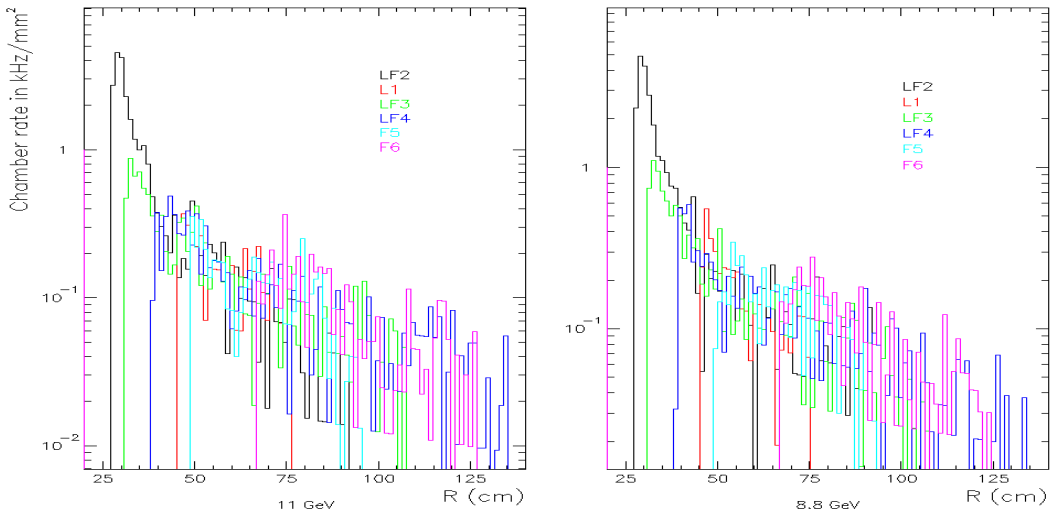

Figure 12: The results of simulated background of 11 (8.8) GeV beam are shown in left (right) panel. The x-axis labels the radius and the y-axis represents the rate. There are six layers of GEM detectors in total. The "L1" labels the first layer in the large-angle. "LF2", "LF3" and "LF4" are shared between the large-angle and forward-angle detection. The "F5" and "F6" are used in the forward-angle only. The position of each GEM detector can be found in Fig. 6.

The results are shown in Fig. 12 for 11 and 8.8 GeV beam energy. The GEMs have been used in a 30 kHz/mm^2 flux in the COMPASS experiment, which is much higher than the estimated rates in our configuration. The multiplicities within a 50 ns TDC window in different layers of chamber are shown in Fig. 13.

In order to justify the design of this configuration, a tracking MC is performed. The simulation is based on the GEANT3 model of SoLID (BaBar magnet) [7]. The GEANT3 package has been checked with previous Hall A data and the agreement is at 50% level. The distribution of the background is based on the results in Fig. 12. The TDC window is assumed to be 50 ns. The detector hitting efficiency is assumed to be 98%. The hit position resolution is assumed to be 200 μm. As discussed previously, the amplitude correlation of the signals from the two planes allows for a suppression of the false U-V combination by a factor of ∼3-5, reducing the number of planes and projections needed for pattern recognition. A reduction factor of 4 is assumed here. Meanwhile, a new tracking algorithm, which is based on the standard Hall A analyzer, is developed based on the idea of progressive searching.

In the standard "progressive" method, the tracking starts from a seed, normally a hit in the first chamber. Then it looks for matched hits in the next chamber, based on the possible trajectory for the particles with designed momentum/angular coverage. With the existing hits, the tracking parameters, such as polar angle, momentum, charge can be narrowed down. The same procedure continues until we reach the last layer of a chamber.

[7]The background levels are very similar for the design based on BaBar magnet and CDF magnet.

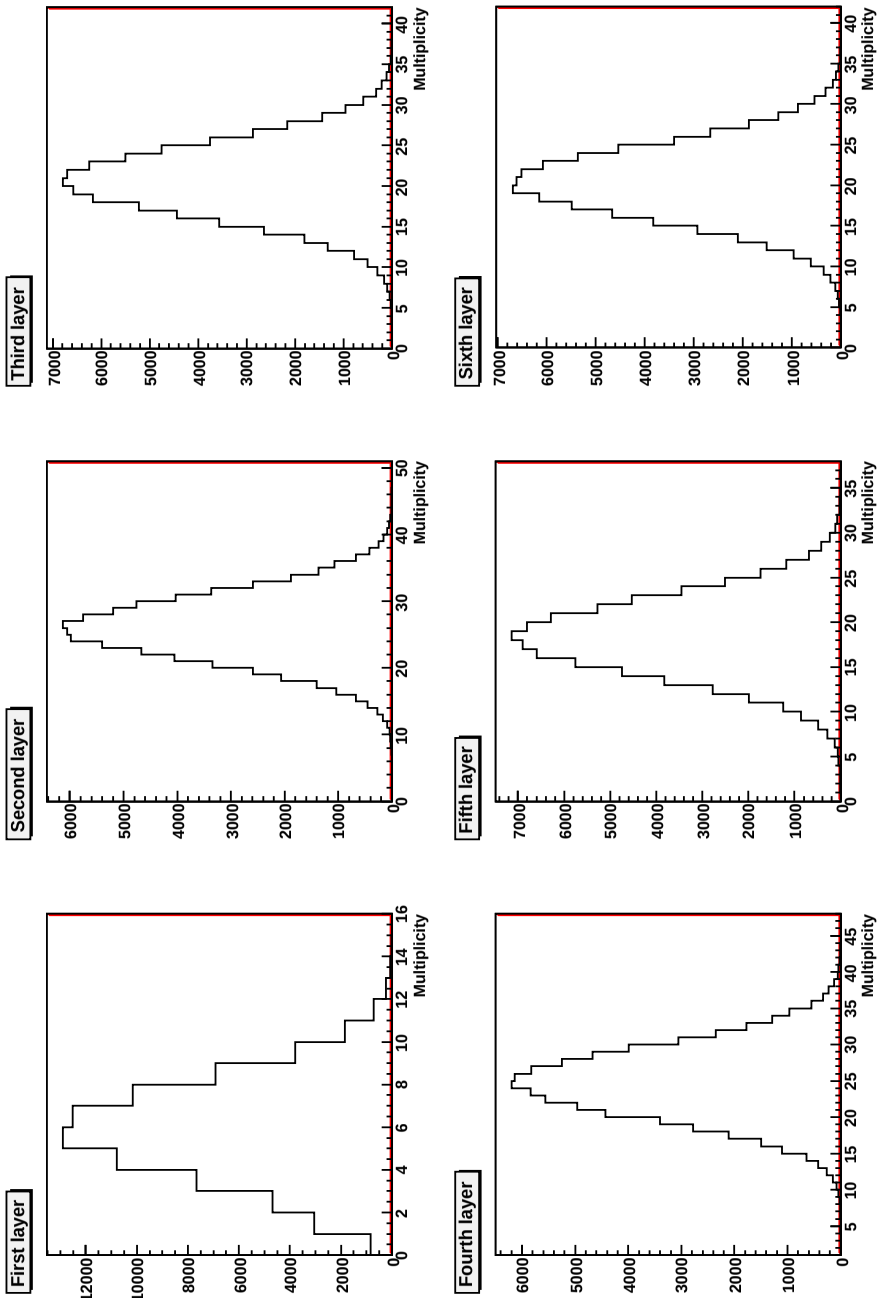

Figure 13: The multiplicities on the GEM chambers, based on the background rates at 11 GeV.

After the coarse tracking, a global fitting is implemented to judge the tracks. Then the "similar tracks" will be merged (de-ghosting).

The results of the tracking MC including background and physics tracks are tabulated in Table. 2. In addition, the calorimeter/MRPC can provide an additional tracking point to de-ghost the false track generated by backgrounds. An improved optics model will further reduce the possibilities in finding false tracks. From the tracking MC study, we conclude that the tracking will not be a problem for the proposed luminosity.

Configuration	Background level	single-track	multi-track	zero-track
large-angle	1	99.4%	0.28%	0.31%
Forward-angle	1	99.2%	0.32%	0.49%
Large-angle	2	95.4%	4.2%	0.32%
Forward-angle	2	95.6%	3.9%	0.44%

Table 2: 3 out of 4 planes (4 out of 5 planes) are required to fire for large-angle (forward-angle) tracking detector for a valid track. When the "Background level" is labeled as 2, we assume the background rates are twice of the simulated rates from GEANT.

The optics of the CDF magnet is studied. The position resolution of GEM tracker is assumed to be 200 μm. Resolutions of momentum, polar angle, azimuthal angle and vertex are shown in Fig. 14 as a function of polar angular θ and momentum. The average momentum resolution, $\delta p/p$ is about 1%. The average polar angle resolution is about 0.3 mr. The average azimuthal angular resolution is about 5 mr. The average vertex resolution is about 0.8 cm.

In addition to the polar and azimuthal angular resolution in the lab frame, we also study the ϕ_h resolution vs the transverse momentum. The coverage of P_T (the hadron transverse momentum with respect to the virtual photon direction) and the $\delta\phi_h$ vs P_T are shown in Fig. 15. Here $\delta\phi_h$ is defined as the angle difference between the ϕ_h with detector resolution effects and the real ϕ_h without the detector resolution effects. In Fig. 15, no clear resolution degration is observed in $\delta\phi_h$. In this study, we assume the average momentum resolution ($\delta p/p$) is 1.2%. The average resolution of polar (azimuthal) angle in the lab frame is assumed to be 0.3 (6) mr. The RMS values of $\delta\phi_h$ are shown in Fig. 16.

5.3 Calorimeter

The background rates of calorimeters are updated in Fig. 17. (Fig. 14 in [1]). The total area that we want to cover is about 12.7 m^2. In comparison, the requested area in PVDIS proposal is about 7.5 m^2. The radiation level in the calorimeter is at least 5-10 times less than that of the PVDIS proposal.

5.4 Target Collimator

The design of the target collimator can be found in Fig. 18. The goal of the target collimator is to shield high energy electrons and photons, which are generated from the

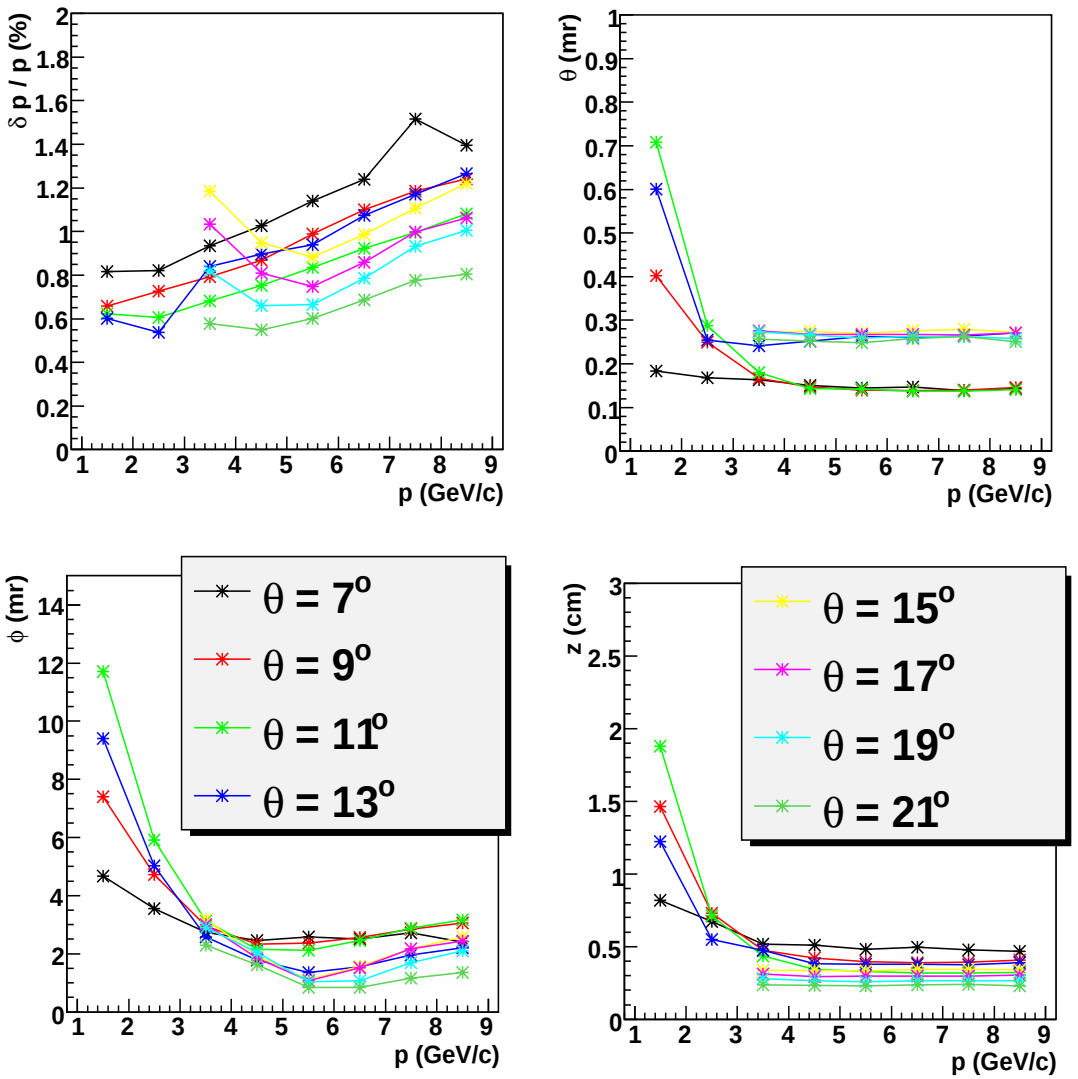

Figure 14: The resolution on reconstructed momentum (top left), polar angle (top right), azimuthal angle (bottom left) and vertex (bottom right).

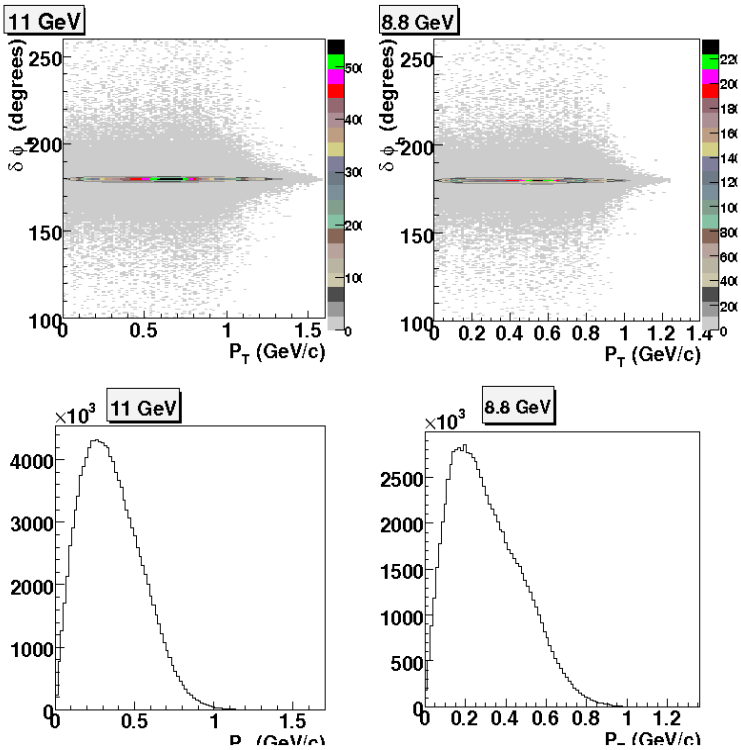

Figure 15: The $\delta\phi_h$ vs P_T are shown in top left (right) panel for 11 (8.8) GeV. The P_T coverage are shown in bottom left (right) panel for 11 (8.8) GeV. The acceptance at very low P_T region is very limited. No clear degration is observed in $\delta\phi_h$.

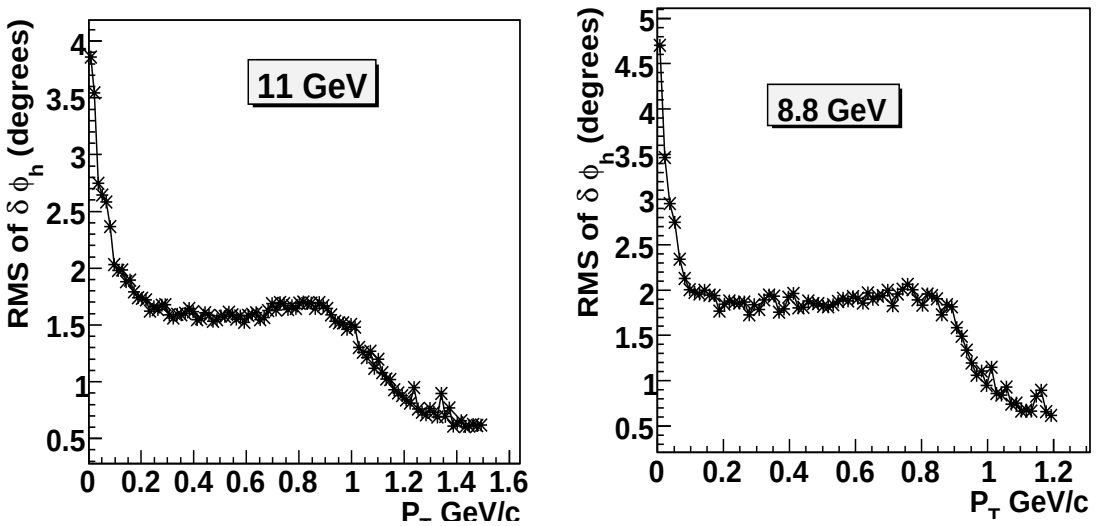

Figure 16: The RMS value of $\delta\phi_h$ vs P_T for 11 (left) and 8.8 (right) GeV. The RMS value of $\delta\phi_h$ is larger at small transverse momentum region.

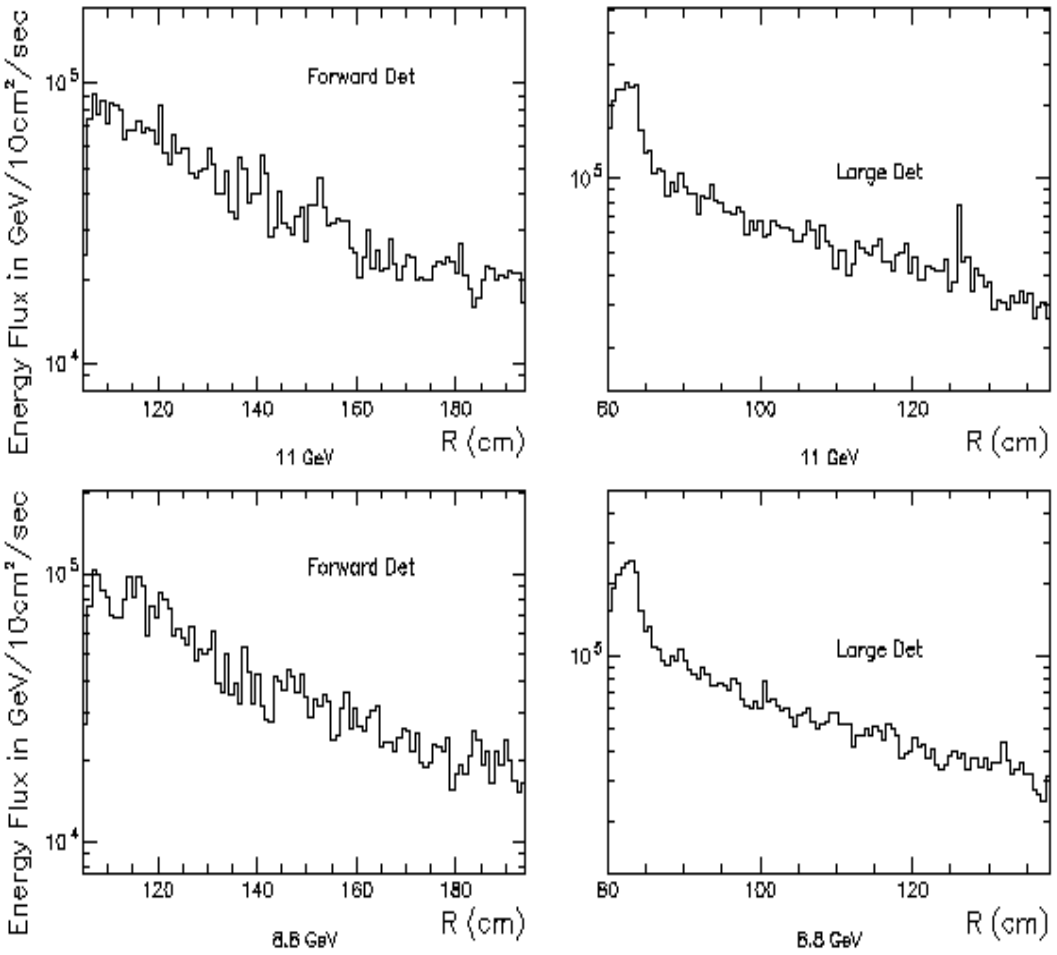

Figure 17: The x-axis is the radius and the y-axis is the energy flux. The left panel shows the background in the calorimeter for the forward-angle detector and the right panel shows the background in the calorimeter for the large-angle detector.

target wall in the forward-angle detector. We also study the acceptance effect for the collimator (see Fig. 19). The target collimator has been successfully implemented in E06-010 experiment (30 degrees) and previous ^3He experiments. For example, the target collimator was successfully implemented in the small angle GDH experiment (E97-110), where the central angles for the HRS spectrometer were 6 and 9 degrees (the acceptance range is $\pm$ 1.5 degrees). The smallest angle is 4.5 degrees which is smaller than the minimum angle (6.6 degrees) in this proposal.

6 Particle Identification: Electron Identification

Following PVDIS detector setup, we plan to divide detectors into 30 sectors in the 2π azimuthal acceptance.

6.1 Electromagnetic Calorimeter

Two sets of electromagnetic calorimeters will be used to identify electron signals in forward and large-angle sides by measuring the energy deposition in the calorimeter through the electromagnetic shower.

As discussed in more details in the PVDIS proposal [2], a "shashlyk"-type calorimeter can be used inside the magnetic field while it is also hard to radiation. The energy resolution will be about $\frac{\delta E}{E} = \sqrt{(2\%)^2 + (\frac{3\%}{\sqrt{E}})^2}$. With a pre-shower/shower splitting, a pion rejection factor of 200:1 can be achieved at $E > 3.5$ GeV and over 100:1 with $E > 1.0$ GeV.

The surface area of the calorimeter required for this experiment to cover a full 2π azimuthal angle, is about 12.3 m^2 (8.5 m^2 for the forward-angle detection and 3.8 m^2 for the large-angle detection), which is similar to the surface area required in PVDIS experiment (7.5 m^2). However, in order to cover the full azimuthal angle, blocks with special shapes will be required.

While the e/π^- ratio is more than 1:1.5 in the large-angle side at high momentum (>3.5 GeV/c) and the calorimeter will do a good electron identification by itself, additional particle identification detectors are required to clean low energy pion background in the forward acceptance.

6.2 Gas Čerenkov Detector

A gas Čerenkov detector of 2.1 m long filled with CO_2 at 1 atmospheric pressure (n=1.00045) gives a π threshold of 4.7 GeV/c. Considering a 80% light collection efficiency and 20% quantum efficiency, this setup is expected to give about 17 photoelectrons for high energy electron. The background rates in the entire light gas Čerenkov is estimated to be 40 MHz. With 30 sectors, and a 20-ns coincidence window, a 40:1 π rejection can be achieved on-line. We expected the off-line rejection ratio to be better than 80:1.

Due to the high radiation background level, the light collection system needs to be carefully designed. A triple-bounce mirror system will be used to reflect and focus the light to PMTs in an endcap pocket which shields away most of the low energy background

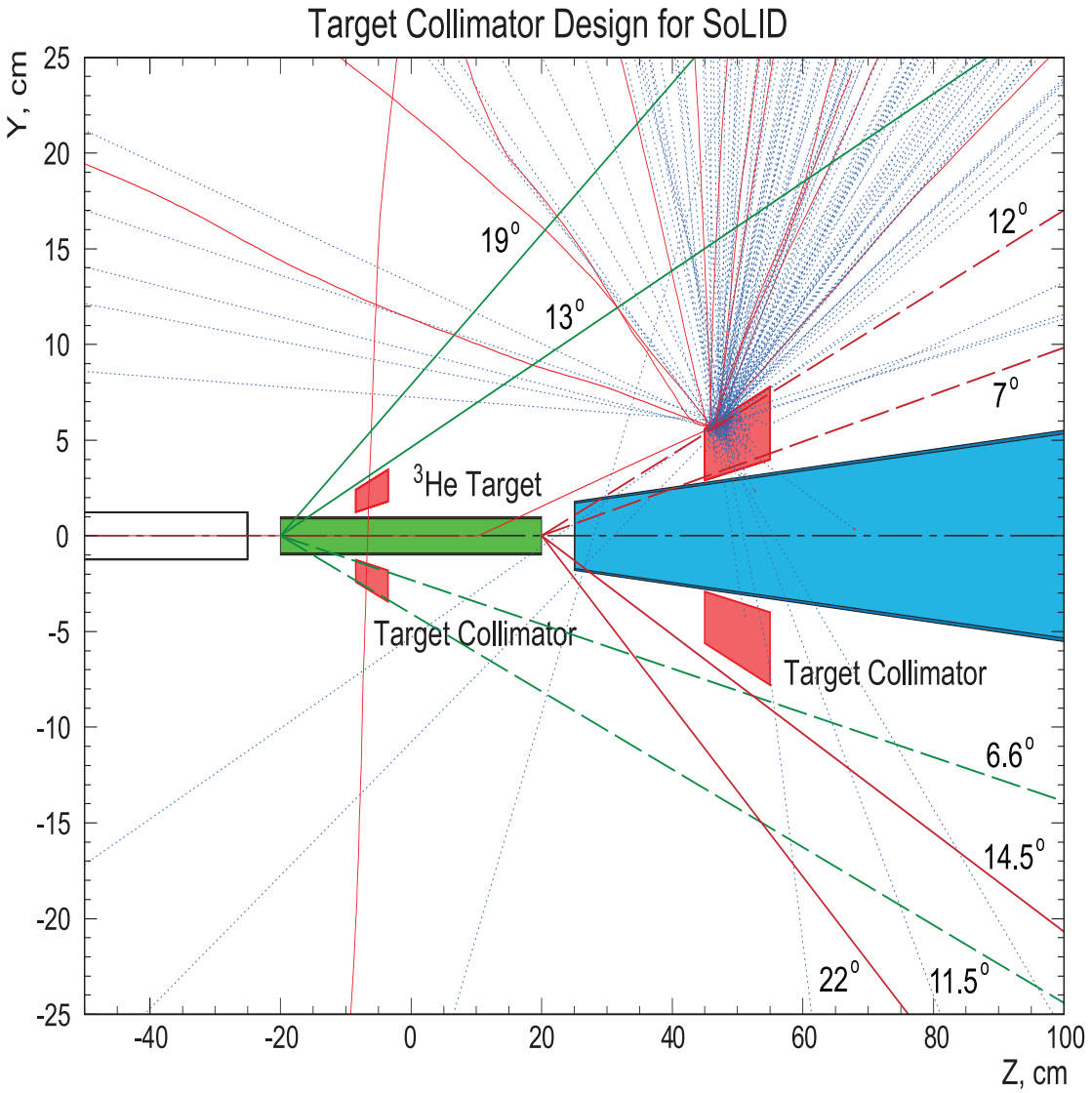

Figure 18: The target collimator is shown as red box in the plot. Their shape is "cone" which is around the beam pipe (blue). The x-axis scale is from -50 to 150 cm, while the y-axis scale is from -25 to 25 cm.

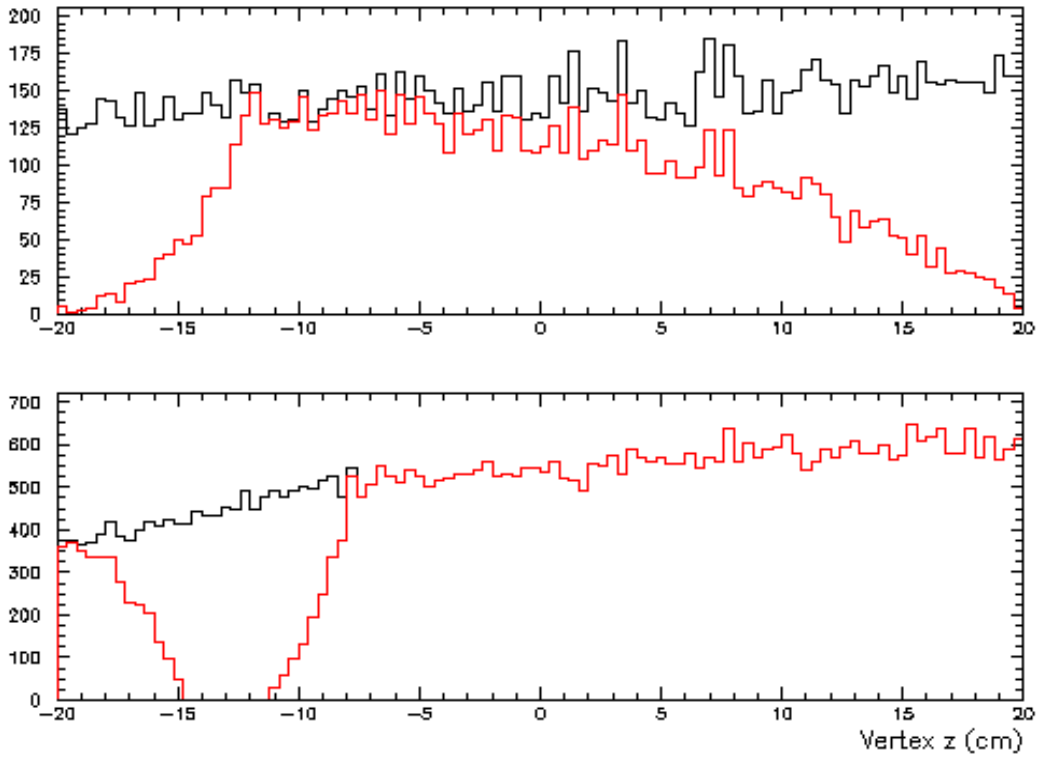

Figure 19: The acceptance effect of the target collimator. The black lines show the acceptance without the collimator and the red lines show the acceptance with the collimator. The upper panel is for the forward-angle detection and the bottom panel is for the large-angle detection. The simulated momentum range is from 0.9 GeV/c to 7.0 GeV/c at forward-angles and 3.5 GeV/c to 7.0 GeV/c at large-angles. The distribution is assumed to be uniform within the simulated momentum ranges.

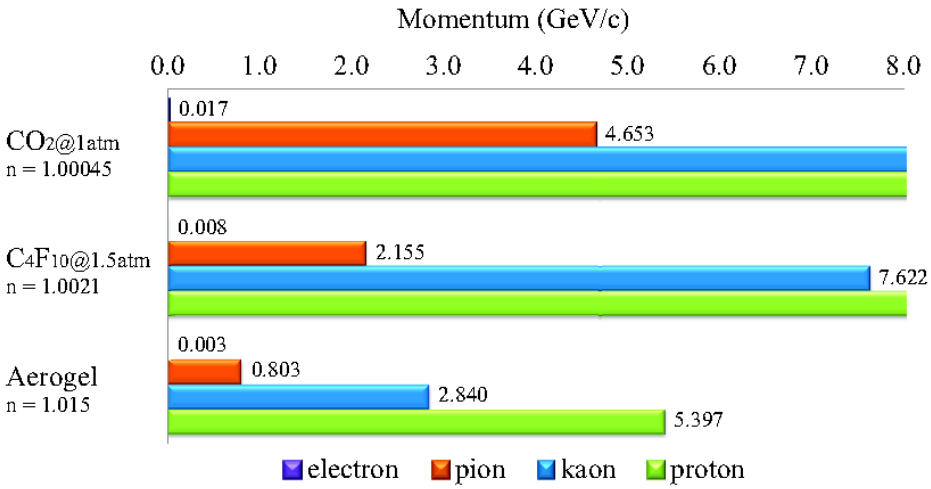

Figure 20: Momentum thresholds of Čerenkov detectors

and prevent direct forward view of the PMTs. Also 3" quartz PMTs are favorable for their less sensitivity to the background. Even though the magnetic field is relatively low (<100 Gauss) in the pocket, a strong magnetic shielding for the PMTs is still needed. Other options are discussed in Sec. 19.1.

6.3 Coincidence Timing/Vertex

The E06-010 (6 GeV transversity) analysis shows that coincidence with hadrons can further help in reducing the π^- contamination in the electron sample by about at least a factor of 5. Assuming a similar suppression factor in the kinematics of this experiment, at large-angle, the pion contamination will be less than 1.5 (π^-/e ratio) / 200 (Calorimeter) / 5 (Coincidence) $\sim$ 0.15% level. At forward angle, the pion contamination will be less than 100 (π^-/e ratio) /100 (Calorimeter) /80 (light gas Čerenkov) /5 (Coincidence) $\sim$ 0.25 % level. In addition, as we will discuss in the following sections, a heavy gas Čerenkov (with π momentum threshold of 2.2 GeV/c) will be added to help the hadron detection. It can further help to suppress the π contamination at momentum lower than 2.0 GeV/c where the π/e ratio is expected to be large. The overall π contamination in the electron sample can be controlled to be less than 0.2% for the coincidence SIDIS events.

7 Particle Identification: Pion Identification

For the forward-angle acceptance, the detection and identification of $\pi^\pm$ with momentum between 0.9 to 7.0 GeV/c will be the major goal of the SIDIS experiment. The CO_2 gas Čerenkov separates the π from other hadrons in the momentum range greater than 4.7 GeV/c. The coincidence timing can separate pions from kaon at low momentum range (from proton in the entire momentum range). And other PID detectors are needed to cover the mid momentum range to separate pions from kaons. Normally, the SIDIS kaon

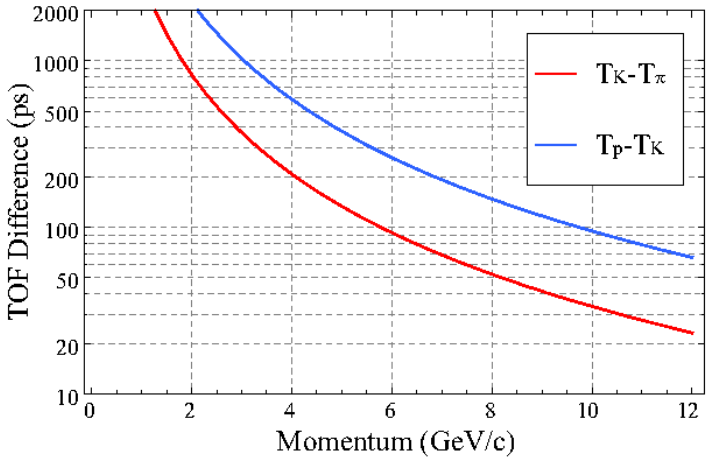

Figure 21: Particle identification through Time-Of-Flight

rates are at least one order of magnitude smaller than the SIDIS π rates. Thus, a 10:1 kaon rejection from the additional PID detectors will reduce the kaon contamination to be less than 1% level.

7.1 Time of Flight Detector

As shown in Figure 6, a layer of multi-resistive plate chamber (MRPC) detector will be inserted before the forward-angle calorimeter. MRPC has been recently used in RHIC STAR and LHC ALICE as their TOFs and its typical time resolution is better than 80 ps. And most importantly, as a gas chamber, MRPC does not need PMT for readout so it can work inside a magnetic field. The simulated background rates on MRPC (Fig. 22) are shown to be less than 0.1 kHz/mm^2. Studies [45] show that the MRPC can work in a environment of background rates of 0.28 kHz/mm^2.

The total path length is around 9 meters from the target and the flight time is calculated by comparing the TOF signal to the beam RF signal. The differences of the TOF of different particles are plotted in Fig. 21.

With a TOF resolution of 100 ps, we can identify π from kaons at a rejection factor of 20:1 up to 2.5 GeV/c. Our collaborators in the engineering department at Tsinghua university have a lot of experience with MRPC and built the TOF for the RHIC STAR. They will lead the effort in building/testing MRPC for this experiment.

7.2 Heavy Gas Čerenkov Detector

A Čerenkov detector filled with C_4F_{10} at 1.5 atmospheric pressure (n=1.0021) will be used to cover the medium momentum range. The thresholds for π and K are 2.2 and 7.6 GeV/c, respectively. A tank with 80 cm depth can give $N_{pe} \sim 25$ for high energy pion. The light collection will be similar to the CO_2 gas Čerenkov detector and proper shielding is needed. The background rates in the entire heavy gas Čerenkov is about 60 MHz. The

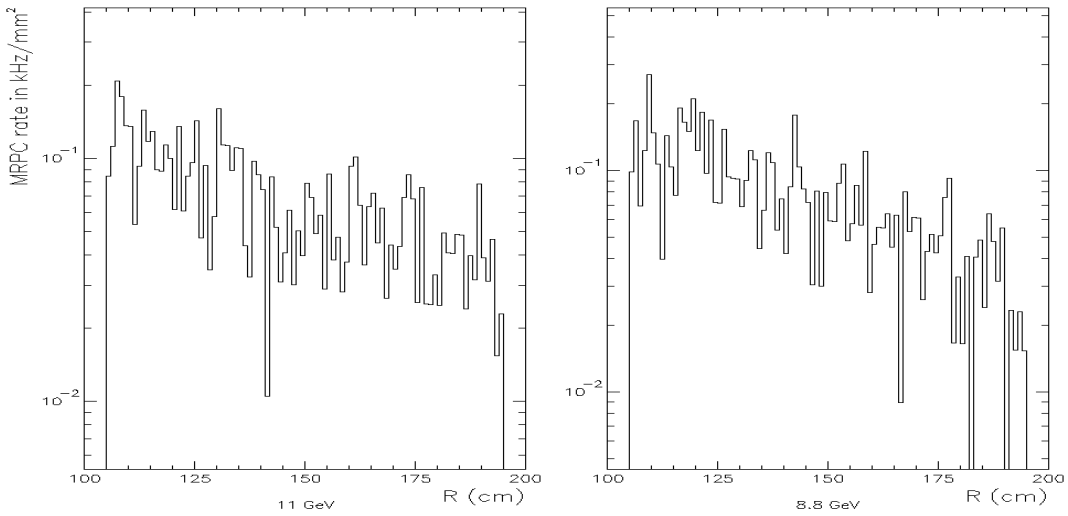

Figure 22: The results of simulated background with 11 (8.8) GeV beam are shown in left (right) panel for MRPC.

off-line rejection is expected to be better than 50:1. In addition, we also explore other options, which can be found in Sec. 19.2. We expect to control the kaon contamination to below 0.25% in the entire momentum range.

8 Trigger Setup and DAQ

With 30 sectors, singles triggers will be first generated in each sector then the coincidence triggers will be formed between sectors. Three types of triggers will be formed and the rates are estimated as following:

8.1 Electron singles trigger

In the large-angle side, the trigger is provided solely by the large-angle Calorimeter with high threshold. With the on-line hadron rejection $R_{LC} = 20$ from the calorimeter, the rates are expected to be

$$\begin{aligned} T_L^e(11\text{ GeV}) &= Y_L^e + Y_L^\gamma + \frac{Y_L^h}{R_{LC}} = 11 + 51.5 + \frac{55.6}{20} = 65\text{ kHz} \\ T_L^e(8.8\text{ GeV}) &= 16.5 + 37 + \frac{36.7}{20} = 55\text{ kHz}. \end{aligned} \quad (1)$$

For the forward-angle acceptance, the electron trigger is formed from the coincidence between large calorimeter signal and CO_2 gas Čerenkov detector. The on-line hadron rejection is about $R_{LC} = 10$ for the calorimeter. The actual hadron/photon rejection performance from the gas Čerenkov depends on the background rates. The background

rates in such a gas Čerenkov detector are studied using GEANT3 simulation. With a 15 μA beam, a 40 cm target and a threshold of 2 photoelectrons, the rates are about 40 MHz. With 30 trigger sectors and a 20 ns coincidence window, the actual online rejection ratio is expected to be about 40. Thus the electron single rates in forward-angle are

$$\begin{aligned} T_F^e(11\text{ GeV}) &= Y_F^e + \frac{Y_F^\gamma}{R_{GC}} + \frac{Y_F^h}{R_{GC}R_C} \\ &= 88.5 + \frac{623}{40} + \frac{6100}{40\cdot 10} = 119\text{ kHz} \\ T_F^e(8.8\text{ GeV}) &= 151 + \frac{596}{40} + \frac{5180}{40\cdot 10} = 179\text{ kHz}. \end{aligned} \quad (2)$$

In total, the electron singles trigger rates will be about 184 kHz and 234 kHz for 11 GeV and 8.8 GeV, respectively. In addition, as an option, the heavy gas Čerenkov and MRPC can be further added to the trigger to suppress the trigger rates from high energy photon and hadrons.

8.2 Charged particle singles trigger

The total energy deposition of the hadrons in the calorimeter is about 300 MeV and the energy resolution associated with it is about 11%. So applying a threshold of 200 MeV on the total energy will help to reject most of the low energy photons. The total rate of photons, including both soft photons and photons from π^o decay, passing this threshold is about 200 MHz for both beam energies.

The calorimeter signal of individual block will first locally match the MRPC detector right in front. The average background rate in MRPC is about 10 kHz/cm^2, and each set of MRPC covers about 500 cm^2 area. With a 10 ns coincidence window, the photon rejection factor is about 20.

To further reduce the photon contamination, a layer of 3 mm thin scintillator will be inserted in front of the heavy gas Čerenkov. By applying an appropriate threshold, the total counting rate in the whole scintillator layer can be controlled to be below 300 MHz, which leads 10 MHz in each sector. Now with a 15 ns coincidence window with the shower+MRPC signal, the photon events can be further suppressed by a factor of 6.5.

The total rates for the charged particle singles trigger are

$$\begin{aligned} T_F^h(11\text{ GeV}) &= Y_F^h + Y_F^e + \frac{Y_F^{\gamma all}}{R_{MRPC}R_S} \\ &= 6.1 + 0.1 + \frac{200}{20\cdot 6.5} = 7.7\text{ MHz} \\ T_F^e(8.8\text{ GeV}) &= 5.2 + 0.15 + \frac{200}{20\cdot 6.5} = 6.9\text{ MHz}. \end{aligned} \quad (3)$$

8.3 Coincidence trigger

The coincidence trigger is formed by electron trigger and charged particle trigger from different sectors to reduce the rate due to the strong correlation of the two triggers in one sector. 30 sectors can be grouped into 10 groups and form 90 coincidence combinations

to reduce the need of coincidence modules. With a 35 ns coincidence window, the final coincidence rates are:

$$\begin{aligned} T^c(11\text{ GeV}) &= T^{phy} + T^h_F \cdot T^e \cdot Window \\ &= 2.8\text{ kHz} + 0.9 \cdot 7.8\text{ MHz} \cdot 184\text{ kHz} \cdot 35\text{ ns} = 48\text{ kHz} \\ T^c(8.8\text{ GeV}) &= 1.6\text{ kHz} + 0.9 \cdot 6.9\text{ MHz} \cdot 234\text{ kHz} \cdot 35\text{ ns} = 53\text{ kHz}. \end{aligned} \quad (4)$$

8.4 Data rate and on-line farm filtering

The typical event size is about 4 kByte. Therefore the data rate of taking coincidence trigger only will be about 200 and 220 MB/sec for 11 and 8.8 GeV. By using the on-line farm, the events without tracks can be filtered out and the data rate can be further reduced by a factor of 5-10.

9 Kinematic Coverage

The updated kinematic coverages are shown in Fig. 23 (Fig. 24) for 11 (8.8) GeV. The polar angle for electrons θ_e and pions θ_h coverage is from 6.6° to 22° and 6.6° to 12°, respectively. The momentum coverage for electrons and pions are from 1.0 GeV/c to 7.0 GeV/c. To ensure DIS kinematics, we will add cuts for $Q^2 > 1$ (GeV/c)^2, W > 2.3 GeV and W' > 1.6 GeV (missing mass) to avoid the resonance region. The final kinematic coverage is $x = 0.05$-0.65, which covers most of the useful region of the d quark transversity distribution, $Q^2 = 1.0$-8.0 (GeV/c)^2. We choose to detect the leading pions with $0.3 < z < 0.7$ to favor the current fragmentation.

The resulting transverse momentum of the hadron, p_T coverage is between 0 and 1.6 GeV/c for 11 GeV incident beam and between 0 and 1.2 GeV/c for a 8.8 GeV beam. The kinematic coverages are plotted in Fig. 23 for a 11 GeV beam and Fig. 24 for 8.8 GeV beam. The kinematic binnings are organized as following: the entire coverage of Q^2 (1-8 $(GeV/c)^2$) is divided into 6 bins; the entire coverage of transverse momentum p_T (0-1.6 GeV/c) is divided into 8 bins; the entire z coverage (0.3-0.7) is divided into 8 bins. Then the entire x coverage (0.05-0.65) is divided into small bins according to the projected statistics within the bin. In the projection, we combine the 11 GeV and 8.8 GeV simulations results together. The total number of bins is about 1400. This will allow for a map of the Single target Spin Asymmetries in 4 dimension (x, Q^2, z and P_T).

The phase space coverage is obtained from a detailed Monte Carlo simulation based on GEANT3 which includes realistic spectrometer models as well as target and detector geometry. The coverage in the (Q^2, x), (W, x) ,(W', x), (p_T, x), (z, x) and (p_T, z) is shown in Fig. 23 for 11 GeV beam and Fig. 24 for 8.8 GeV beam. Due to the nature of the large acceptance solenoid detector, we will have a complete 2π coverage for the ϕ^l_S. The full 2π azimuthal angular coverage and the large ϕ_h azimuthal angular coverage are very important in disentangling different asymmetries (Collins, Sivers and Pretzelosity) to the precision that we propose, since there potentially could be contributions from other azimuthal angular dependent terms from higher-twist contributions ($\sin(\phi_S)$ and $\sin(2\phi_h -$

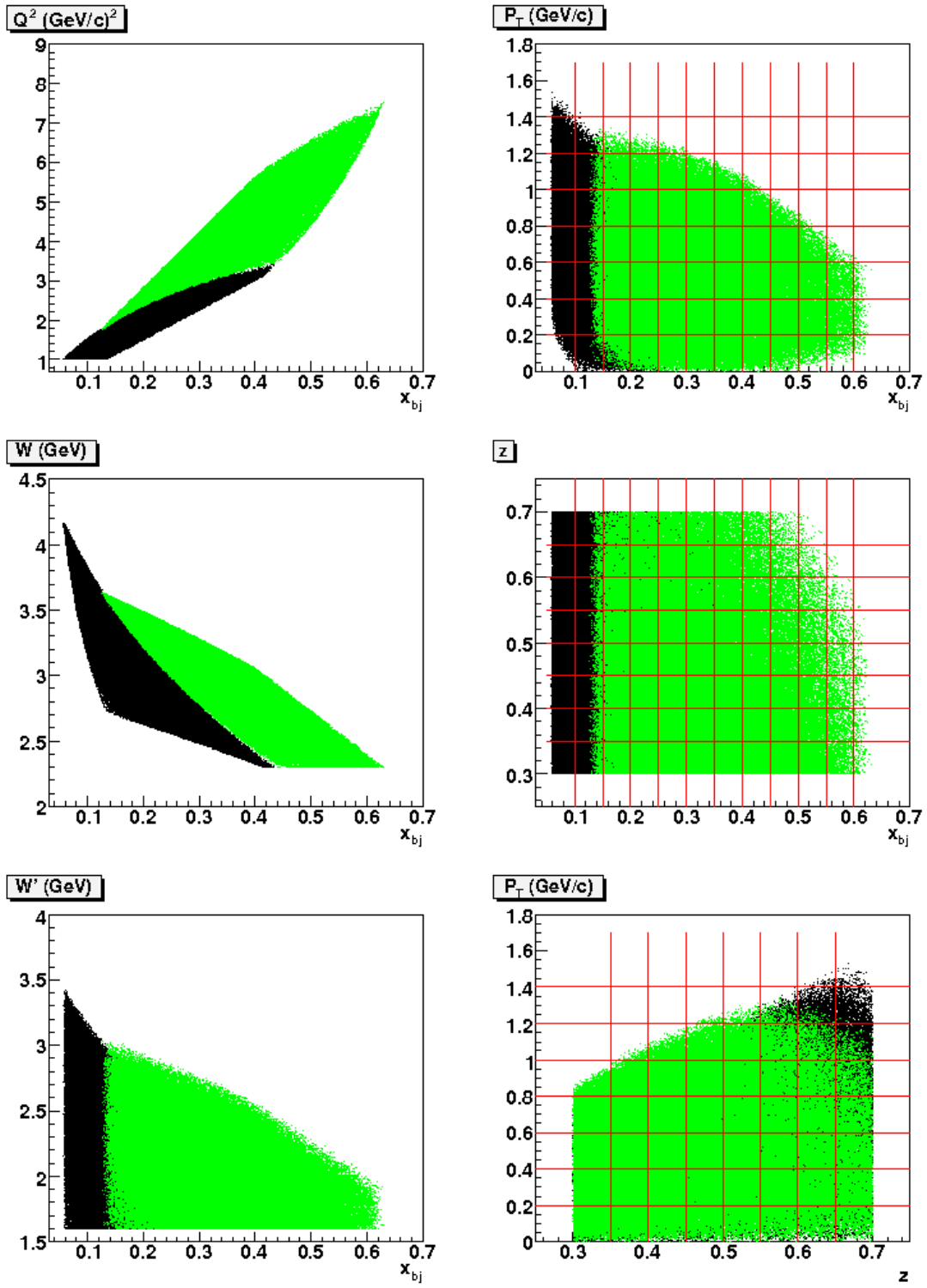

Figure 23: Kinematic coverage for the solenoid detector with a 11 GeV electron beam. The black points show the coverage for the forward-angle detectors and the green points show the coverage for the large-angle detectors.

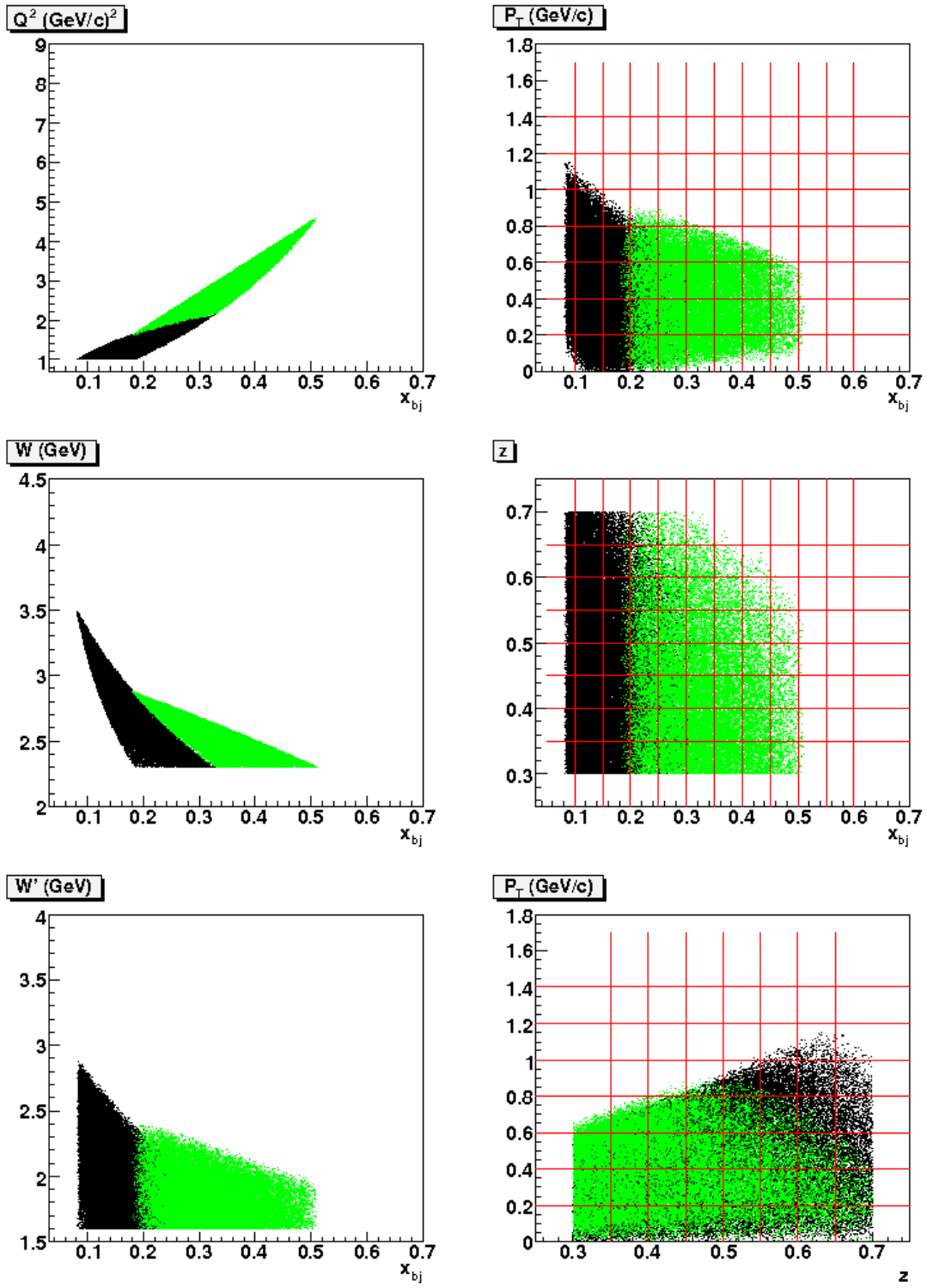

Figure 24: Kinematic coverage for the solenoid detector with a 8.8 GeV electron beam. The black points show the coverage for the forward-angle detectors and the green points show the coverage for the large-angle detectors.

ϕ_S)). In Sec. 17, we presented the p_T vs ϕ_h results for all our x, z and p_T [8]

10 Updated Rates Estimation

The updated event rates are listed in Table. 3 for the $(e, e'\pi^{\pm})$ reaction. We have assumed a beam current of 15 μA, a target length of 40 cm with 10 amgs of ^{3}He gas and a target polarization of 60% with a spin flip every 10 minutes. The collimator effect has been taken into account in the GEANT3 simulation of the acceptance. The overall detection efficiency is assumed to be 85% which includes the detection efficiency, computer dead time and electronic dead time. The updated single rates are also presented. The high energy photon (relevant to the electron triggers) rates are estimated by the π^o rates, where the π^o production cross section is assumed to be twice of the sum of π^+ and π^- at high energy. We compared the rates estimation from Whitlow [46]/QFS [47] and Wiser [48] with data from E06-010 using a simple calculation for HRS and a GEANT3 based model for the BigBite spectrometer. Corrections are added to match the data. Details can be found in Sec. 15. Despite the DIS electrons estimated from whitlow, the rate of "photon"-induced electrons, including electrons from π^o decay, and electrons generated by photons when they pass through materials, is estimated and included in the singles electron rate. The low energy photon (energy larger than 200 MeV, relevant to the hadron trigger in forward-angle detectors) rates are estimated from two sources. The soft photon rates, which dominate the total photon rates, are simulated by GEANT including all forward scattering processes. The hard photon rates are estimated by simulating the π^o decay through GEANT Monte-Carlo.

The total coincidence rate and singles rate can be found in Table. 3. The low momentum cut-off for the forward detection is about 0.9 GeV/c which is from the natural momentum cut-off of the magnetic field (See Sec. 18). The low momentum cut-off for the large-angle detection is 3.5 GeV/c, which is from the trigger threshold. In the single rates estimation, we did not apply the 85% detection efficiency. The average signal to background ratio is above 150 for π^+ and π^- assuming a 2.0 ns coincidence timing window and a factor of 4 (in average) from vertex position cut. The smallest signal to background ratio is at high P_T where the signal to noise ratio is about 5 (10) for 11 (8.8) GeV beam. The statistical uncertainties of the physics asymmetries from ^{3}He are translated into statistical uncertainties on neutron asymmetries $A_{UT}^{\pi^+}(n)$ and are also listed in Ref. [49] together with the corresponding dilution factors. An effective neutron polarization of 86% in ^{3}He ground state has been taken into account.

[8] Instead of binning in Q^2, we divided the x coverage into eight kinematic bins. In the projected results, we include the effects of incomplete coverage in ϕ_h for all 1400 kinematic bins, based on simulated ϕ_h distribution within each kinematics bin.

Process	Rate Forward angle 11 GeV	Rate Large angle 11 GeV	Rate Forward angle 8.8 GeV	Rate Large angle 8.8 GeV
(e,eπ^+)	1467 Hz	192 Hz	810 Hz	117 Hz
(e,eπ^-)	1010 Hz	120 Hz	554 Hz	73 Hz
single e^-	88.5 kHz	11.0 kHz	151 kHz	16.5 kHz
high energy photon	623 kHz	51.5 kHz	596 kHz	37 kHz
single π^+	2.90 MHz	20.2 kHz	2.5 MHz	13.4 kHz
single π^-	1.77 MHz	14.5 kHz	1.47 MHz	9.2 kHz
single K^+	226 kHz	5.9 kHz	185 kHz	4.1 kHz
single K^-	54.6 kHz	1.2 kHz	39.9 kHz	0.6 kHz
single proton	1.15 MHz	13.8 kHz	0.99 MHz	9.4 kHz
low energy photon	200 MHz	-	200 MHz	-

Table 3: Total coincidence rate and single rates for both positive/negative charged particles and low/high energy photons with 11 and 8.8 GeV beam. The high energy photon cutoffs are 0.9 (3.5) GeV at forward (large) angle. The low energy photon cutoff is 200 MeV.

11 Requested Time and Projections

11.1 Beam time request

The beam time request is listed in Table 4. We request 90 days of total beam time with 15 μA, 11/8.8 GeV electron beams on a 40-cm long, 10 amgs transversely polarized ^{3}He target. 69 days is for beam on the polarized ^{3}He target. A total overhead time of 8 days is requested. This overhead time will be shared among activities such as unpolarized target runs, target spin flip and target polarization measurements, as has been done in the past during other Hall A polarized ^{3}He target experiments. Major target related down times can also be arranged to coincide with the scheduled accelerator maintenance activities in order to reduce overhead time. In addition, we request 10 days for dedicated study of the naive $x - z$ factorization with Hydrogen and Deuterium gas using our reference cell. We also request 3.0 days with longitudinal polarization to study the systematics of A_{UL} contamination. Although beam polarization is not required for the proposed SSA measurements, we request a polarized beam for a parasitic measurement of the A_{LT} which can be used to access another leading twist distribution, g_{1T}.

12 Projected Results

The projections combine both 11 GeV data and 8.8 GeV data. The projected results for π^+ Collins and Pretzelosity (Sivers) asymmetries at one typical kinematics bin, $0.45 > z > 0.4$, $3 > Q^2 > 2$, are shown in Fig. 25 (Fig. 26) together with theoretical predictions of Collins asymmetries from Anselmino *et al.* [38], Vogelsang and Yuan [36] and predictions

Table 4: Beam time request.

	Time (Hour)	Time (Day)
Production on Pol. ^{3}He at 11 GeV	**1152**	48
Production on Pol. ^{3}He at 8.8 GeV	**504**	21
Longitudinal on Pol. ^{3}He at 11 GeV	38	2
Longitudinal on Pol. ^{3}He at 8.8 GeV	24	1.
Dedicated Hydrogen run at 11 GeV	84	3.5
Dedicated Deuterium run at 11 GeV	84	3.5
Dedicated Hydrogen run at 8.8 GeV	36	1.5
Dedicated Deuterium run at 8.8 GeV	36	1.5
Reference cell runs, optics and detector check	72	3.
Target Overhead: spin rotation, polarization measurement	120	5.
Total Time Request	**2160**	**90 days**

Table 5: Details of the beam time request.

of Collins/Pretzeloity asymmetries from Pasquini [50]. The projected E06-010 results are shown in back points. The x-axis is x_{bj}. The y-axis on the left side is P_T which is the transverse momentum. The y-axis on the right side shows the scale of the asymmetry. The y-position of the projections shows the average P_T value for the corresponding kinematic bin. The statistical uncertainties follow the scale on the right side y-axis. The scale of the theoretical calculations follow the right side y-axis. The Sivers asymmetries for π^+ (π^-) at one typical kinematics bin, $0.45 > z > 0.4$, $3 > Q^2 > 2$, are shown in Fig. 27 (Fig. 28).

The complete projections for π^+ (π^-) Collins/Pretzelosity asymmetries are shown in terms of 4-D (x, z, P_T and Q^2) kinematic bin in Fig. 29 (Fig. 30). Theoretical predictions of Collins asymmetries from Anselmino *et al.* [38], and predictions of Collins/Pretzeloity asymmetries from Pasquini [50] are shown in the first panel only. The Q^2 and z values for these calculations are the average value of the entire kinematics. Theoretical predictions of Collins asymmetries from Vogelsang and Yuan [36] are shown in panels in the first row. The Q^2 value for the calculations is the average value of the entire kinematics. The x-dependence of asymmetries in different z bins is shown in different panels. The complete projections for π^+ (π^-) Sivers asymmetries are shown in terms of 4-D (x, z, P_T and Q^2) kinematic bin in Fig. 31 (Fig. 32). Theoretical predictions of Sivers asymmetries from Anselmino *et al.* [38] and Vogelsang and Yuan [36] are shown in comparison [9]. We also include the current E06-010 projections in the first panel.

For the $x - z$ factorization test with unpolarized hydrogen and deuterium target. We will integrate the entire P_T bin for each x and z bin. The expected precision for $D'(z)$, r_h, r_1 and r_2 is plotted in Fig. 33 together with calculations based on the CTEQ [51] and

[9]The projections on Sivers asymmetry are shown separately from the projections of Collins and Pretzelosity asymmetries, since the projection statistical uncertainties are different due to ϕ_h coverage.

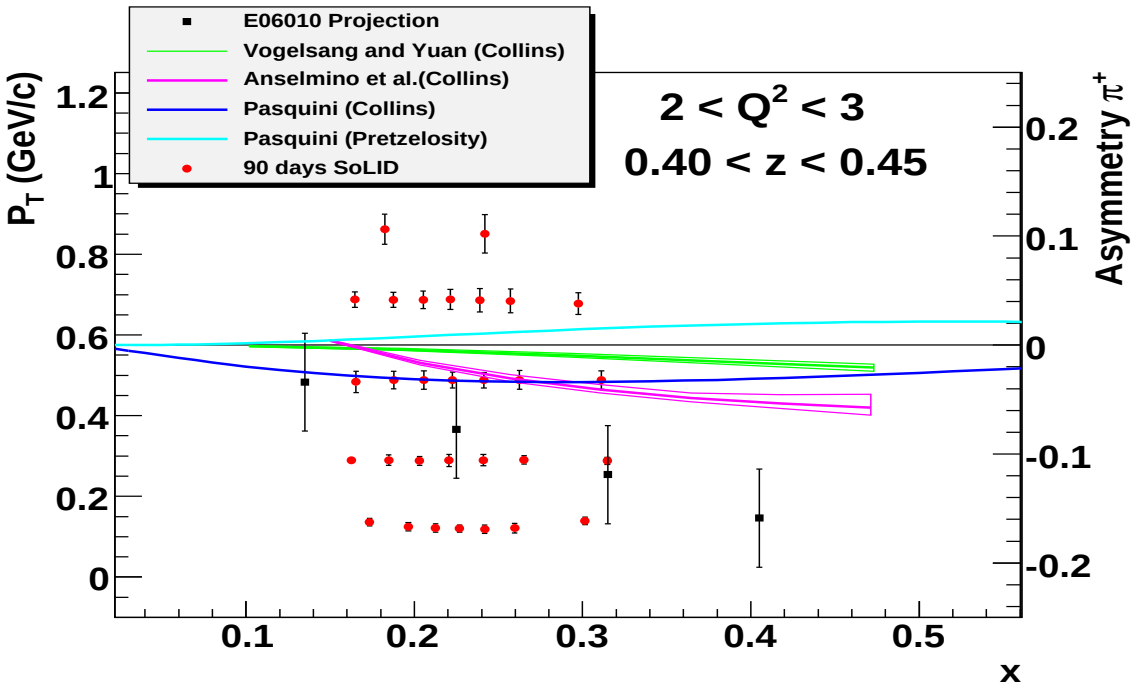

Figure 25: 12 GeV Projections with SoLID. π^+ Collins/Pretzelosity asymmetries at 0.3 $> z >$ 0.35, 2 $> Q^2 >$ 1.

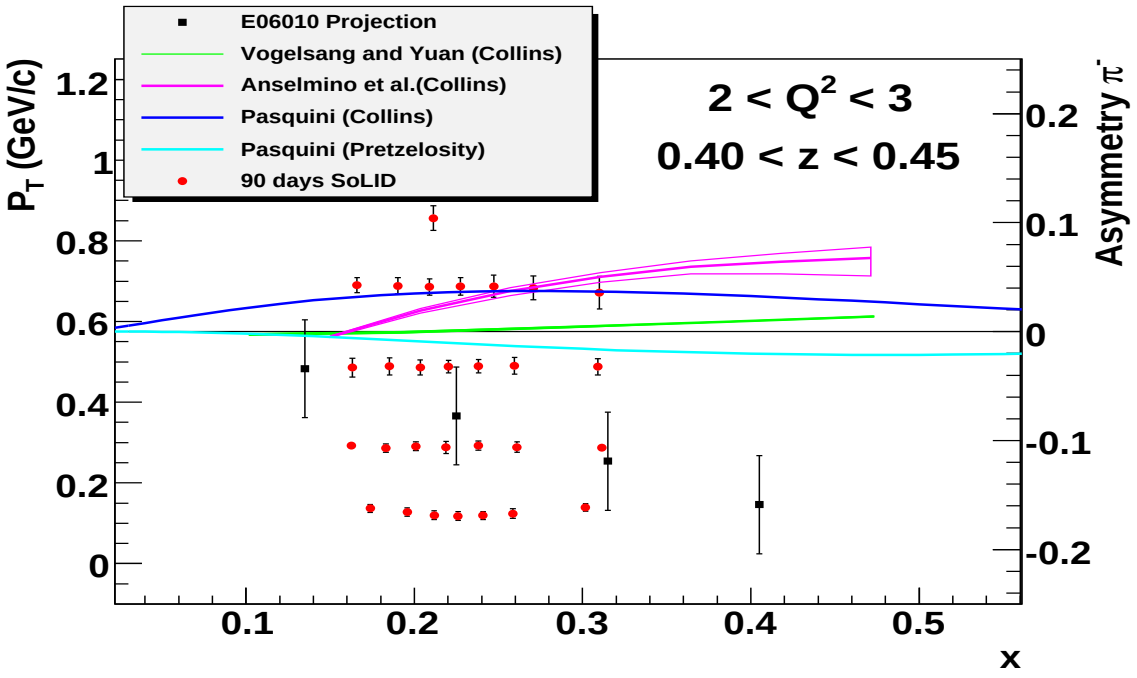

Figure 26: 12 GeV Projections with SoLID. π^- Collins/Pretzelosity asymmetries at 0.3 $> z >$ 0.35, 2 $> Q^2 >$ 1.

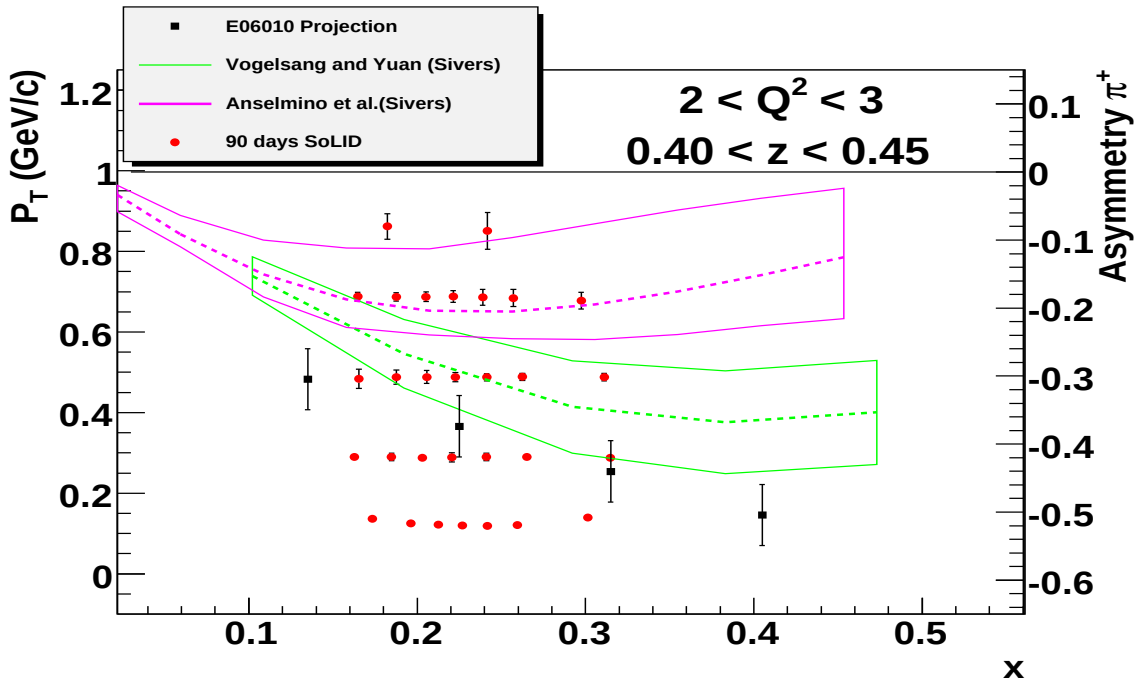

Figure 27: 12 GeV Projections with SoLID. π^+ Sivers asymmetries at $0.3 > z > 0.35$, $2 > Q^2 > 1$.

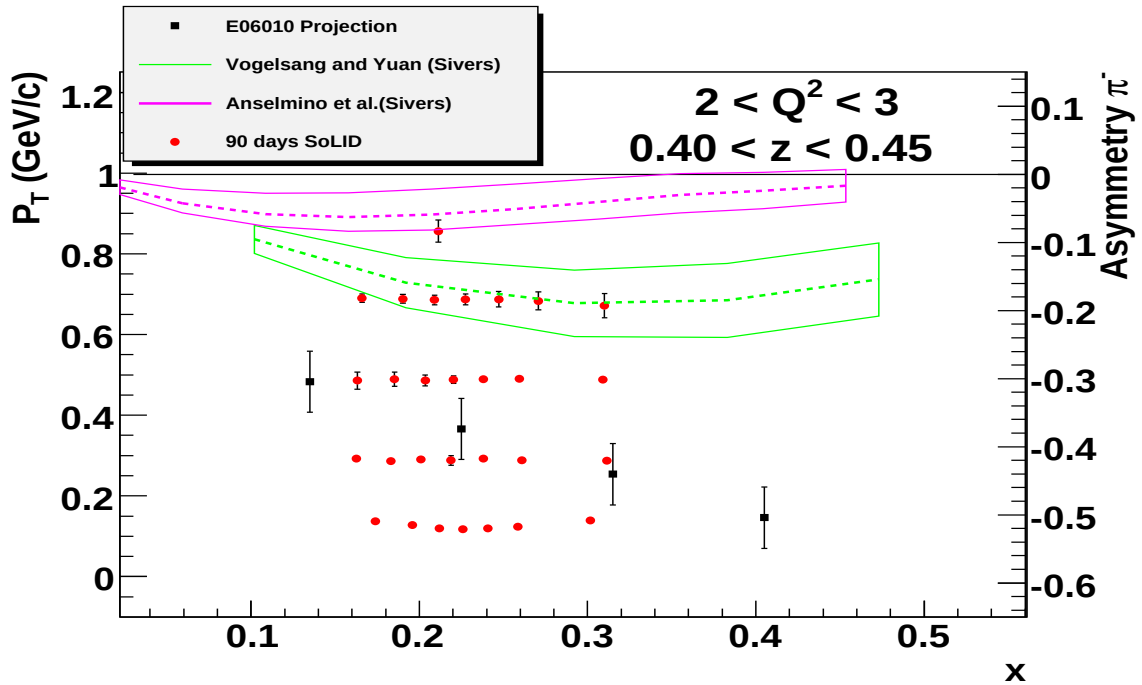

Figure 28: 12 GeV Projections with SoLID. π^- Sivers asymmetries at $0.3 > z > 0.35$, $2 > Q^2 > 1$.

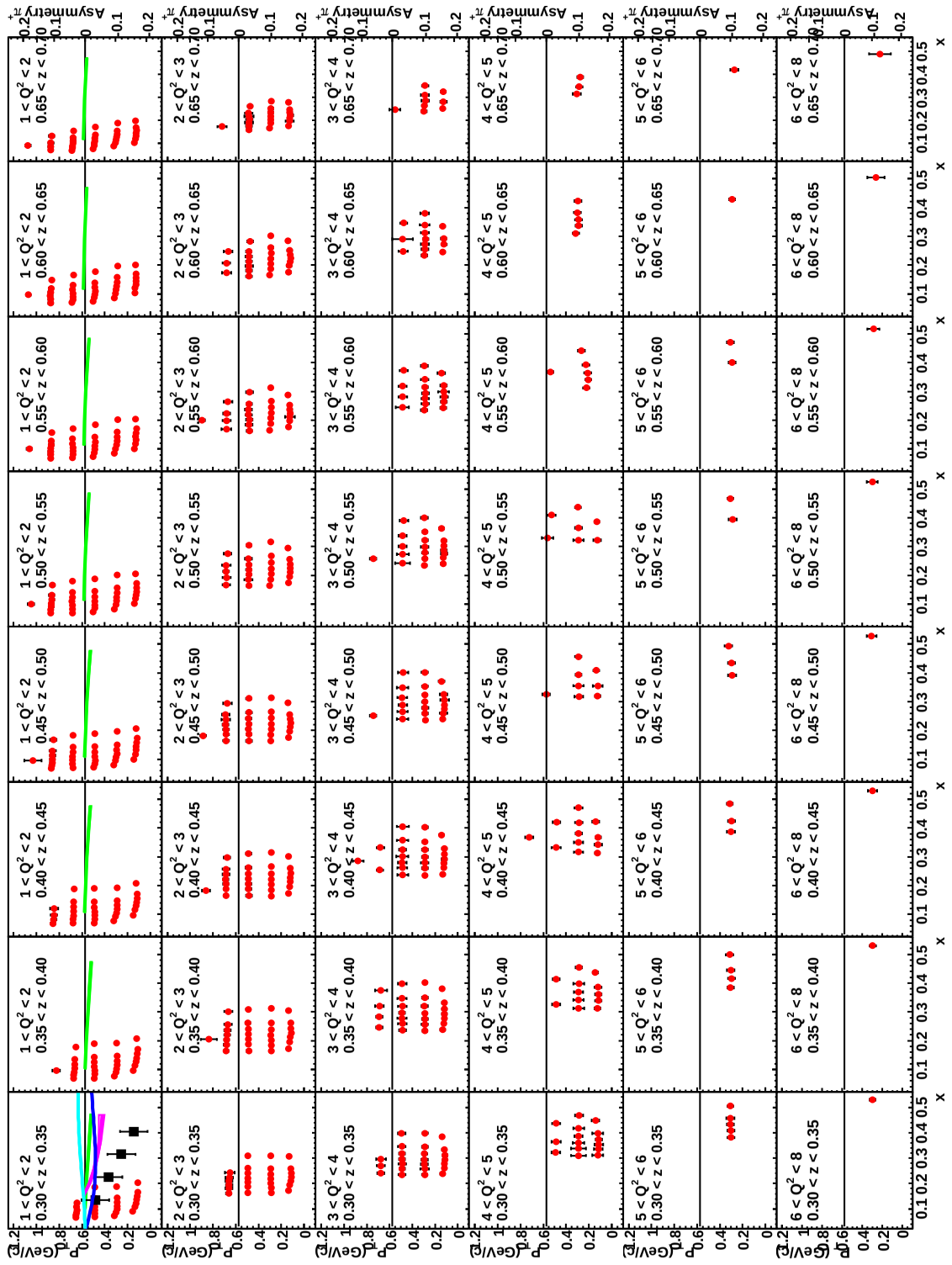

Figure 29: 12 GeV Projections with SoLID. π^+ Collins/Pretzelosity asymmetries for all kinematic bin in terms of different z and Q^2 bin.

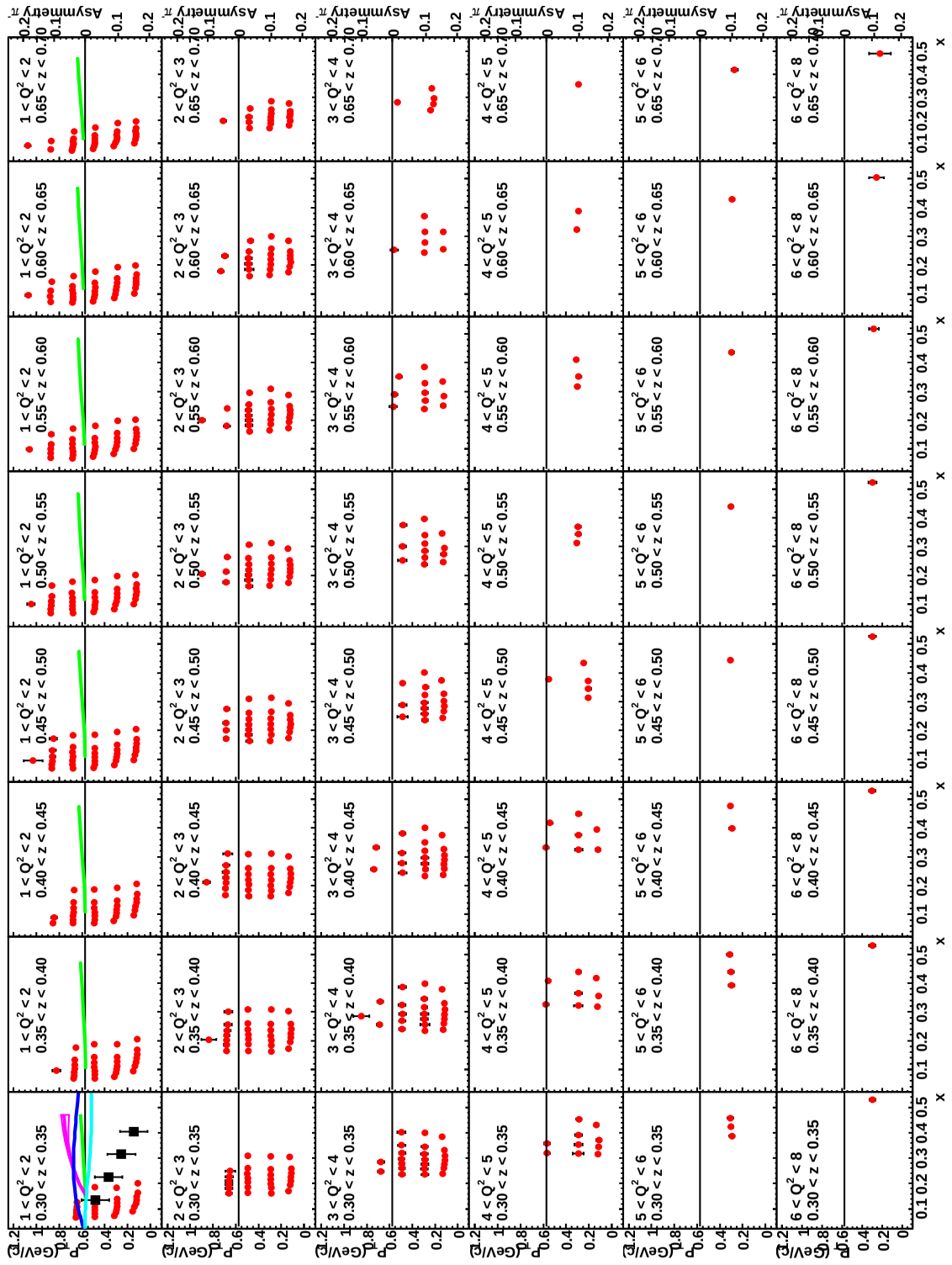

Figure 30: 12 GeV Projections with SoLID. π^- Collins/Pretzelosity asymmetries for all kinematic bin in terms of different z and Q^2 bin.

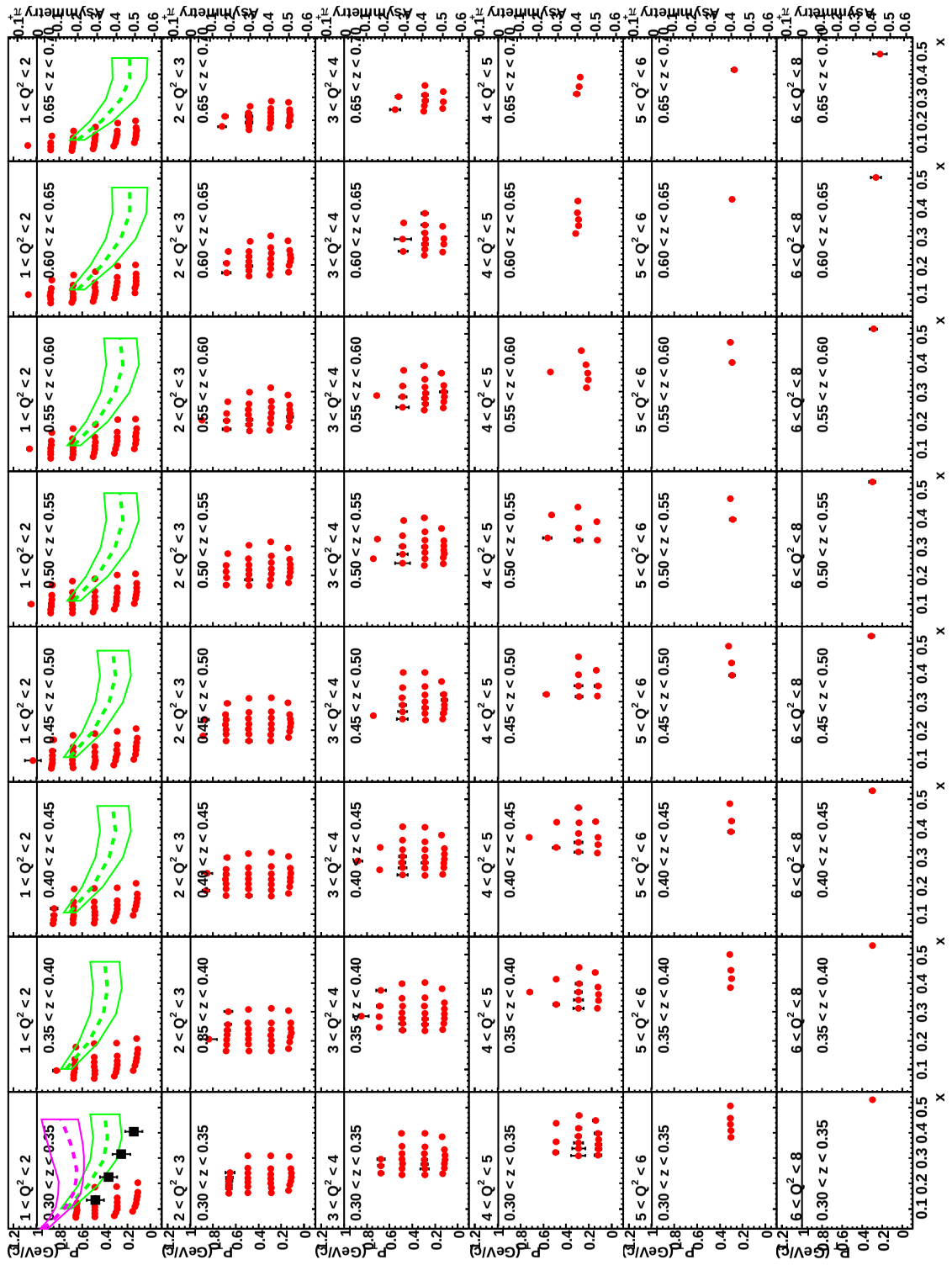

Figure 31: 12 GeV Projections with SoLID. π^+ Sivers asymmetries for all kinematic bin in terms of different z and Q^2 bin.

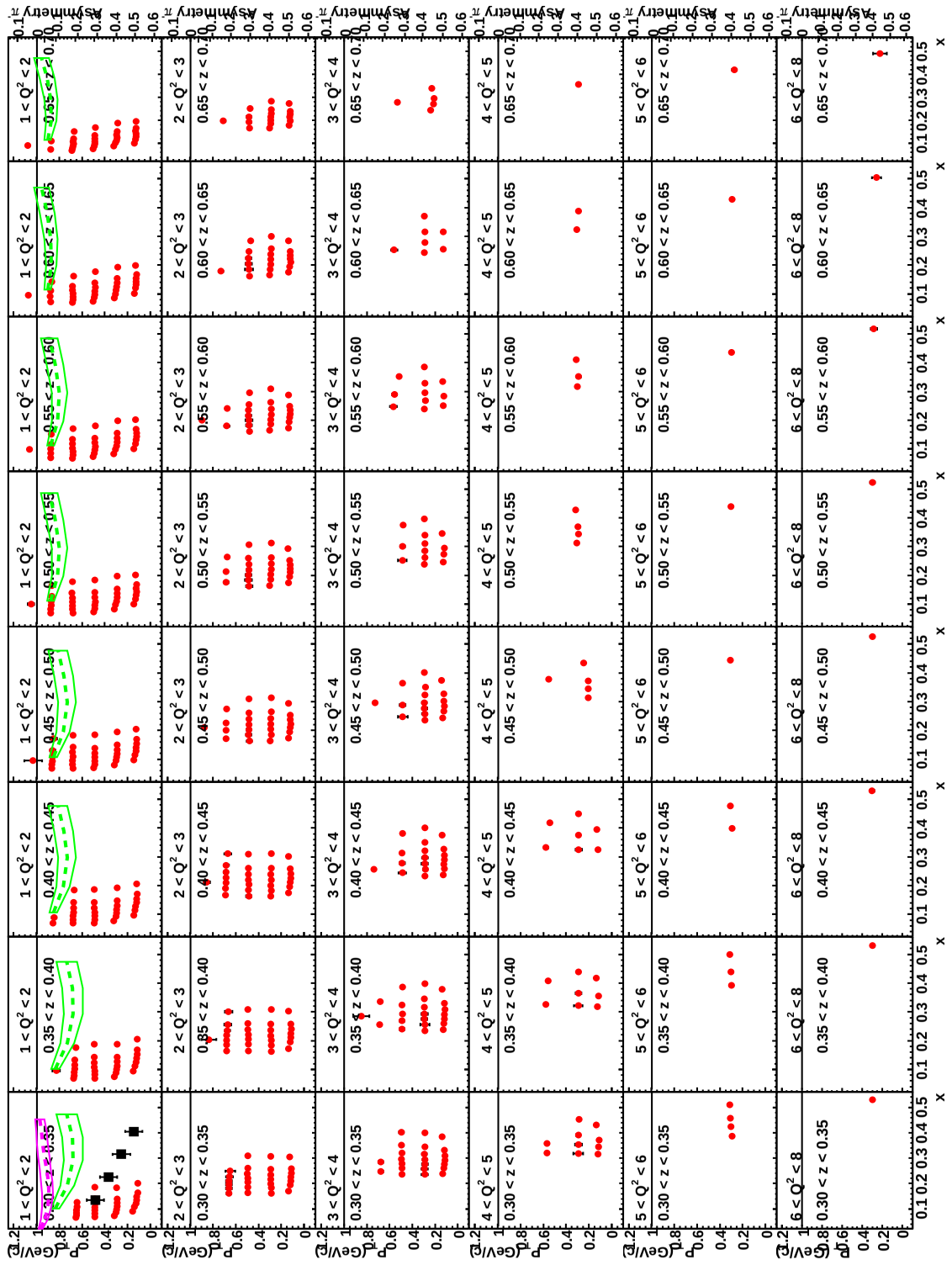

Figure 32: 12 GeV Projections with SoLID. π^- Sivers asymmetries for all kinematic bin in terms of different z and Q^2 bin.

the BKK parametrization [52] for fragmentation function. We requested 3.5 (1.5) days of data taking on hydrogen and 3.5 (1.5) days running on deuterium at 11 (8.8) GeV. The data can also be binned in P_T to test the naive $x - z$ factorization.

12.1 Impacts

From the projections, we can see that the results from the proposed experiment will have great impact on the current theoretical understanding of the transverse spin physics. Firstly, we will extend the study of the SIDIS to a real 4-D manner (x, Q^2, z and P_T). Secondly, we will extend the measurement of the transversity distribution to the large x region which is essential in extracting the tensor charge. Thirdly, the Sivers distribution and Pretzelosity distribution functions, which are crucial to understand the relativistic effect and the role of quark orbital angular momentum, will be mapped precisely in 4-D. Fourthly, we will cover a large P_T region which is important in testing various theoretical ideas. Finally, we will cover a relatively large Q^2 region which can study higher-twist contributions [10].

Probing TMDs, in particular transversity distribution, the least known leading-twist quark distribution function, which is non-zero upon integrating over the quark transverse momentum, is among the goals of several ongoing and future experiments. The experimental study of TMDs, which is now only at its inception, promises to have a very exciting future. Understanding the TMDs for different quark flavor is certainly a complex task which demands major efforts in different laboratories in studying many different processes ranging over a wide kinematic region.

This is a fast evolving field with growing interest worldwide. It is important for JLab to be a major player in this important frontier. Measuring the transversity distribution and probing the TMDs through SIDIS at Jefferson Lab has attracted a lot of attentions by many theorists and experimentalists [53] (a recent review of the workshop on transverse spin at Jefferson Lab; this served as an input to the Nuclear Physics Long Range Plan on QCD and Hadron Physics). It will have impact on other related programs and particularly on the design of future facilities with TMDs study as one of their important physics goals, for example the EIC, the FAIR project at GSI, and J-PARC. The proposed 11 GeV experiment will also help to move theory forward in understanding and in modeling the quark TMDs significantly.

12.2 A combined analysis

A combined analysis between our neutron results and the future proton results, will be carried out to extract the tensor charge of the u and d quark. The high statistics data from both the proton and the neutron will lead to a unprecedented precise determination of tensor charge in a model-independent way. Such a precision will provide important tests of Lattice QCD predictions for the tensor charge.

[10] Higher twist effects can also be observed with contributions with $\sin(\phi_S)$ and $\sin(2\phi_h - \phi_S)$ angular modulation.

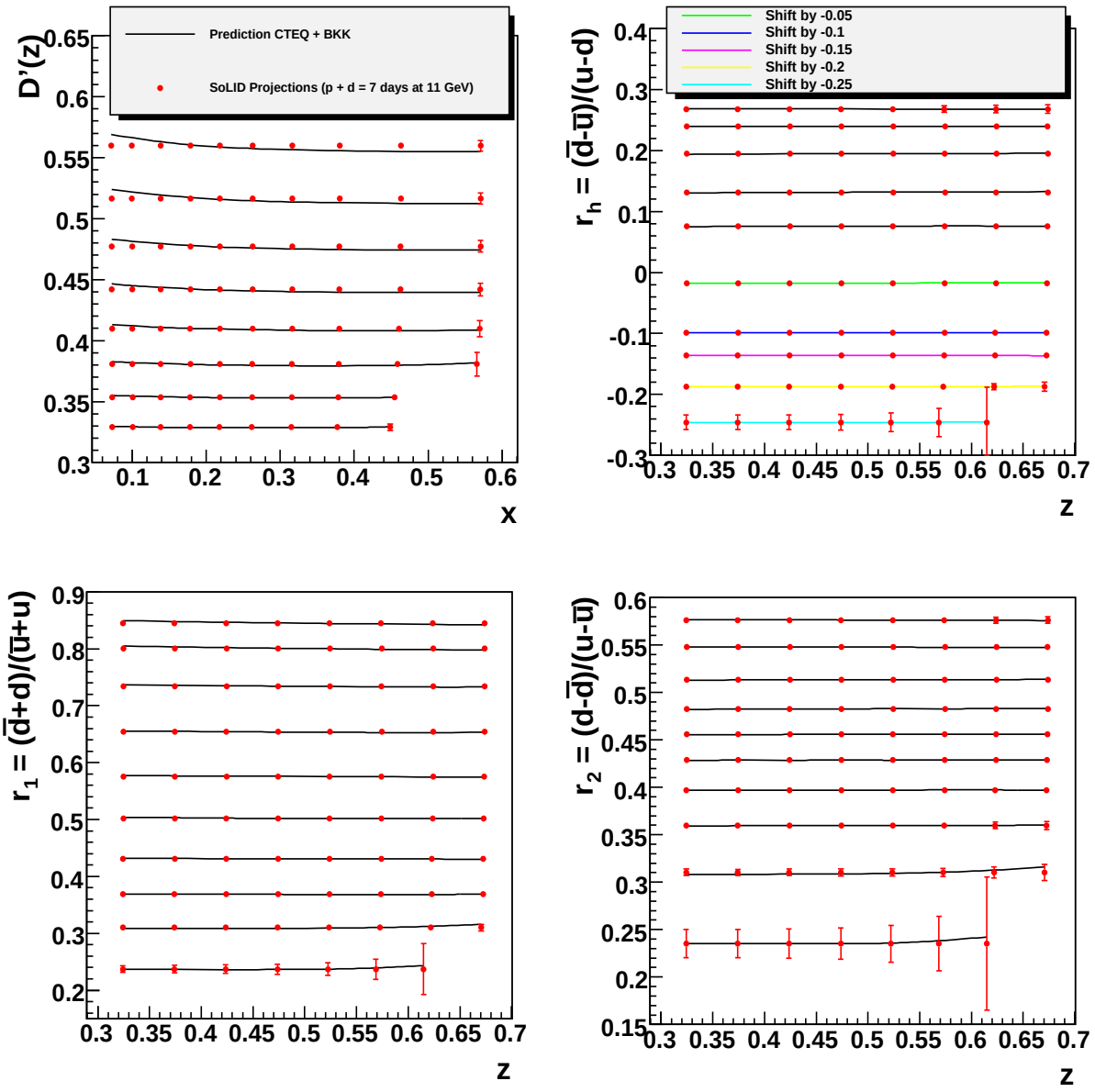

Figure 33: The top left shows $D'(z)$ for different z bins vs x. The different lines are corresponding to different z bins. The other three plots show $r_h(x)$, $r_1(x)$ and $r_2(x)$ for different x bin vs z. Different lines are corresponding to different x bins. Some lines are shifted for clarity. These projections correspond to a total 7 days of data taking time on the proton and the deuteron target at 11 GeV.

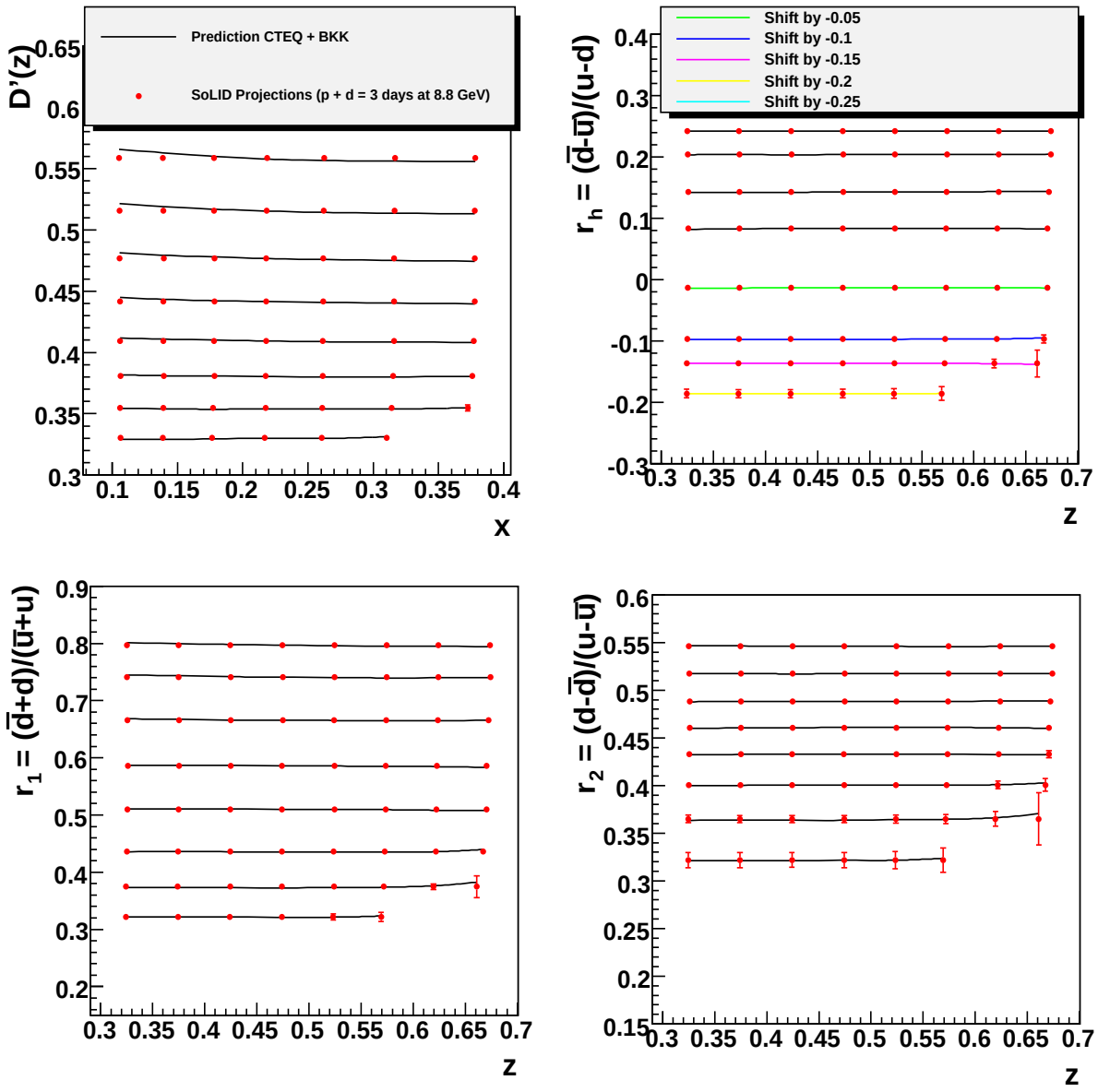

Figure 34: The top left shows $D'(z)$ for different z bins vs x. The different lines are corresponding to different z bins. The other three plots show $r_h(x)$, $r_1(x)$ and $r_2(x)$ for different x bin vs z. Different lines are corresponding to different x bins. Some lines are shifted for clarity. These projections correspond to a total 3 days of data taking time on the proton and the deuteron target at 8.8 GeV.

12.3 By-products

Azimuthal asymmetry in the unpolarized cross section will be obtained together with the the polarized ^{3}He data. In addition, the data from the $x - z$ factorization test on hydrogen and deuterium will also be used to understand the azimuthal asymmetry in the unpolarized cross section for both the proton and the neutron, which is one source of the systematic uncertainty for the SSAs.

Double-spin asymmetries g_{1T}^n will be obtained as a by-product. In our proposed measurement on SSAs, we do not need a polarized beam. However, the polarized beam will be used to extract the double-spin (beam longitudinally polarized, target transversely polarized) azimuthal asymmetry which can be used to study another TMD, g_{1T}^n.

Inclusive double-spin asymmetries will allow for the extraction of the g_2 on the neutron.

Inclusive electron Single Spin asymmetries will probe A_y which is sensitive to two-photon effects.

13 Systematic uncertainties

To achieve the proposed precision, it is very important to control the systematic uncertainties. The full 2π azimuthal angular coverage plays an important role in reducing the experimental systematic uncertainties. The large signal-to-noise ratio will also help to reduce the systematic uncertainties in subtracting backgrounds.

13.1 The experimental observable

In E06-010 experiment, the target single spin asymmetry$A_{UT}^h(\phi_h, \phi_S)$ was obtained directly from the luminosity-normalized yield:

$$A_{UT}^h(\phi_h, \phi_S) = \frac{1}{(p_T)} \cdot \frac{N_1(\phi_h, \phi_S) - N_2(\phi_h, \phi_S + \pi)}{N_1(\phi_h, \phi_S) + N_2(\phi_h, \phi_S + \pi)} \tag{5}$$

The relative luminosity was monitored by various spectrometer singles rates and the downstream luminosity monitors. In addition, frequent target spin flips, every 20 minutes, were required, since the N_1 and N_2 were obtained at different time periods with the target spin direction flipped. This is one of the major limitations in the systematic uncertainties, because the target flip can not be performed at a higher rate, without a large loss in the polarization [11].

For the large acceptance solenoid detector, thanks to the full 2π azimuthal coverage, we have unique advantage in reducing the systematic uncertainties associated with detection efficiencies and luminosity. Our experimental target single spin asymmetry is defined as:

$$A_{UT}^h(\phi_h, \phi_S) = \frac{2}{P_T^1 + P_T^2} \cdot \frac{\sqrt{N_1(\phi_h, \phi_S) N_2(\phi_h, \phi_S + \pi)} - \sqrt{N_1(\phi_h, \phi_S + \pi) N_2(\phi_h, \phi_S)}}{\sqrt{N_1(\phi_h, \phi_S) N_2(\phi_h, \phi_S + \pi)} + \sqrt{N_1(\phi_h, \phi_S + \pi) N_2(\phi_h, \phi_S)}} \tag{6}$$

[11] Recent studies shows that this time can be reduced to 10 mins with rotation of field. In this proposal, we assume the average time is 10 mins between two spin flips.

Here the $N_1(\phi_H, \phi_S)$ and $N_1(\phi_H, \phi_S + \pi)$ [12] are taken at the same time while the target polarization is P_T^1. And the $N_2(\phi_H, \phi_S)$ and $N_2(\phi_H, \phi_S + \pi)$ are taken at the same time while the target polarization is P_T^2, when the target spin is flipped 180°. Thus, the luminosity at different times will be canceled in the above equation. Furthermore, to first order, the acceptance, detector efficiency will also cancel, since $N_1(\phi_h, \phi_S)$ and $N_2(\phi_h, \phi_S+\pi)$, $N_1(\phi_h, \phi_S+\pi)$ and $N_2(\phi_h, \phi_S)$ are taken in the same region of the detectors.

The raw asymmetry is not sensitive to the target polarization difference between the two time periods either. This is important to achieve the desired precision in this proposal. The same trick can not be applied to E06-010, since the $N_1(\phi_H, \phi_S)$ and $N_1(\phi_H, \phi_S + \pi)$ can not be taken at the same time due to the incomplete azimuthal angular coverage.

13.2 Raw Asymmetry

From Eqn. 6, we can see all the systematic uncertainties in luminosity (each term shares the same luminosity), acceptance (each term shares the same acceptance), polarization, detector efficiency (the time-independent part) will cancel to first order, by taking advantage of the full 2π azimuthal angular coverage. At the second order, there are only three kinds of systematic uncertainties:

1. The first one is the systematic uncertainty corresponding to the time-dependent part of the detector efficiencies. Singles data will be used to monitor the time-dependent detector efficiencies. We expect to control the systematic uncertainties of detection efficiencies (time dependent part) to less than 1% in each pair by monitoring the singles electron/pion rates. With a 10-min, which is target spin flip rate, in 48 days at 11 GeV, we will have 3456 pairs of spin flip (20 mins for each pair). Then the systematic uncertainty for the raw asymmetry is about $1.0\%/\sqrt{3456}$ about 1.7E-4. In the separated physics asymmetry, the 1.7E-4 will be transformed to be less than 1E-3 in the separated physics asymmetry, much smaller than the average statistical uncertainty, 3.7E-3.

2. The second one is the systematic uncertainty corresponding to the knowledge of the target polarization. The knowledge on the target polarization is at 3% level, which will give a 3% relative uncertainty. The second order effect of the target polarization in the raw asymmetry is suppressed by P^2A^3, which is P^2A^2 for the relative uncertainty. Assuming an average of 10% physics asymmetry, the second order effect of the target polarization is less than 0.5% (relative).

3. The third one is the systematic uncertainty corresponding to the knowledge of the target polarization direction. The knowledge about this direction is about 0.2°. The effect on each asymmetry can be estimated as $1 - \cos(\Delta\theta) \approx \frac{\Delta\theta^2}{2} \approx 1e-5$. (relative) The knowledge of the electron scattering azimuthal angle is also about 0.2°. The largest effect is on the pretzelosity asymmetry which is about $1 - \cos(2\Delta\theta) \approx \frac{4\Delta\theta^2}{2} \approx 4e-5$. (relative) The combined effect of these two angles will not bigger than $1e-4$ (relative). In addition, the effect of the asymmetry mixing due to the inaccuracy of the two angles is negligible due to the integration over them (ϕ_h and ϕ_S).

[12] Here, $N_1(\phi_H, \phi_S + \pi)$ is obtained by maintaining the target spin direction. In the lab frame, the SoLID has full azimuthal coverage and symmetry. Thus target spin flip is equivalent to a rotation of both electron and pion azimuthal angles by 180 degrees. Thus $N_1(\phi_H, \phi_S + \pi)$ is taken at different region of SoLID.

13.3 Subtraction of the Random Coincidence Events

The average signal to noise ratio at our kinematics is above 50 for π^+ and π^- assuming a 6.0 ns coincidence timing window and a factor of 4 [13] from vertex position cut. The random coincidence events play a role as dilution. Assuming a 20% systematic uncertainty in the background subtraction procedure, we have on average less than a 0.5% relative systematic uncertainty from the background subtraction. At high P_T, the signal to noise ratio becomes smaller, since the SIDIS cross section roughly follows a $e^{-aP_T^2}$ distribution. In the worst scenario, the signal-to-noise ratio is about 5.

13.4 Azimuthal Angular Asymmetry in A_{UL}

In the lab frame, when the ^3He is transversely polarized with respect to the beam direction. However, in the definition of A_{UT}, the S_T is defined as the transverse polarization with respect to the virtual photon direction, which has a small angle with the z-axis. Therefore, there will be a small S_L component. When the target spin is flipped, The S_L will also flip. Thus there will be a false asymmetry from the S_L contamination. In Fig. 35, we show the size of this S_L with the SoLID configuration.

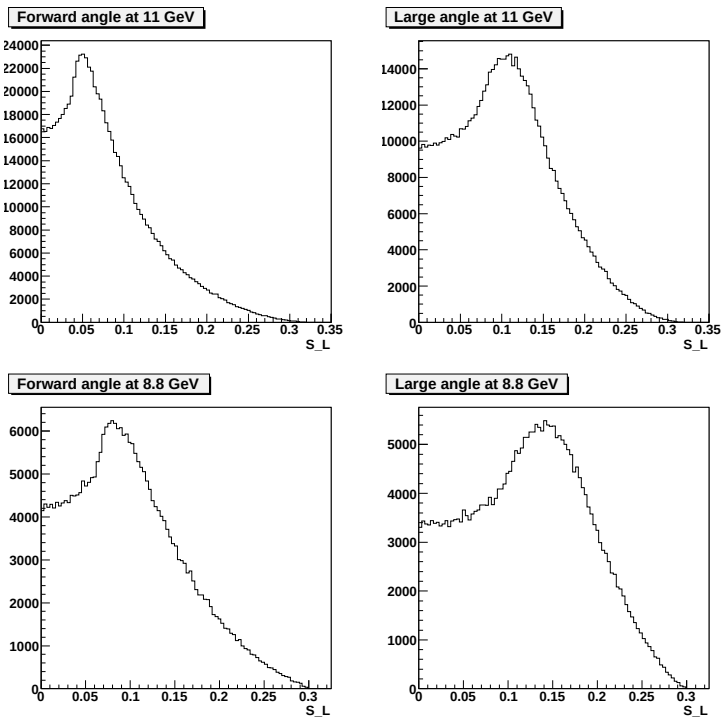

Figure 35: The S_L component for different configuration and different beam energy.

One way to correct for the contribution from this term is to include it in the fitting procedure. This would reduce the sensitivities to normal terms in A_{UT} when the azimuthal angle is incomplete. A more general way is to measure it directly with the longitudinally

[13] The average vertex resolution $\sigma = 1.5$ cm. Thus, $6\sigma = 9$ cm ≈ 40 / 4 cm.

polarized ^3He target. Since the statistics in the asymmetry goes with $1/\sqrt{N}$, but linearly in target polarization. Thus the required statistical precision with longitudinal data is suppressed by $1./S_L^2$. We plan to take 2 (1) days data at 11 (8.8) GeV with longitudinally polarized ^3He.

13.5 Higher Twist effect

The higher twist effects will be examined with the unpolarized Hydrogen and Deuterium data from the $x - z$ factorization test. In addition, one important feature for the single-target spin asymmetry is that some of the higher twist terms have different azimuthal angular dependence. In this case, a direct fitting of the data with more azimuthal angular dependent terms provide a direct measure of the higher-twist contribution. We discuss the effect of including the additional sub-leading twist terms in the fitting procedure in Sec 16.4.

13.6 Target fragmentation and vector meson production

In the high-z settings of this experiment ($0.3 < z < 0.7$), the target fragmentation contamination is expected to be small, as has been shown by the HERMES LUND [54] based Monte Carlo simulation.

The contributions of the π from the vector meson, especially ρ meson decay, can usually be divided into two categories. The first category is the ρ meson production in the Deep-Inelastic Scattering (DIS) kinematics. In principle, this contribution is included in the standard π fragmentation function. The second category is the diffractive ρ production. At high energies, the contribution of the diffractive ρ production can be as large as 10-14% of the inclusive scattering. At our kinematics, the contribution of the pions from the decay of the diffractive ρ production is estimated based HERMES tuned Pythia [55]. The average contamination from the diffractive ρ production on neutron is about 7% and 8% for π^+ and π^-, respectively. The kinematic dependence of the contamination from the diffractive ρ production is plotted in Fig. 36. Currently, there is no measurement of the single target spin asymmetries from the diffractive ρ production. Theoretical predictions [56] show that the SSA in diffractive ρ production is at a couple of percentage level, and it follows the same azimuthal angular distribution as that of the Sivers asymmetry.

The SoLID can be used to detect ρ meson directly through detecting two pions from its decay at the forward-angle in coincidence with the electron. The acceptance for the ρ meson production is about 3.3 msr for the ρ meson produced between 3.0 and 6.0 GeV/c. The acceptance with a uniformly distributed ρ meson in momentum and solid angle is shown in Fig. 37.

13.7 Systematic Uncertainty Budget

The systematic uncertainties are summarized in Table. 6.

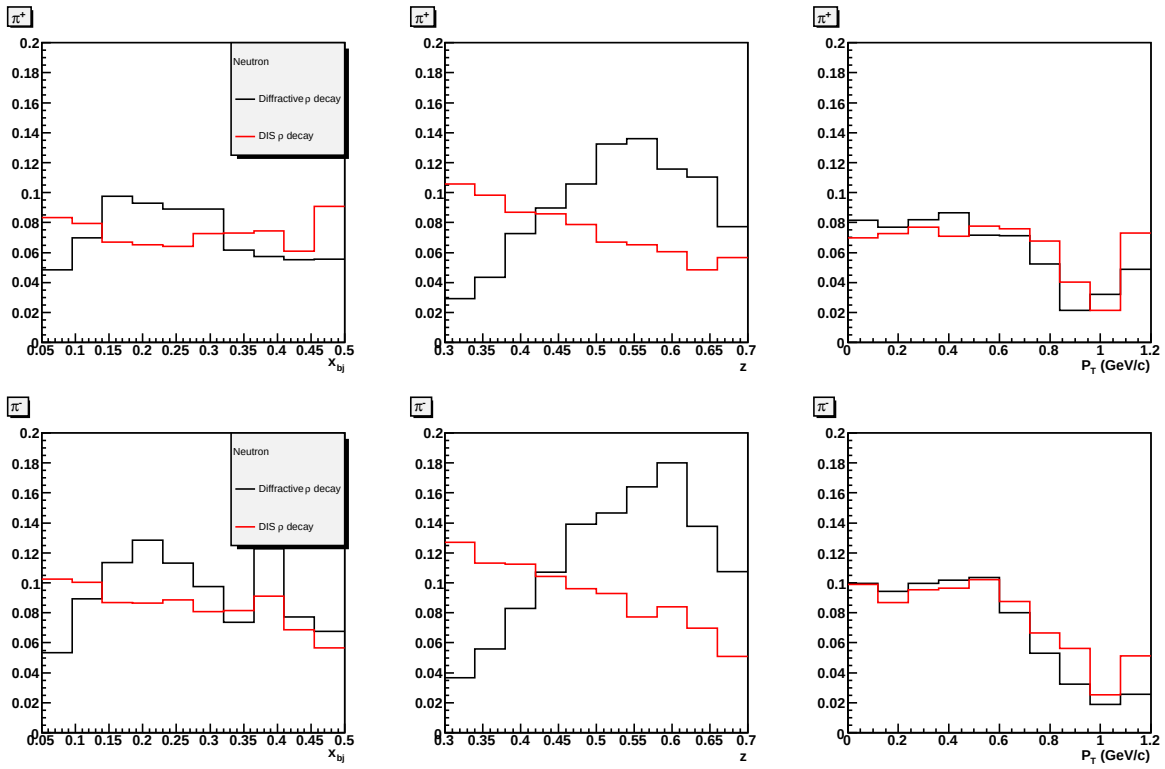

Figure 36: The contamination from the diffractive ρ production is shown for neutron for both π^+ and π^-. In addition, we also plot the pion production from the DIS ρ production for comparison.

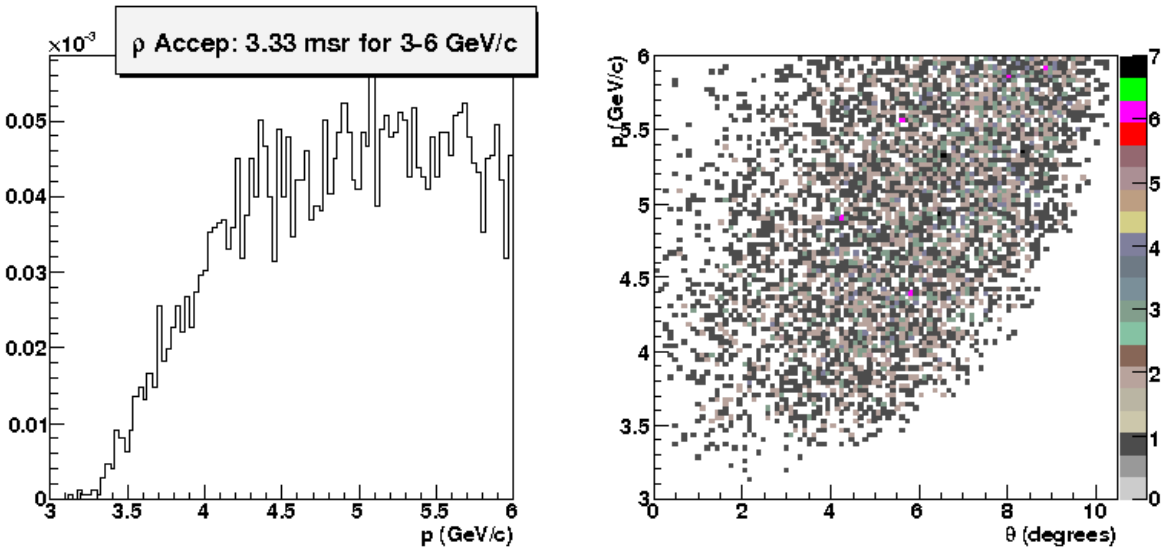

Figure 37: The momentum distribution of ρ meson is shown on the left panel. The distribution of the polar angle θ in respect of the momentum are shown on the right panel.

Sources	Type	Collins π^+	Collins π^-	Sivers π^+	Sivers π^-
Raw asymmetry	absolute	1E-3	1E-3	1E-3	1E-3
Background Subtraction	relative	1.0%	1.0%	1.0%	1.0%
Detection resolution	relative	negligible	negligible	negligible	negligible
Nuclear Effects	relative	4% +1.2%	4% + 1.2%	5% + 1.2%	5% + 1.2%
Diffractive Vector Meson	relative	3%	2%	3%	2%
Radiative Correction	relative	2%	2%	2%	2%
^{3}He Polarization	relative	3% +0.5%	3% + 0.5%	3% +0.5%	3% + 0.5%
Total	relative	6.4%	6.0%	7.0 %	6.7%
	absolute	1E-3	1E-3	1E-3	1E-3

Table 6: Systematic uncertainties on the separated asymmetries for the proposed experiment. The average statistical uncertainties on the separated asymmetries will be around 3.7E-3 (absolute) with 1400 bins.

14 Summary

In this update, we present studies carried out to address concerns raised by PAC34 towards our proposal PR12-09-014 specifically as well as general concerns towards all SIDIS proposals. We also present studies and updated projections based on the option of using the CDF solenoid magnet, while proposal PR12-09-014 was based on the BABAR solenoid magnet. In addition to a 11 GeV incident electron beam energy, we also propose to take data at 8.8 GeV. Our total beam request is 90 days.

15 Appendix I: Single Rates Estimation – Comparison with E06-010 data

The single rates estimation was checked against the data from E06-010 (6 GeV transversity experiment). In E06-010, the BigBite spectrometer is set to detect electron at 30 degrees, in coincidence with the left HRS spectrometer detecting hadrons at 16 degrees. The beam energy is 5.892 GeV. The HRS momentum setting is 2.35 GeV/c. The BigBite momentum coverage is from 0.6 GeV/c to 2.5 GeV/c. The polarized ^3He target is 40 cm long. The target density is about 10 amagats. The average beam current is about 12 μA through out the whole experiment. In addition to the coincidence trigger, the single arm trigger are recorded with certain prescale factor on both BigBite and HRS side. In this section, we compared the our estimation on the single rate with the single arm trigger data on BigBite and HRS.

On the HRS side, we used the Wiser code to estimate the rates for π^+, π^- and proton. We used the Whitlow code to estimate the electron rate. The HRS acceptance is assumed to be 6.7 msr. The momentum acceptance is about $\pm$ 5%. The comparisons are shown in the Table. 7. For pions, the wiser over estimate the data by about factor of 2. For the electron, the whitlow code reasonably describe the data. For the proton, the wiser code over estimate about 40%. The estimation with the correction obtained in this study is also presented.

	π^+	π^-	e-	p
Calculation	105	62.4	11.6	71
Corrected Calculation	62.6	37.2	-	51
Data	54.8	34	12.4	49.6

Table 7: The units is in events/μC.

For the BigBite spectrometer, we used a GEANT3 Monte-Carlo simulation to simulate the detector response (MWDC, lead glass calorimeter). The simulated detector response are analyzed with the same Hall A analysis software, including the tree search pattern match tracking code, the calorimeter clustering software and the BigBite optics module. The BigBite optics model, the BigBite acceptance, the effect of the target collimator and the calorimeter energy resolution are properly modeled in the MC. During the simulation process, we generated electron/charged pion and π^o events uniformly in the phase space. Then, we weighted the events with the cross section generated by wiser/whitlow code for different particles. The photon events are simulated through the π^o production from the target. About 99% of the π^o decay into two photons and about 1% of the π^o decay into one photon and a pair of electron and positron.

For the charged pion rates, the wiser code overestimate the data at the low transverse momentum side, while it agrees with data quite well at high transverse momentum side. For the electron rate, the whitlow code under-estimate the data in the low momentum side. The discrepancy can be understood as the π^o decay to photon and electron positron pair, or the photo pair production when photon pass through materials. The π^o production

cross section is assumed to be twice of the sum of the π^+ and π^- production cross section. The resulting photon rates from the π^o data significantly overestimate the data. In order to obtain a reasonable agreement with data, a p_T dependent correction is applied to the wiser code at low transverse momentum region to match the charged pion rate observed in the data. Similarly, an additional p_T dependent correction is applied on the π^o production cross section (twice of the sum of π^+ and π^- cross section). The results with correction are compared with data in Fig. 38. The estimation can reasonably describe the data with corrections.

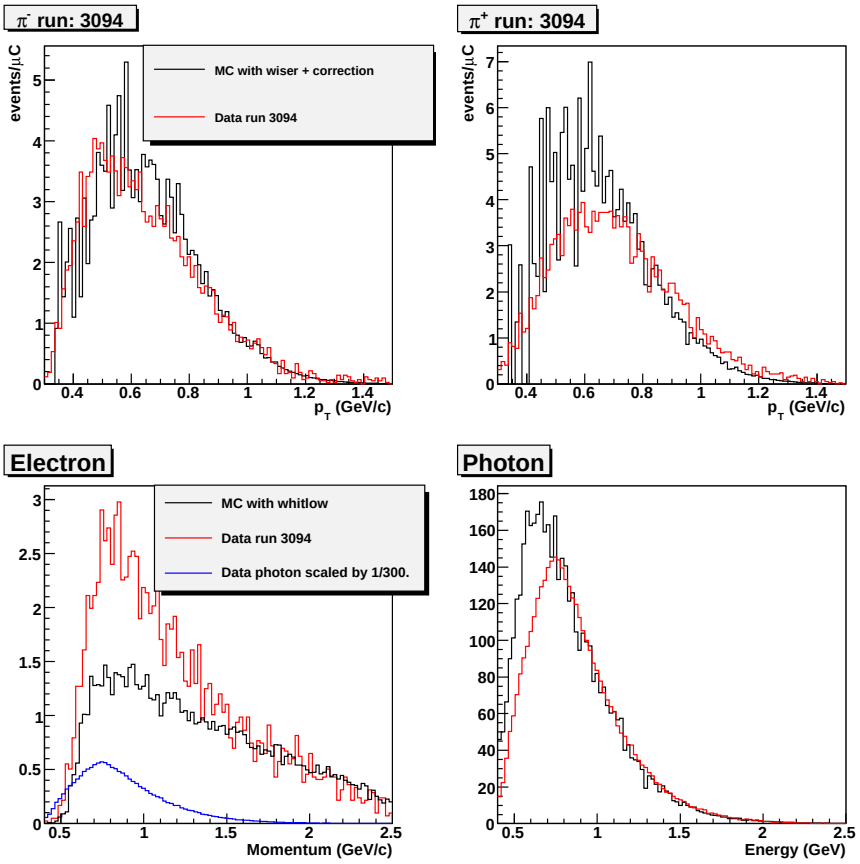

Figure 38: The GEANT3 based single rate estimations are compared with data for π^- (top left), π^+ (top right), e^- (bottom left) and photon (bottom right). For the electron rate, the "photon"-induced electron (or electron decayed from π^o) can be used to explain the enhancement seen in the low momentum region.

Using this calibrated wiser/whitlow code, we estimated the single rate for different particles for in proposal. The total rates can be found in Table. 3. In addition, we also present the rate seen on the calorimeter in Fig. 39. The rates are presented in the units of $kHz/100cm^2$. For the large angle, we only present the rate for particles with momentum higher than 3.5 GeV/c.

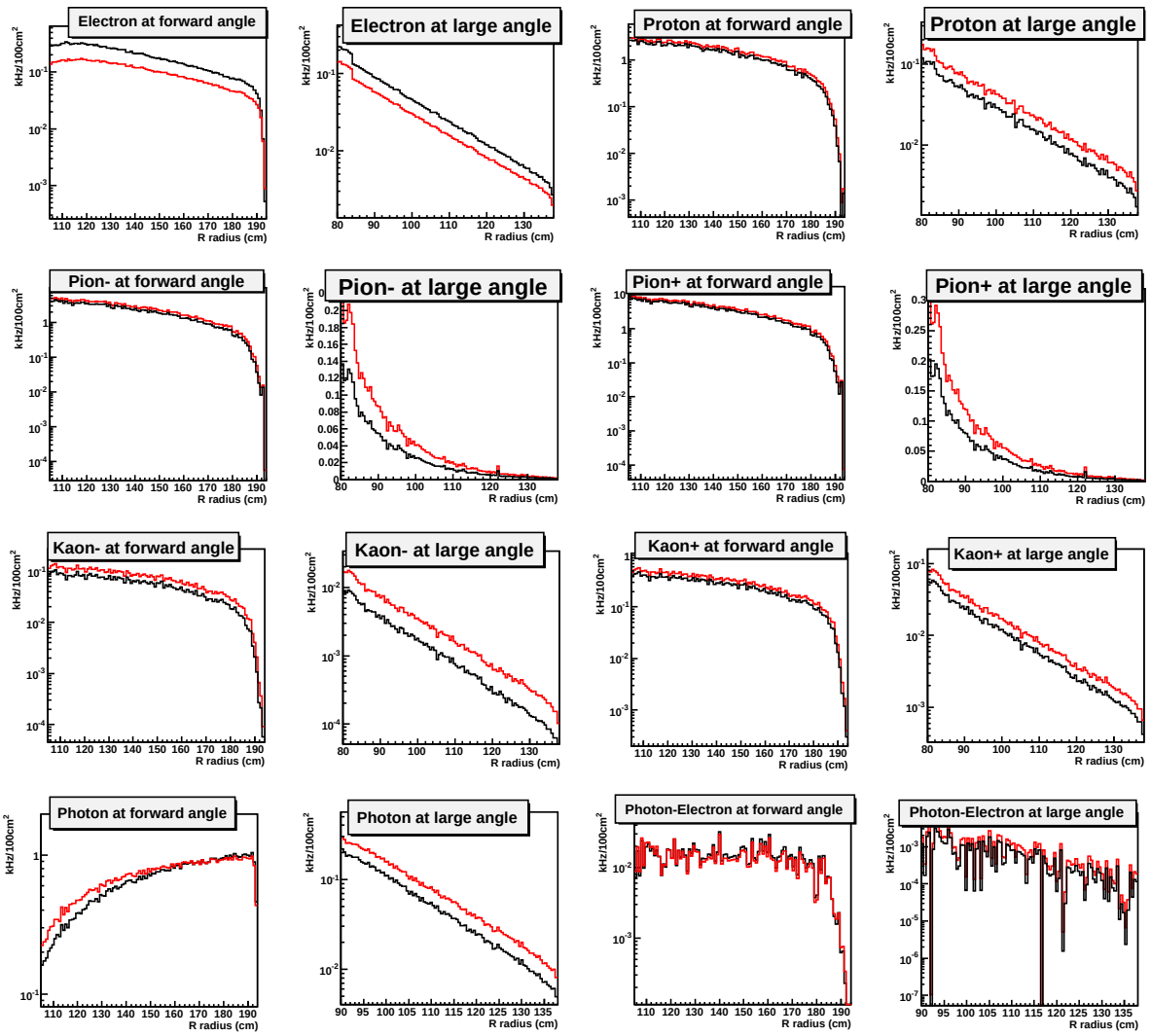

Figure 39: The single rates seen on the calorimeter for this proposal. The results on the large angle and forward angle are shown separately. The 11 (8.8) GeV results are shown in red (black) lines. The total rates are summarized in Table. 3.

16 Appendix II: Statistical Uncertainties Estimation

In this section, we describe the formalism to estimate the statistical uncertainties of the separated Collins, Sivers and Pretzelosity asymmetries from the measured raw asymmetries. The statistical uncertainties of the separated asymmetries will depend on the azimuthal angular coverage of both ϕ_S and ϕ_h, event distribution (detection efficiency and acceptance), number of events in the kinematic bins, and number of terms involved in the fitting procedure. In the projections, we only include the leading twist contributions (Collins, Sivers, and Pretzelosity) in the fitting procedure. The formalism has been checked with the actual 2-D (ϕ_S and ϕ_h) χ^2 fitting on many different kinematic bins with different event angular distributions. In Sec. 16.1, we simplified the problem by assuming the azimuthal angular coverage is perfect, no distributions through the entire acceptance and including only three leading twist terms in the fitting. In Sec. 16.2, we examine the effect of incomplete ϕ_h angular coverage. In Sec. 16.3, we prove that the method that we used in Sec. 16.1 and Sec. 16.2 to do separation is the best. In Sec. 16.4, we include the two sub-leading twist terms into the fitting procedure and discuss their effect to the statistical uncertainties of the three leading twist terms.

16.1 Full azimuthal angular coverage and flat distribution

In general, the transverse single target spin asymmetry can be written as with all three leading twist terms:

$$\begin{aligned} A_{UT} &= A_{Sivers}\sin(\phi_h-\phi_S) + A_{Collins}\sin(\phi_h+\phi_S) + A_{Pretzelosity}\sin(3\phi_h-\phi_S) \\ &= a\sin(\phi) + b\sin(2\phi_h-\phi) + c\sin(2\phi_h+\phi) \\ &= a\sin(\phi) + (b+c)\sin(2\phi_h)\cos(\phi) + (c-b)\cos(2\phi_h)\sin(\phi) \end{aligned} \quad (7)$$

where the $\phi \equiv \phi_h - \phi_S$ is the Sivers angle, a, b and c represent Collins, Sivers and Pretzelosity asymmetries, respectively.

If we assume a full 2π azimuthal coverage on both ϕ_h and ϕ, we can integrate the ϕ and ϕ_h angles by multiplying $\sin(\phi)$ at both the left and right sides of Eqn. 7 first. The last two terms in the right side of Eqn. 7 vanish:

$$\begin{aligned} \int_0^{2\pi}\int_0^{\pi} A_{UT}\sin\phi d\phi d\phi_h &= a\cdot\int_0^{2\pi}\int_0^{\pi}\sin^2\phi d\phi d\phi_h \\ &= \pi^2 a \end{aligned} \quad (8)$$

Thus

$$\begin{aligned} \delta a &= \frac{1}{\pi^2}\sqrt{\int_0^{2\pi}\int_0^{\pi}(\delta A_{UT})^2\sin^2\phi d^2\phi d^2\phi_h} \\ &= \frac{1}{\pi^2}\sqrt{(\delta A_{UT})^2 d\phi d\phi_h \pi^2} \\ &= \sqrt{\frac{2}{N}} \end{aligned} \quad (9)$$

where the N is the total number of events. In the last step of Eqn. 9, we used the relation:

$$(\delta A_{UT})^2 d\phi d\phi_h = \frac{2\pi^2}{N} \tag{10}$$

The $2\pi^2$ is due to the integration of ϕ is 2π, while the integration of ϕ_h is only π. If we assume that ϕ is divided into m small bins, and ϕ_h is divided into n small bins, the events in this particular bin is $N/(m \cdot n)$, where N is the total number of events (we assume a flat distribution). Then $(\delta A_{UT})^2 = m \cdot n/N$, $d\phi = \pi/m$ and $d\phi_h = 2\pi/n$. Thus $(\delta A_{UT})^2 d\phi d\phi_h = \frac{2\pi^2}{N}$.

Then we can multiply $\sin\phi\cos 2\phi_h$ and $\cos\phi\sin 2\phi_h$ to both sides of Eqn. 7:

$$(c-b)\frac{\pi^2}{2} = \int_0^{2\pi}\int_0^{\pi} A_{UT}\sin\phi\cos 2\phi_h d\phi d\phi_h \tag{11}$$

$$(c+b)\frac{\pi^2}{2} = \int_0^{2\pi}\int_0^{\pi} A_{UT}\cos\phi\sin 2\phi_h d\phi d\phi_h \tag{12}$$

which are

$$c = \frac{1}{\pi^2}\int_0^{2\pi}\int_0^{\pi} A_{UT}\sin(2\phi_h+\phi) d\phi d\phi_h \tag{13}$$

$$b = \frac{1}{\pi^2}\int_0^{2\pi}\int_0^{\pi} A_{UT}\sin(2\phi_h-\phi) d\phi d\phi_h \tag{14}$$

. Then

$$\begin{aligned}
\delta b &= \frac{1}{\pi^2}\sqrt{\int_0^{2\pi}\int_0^{\pi}(\delta A_{UT})^2\sin^2(\phi+2\phi_h) d^2\phi d^2\phi_h} \\
&= \frac{1}{\pi^2}\sqrt{\frac{2\pi^2}{N}\int_0^{2\pi}\int_0^{\pi}\sin^2(\phi+2\phi_h) d\phi d\phi_h} \\
&= \sqrt{\frac{2}{N}} \\
&= \delta c
\end{aligned} \tag{15}$$

In comparison to the usual estimation of the statistical uncertainties of the asymmetry $\delta A = \sqrt{\frac{1}{N}}$, the separated asymmetry (Collins, Sivers and Pretzelosity) obtain an extra factor $\sqrt{2}$ due to the separation.

16.2 Real azimuthal angular coverage and flat acceptance

In the real SoLID case, we have full π azimuthal angular coverage for ϕ, when forming asymmetry. The ϕ_h coverage in each bin is symmetric with respect to the plane of $\phi_h = 0$, which we assume [x,y] and [-y,-x] here. To simplify the derivation, we assume the acceptance is flat within the [x,y] and [-y,-x].

Starting with Eqn. 7, we multiply $\sin(\phi)$, $\sin(2\phi_h-\phi)$, and $\sin(2\phi_h+\phi)$ at both sides of Eqn. 7 and integrate over the ϕ and ϕ_h angles, and obtain the following three equations:

$$\begin{aligned}
I_1 &= \left(\int_x^y + \int_{-y}^{-x}\right)\int_0^{\pi} A_{UT}\sin\phi d\phi d\phi_h \\
&= \left(\int_x^y + \int_{-y}^{-x}\right)\int_0^{\pi}(a\sin(\phi) + b\sin(2\phi_h-\phi) + c\sin(2\phi_h+\phi))\sin\phi d\phi d\phi_h
\end{aligned}$$

$$
\begin{aligned}
I_2 &= (\int_x^y + \int_{-y}^{-x}) \int_0^\pi A_{UT} \sin 2\phi_h \cos\phi d\phi d\phi_h \\
&= (\int_x^y + \int_{-y}^{-x}) \int_0^\pi (a\sin(\phi) + b\sin(2\phi_h - \phi) + c\sin(2\phi_h + \phi)) \sin(2\phi_h - \phi) d\phi d\phi_h
\end{aligned}
$$

$$
\begin{aligned}
I_3 &= (\int_x^y + \int_{-y}^{-x}) \int_0^\pi A_{UT} \cos 2\phi_h \sin\phi d\phi d\phi_h \\
&= (\int_x^y + \int_{-y}^{-x}) \int_0^\pi (a\sin(\phi) + b\sin(2\phi_h - \phi) + c\sin(2\phi_h + \phi)) \sin(2\phi_h - \phi) d\phi d\phi_h
\end{aligned}
$$

Then, we can rewrite it into matrix format:

$$
\begin{pmatrix} I_1 \\ I_2 \\ I_3 \end{pmatrix} = \mathbf{M} \begin{pmatrix} a \\ b \\ c \end{pmatrix} \tag{16}
$$

in which, M is defined as the coefficient matrix of (a, b, c).

We can solve this equation group, by inverting the coefficient matrix M, then the equation group can be written as:

$$
\begin{pmatrix} a \\ b \\ c \end{pmatrix} = \mathbf{M^{-1}} \begin{pmatrix} I_1 \\ I_2 \\ I_3 \end{pmatrix} \tag{17}
$$

Assuming

$$
\mathbf{M^{-1}} = \begin{pmatrix} a_1 & a_2 & a_3 \\ b_1 & b_2 & b_3 \\ c_1 & c_2 & c_3 \end{pmatrix} \tag{18}
$$

Then

$$
a = (\int_x^y + \int_{-y}^{-x}) \int_0^\pi A_{UT}(a_1 \sin\phi + a_2 \sin(2\phi_h)\cos\phi + a_3 \cos(2\phi_h)\sin\phi) d\phi d\phi_h \tag{19}
$$

$$
b = (\int_x^y + \int_{-y}^{-x}) \int_0^\pi A_{UT}(b_1 \sin\phi + b_2 \sin(2\phi_h)\cos\phi + b_3 \cos(2\phi_h)\sin\phi) d\phi d\phi_h \tag{20}
$$

$$
c = (\int_x^y + \int_{-y}^{-x}) \int_0^\pi A_{UT}(c_1 \sin\phi + c_2 \sin(2\phi_h)\cos\phi + c_3 \cos(2\phi_h)\sin\phi) d\phi d\phi_h \tag{21}
$$

Thus:

$$
\delta a = \sqrt{(\int_x^y + \int_{-y}^{-x}) \int_0^\pi (\delta A_{UT})^2 (a_1 \sin\phi + a_2 \sin(2\phi_h)\cos\phi + a_3 \cos(2\phi_h)\sin\phi)^2 d^2\phi d^2\phi_h}
$$

$$
\delta b = \sqrt{(\int_x^y + \int_{-y}^{-x}) \int_0^\pi (\delta A_{UT})^2 (b_1 \sin\phi + b_2 \sin(2\phi_h)\cos\phi + b_3 \cos(2\phi_h)\sin\phi)^2 d^2\phi d^2\phi_h}
$$

$$\delta c = \sqrt{(\int_x^y + \int_{-y}^{-x}) \int_0^\pi (\delta A_{UT})^2 (c_1 \sin\phi + c_2 \sin(2\phi_h)\cos\phi + c_3 \cos(2\phi_h)\sin\phi)^2 d^2\phi d^2\phi_h}$$

Here, assuming the acceptance is flat, we have the following relation:

$$(\delta A_{UT})^2 d\phi d\phi_h = \frac{2\pi(y-x)}{N} \tag{22}$$

in which the integration of ϕ is π, while the integration of ϕ_h is $2(y-x)$.

16.3 Why should we multiply $\sin(\phi)$, $\sin(2\phi_h)\cos(\phi)$, and $\cos(2\phi_h)\sin(\phi)$?

This fact can be derived from analysis of the least χ^2. For example, we have an asymmetry has the form:

$$A = a\sin(\phi) \tag{23}$$

We can then form χ^2

$$\chi^2 = \sum \frac{(A_i - a\sin(\phi_i))^2}{(\delta A_i)^2} \tag{24}$$

where δA_i is the uncertainty of A_i. With least χ^2 condition, we have

$$\frac{\partial \chi^2}{\partial a} = 0 \tag{25}$$

which yields

$$a \sum \frac{\sin(\phi_i)^2}{(\delta A_i)^2} = \sum \frac{A_i \sin(\phi_i)}{(\delta A_i)^2} \tag{26}$$

In the flat acceptance case, and if we assume the distribution of events are flat, we have

$$a \int \sin(\phi)^2 d\phi = \int A\sin(\phi) d\phi \tag{27}$$

If there is acceptance effect, or there is a uneven event distribution due to detector efficiency, we have

$$a \sum \frac{\sin(\phi_i)^2}{(\delta A_i)^2} = \sum \frac{A_i \sin(\phi_i)}{(\delta A_i)^2} \tag{28}$$
$$a \int \sin(\phi_i)^2 \cdot g(\phi) d\phi = \int A g(\phi)\sin(\phi_i) d\phi$$

where $\delta A_i^2 = \frac{1}{N_i}$, and N_i is the events in this particular bin. Then we can define $g(\phi_i) = N_i/N_{mean}$. In this case, we can conclude that instead multiplying the terms by $\sin(\phi)$, we should multiply it by $g(\phi)\sin(\phi)$.

We can easily extend the discussion to multi-terms. For example, if we have

$$A = a \cdot f_1(\phi) + b \cdot f_2(\phi) + ... + c \cdot f_n(\phi) \tag{29}$$

From the least Chi2 condition, we have

$$\sum \frac{(A_i - a \cdot f_1(\phi_i) + b \cdot f_2(\phi_i) + ... + c \cdot f_n(\phi_i)) f_1(\phi_i)}{\delta A_i^2} = 0 \tag{30}$$

$$...$$

$$\sum \frac{(A_i - a \cdot f_1(\phi_i) + b \cdot f_2(\phi_i) + ... + c \cdot f_n(\phi_i)) f_n(\phi_i)}{\delta A_i^2} = 0 \tag{31}$$

and

$$\int \frac{(A_i - a \cdot f_1(\phi_i) + b \cdot f_2(\phi_i) + ... + c \cdot f_n(\phi_i)) f_1(\phi_i)}{\delta A_i^2} = 0 \tag{32}$$

$$...$$

$$\int \frac{(A_i - a \cdot f_1(\phi_i) + b \cdot f_2(\phi_i) + ... + c \cdot f_n(\phi_i)) f_n(\phi_i)}{\delta A_i^2} = 0 \tag{33}$$

We can reorganize the above equation group including the acceptance effect $g(\phi)$ as:

$$\int A f_1(\phi) g(\phi) d\phi = \int (a \cdot f_1(\phi) + b \cdot f_2(\phi) + ... + c \cdot f_n(\phi)) f_1(\phi) g(\phi) d\phi \tag{34}$$

$$...$$

$$\int A f_n(\phi) g(\phi) d\phi = \int (a \cdot f_1(\phi) + b \cdot f_2(\phi) + ... + c \cdot f_n(\phi)) f_n(\phi) g(\phi) d\phi$$

Effectively, we are weighting our data for $f_{1,2,...}(\phi) g(\phi)$

16.4 What is the effect of including the two sub-leading twist terms in the fitting?

In previous section, we only consider the three leading twist contributions (Collins, Sivers, and Pretzelosity). In this section, we examine the effects of including the additional two sub-leading twist terms into the fitting procedure. Eqn. 7 can then be written as

$$\begin{aligned} A_{UT} &= A_{Sivers} \sin(\phi_h - \phi_S) + A_{Collins} \sin(\phi_h + \phi_S) + A_{Pretzelosity} \sin(3\phi_h - \phi_S) \\ &+ d \sin\phi_S + e \sin(2\phi_h - \phi_S) \\ &= a \sin(\phi) + b \sin(2\phi_h - \phi) + c \sin(2\phi_h + \phi) + d \sin(\phi_h - \phi) + e \sin(\phi_h + \phi) \end{aligned}$$

where the $\phi \equiv \phi_h - \phi_S$ is the Sivers angle, d and e are the two sub-leading twist terms.

First, if we assume the two sub-leading twist terms have similar contribution as the three leading twist terms, we will have $5x5$ equation group:

$$\begin{pmatrix} a \\ b \\ c \\ d \\ e \end{pmatrix} = \mathbf{M^{-1}} \begin{pmatrix} I_1 \\ I_2 \\ I_3 \\ I_4 \\ I_5 \end{pmatrix} \tag{35}$$

Following the similar calculation procedures in Sec. 16.2, and taking the acceptance into account, we can get the uncertainties of each asymmetry term. As an example,

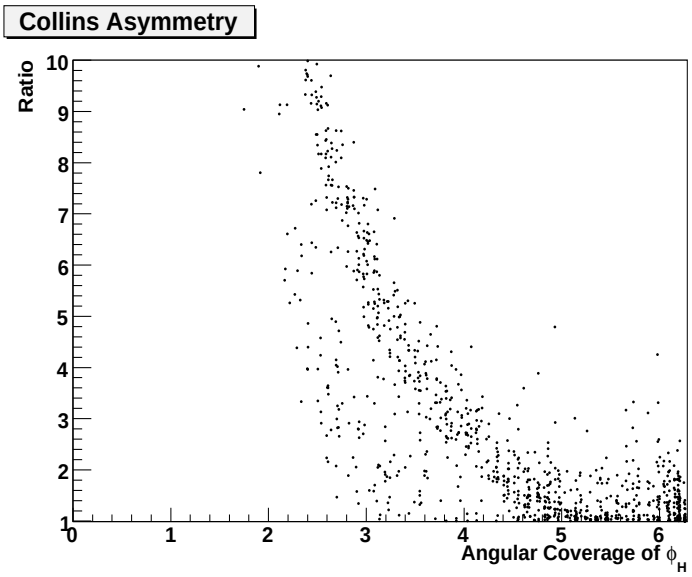

Figure 40: Collins asymmetry uncertainty ratio of 5 terms to 3 terms SSA definition.

we show the Collins asymmetry uncertainty ratio of 5 terms fitting to 3 terms fitting in Fig. 40.

However, the two sub-leading twist asymmetries are not likely on the same scale as the three leading twist asymmetries. Assuming the two sub-leading twist terms are small and do not vary a lot through the acceptance, we can combine the results of many kinematics bins together (In each kinematics bin, we fit the raw asymmetries with 5 terms). Then we can plug the results of d and e back, and fit the raw asymmetries with 3 terms only. As an example, we assume the statistical uncertainties of d and e is about factor of 2 smaller than the statistical uncertainties of raw asymmetry. Then the ratios of Collins asymmetry statistical uncertainties of this method and the method with fitting only three leading twist terms is less than 1.1 (10% increase comparing with the statistical uncertainties of fitting only three leading twist terms).

17 Appendix III: Kinematic Coverage

In this section, we present the p_T vs ϕ_h coverage for our kinematic bin at 11 GeV and 8.8 GeV as requested in the PAC report. We bin our data in 3-D, 12 x bins from 0.05 to 0.65, 8 z bins from 0.3 to 0.7, 8 P_T bins from 0.0 to 1.6 GeV/c. Here, only one example plot is shown. The rest of plots can be found at
`http://www.jlab.org/~xqian/SoLID/phi_coverage.pdf`
(username: "12transversity"; password: "SoLID").

18 Appendix IV: SoLID GEANT Simulation

The simulation of the experiment was done with GEANT3 [57]. The interaction point was uniformly distributed over the 40 cm length of the polarized ^3He target, the size of

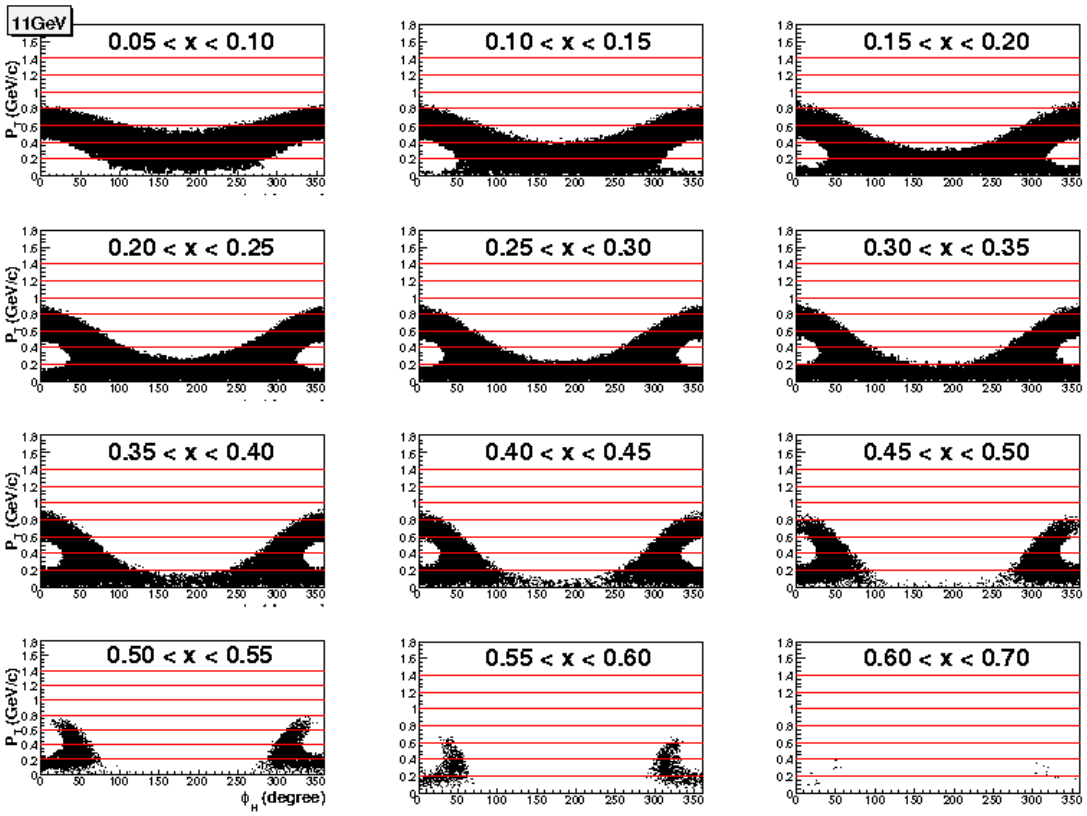

Figure 41: The p_T vs ϕ_h coverage for (0.3,0.35) of z bin for 11 GeV beam.

the beam spot was assumed to be 2x2 mm^2. Each of the two target windows has similar radiation length as the 40 cm 10 atm ^{3}He. The magnetic field calculated by Superfish [44] was used. In order to calculate the backgrounds and the resolutions, we put in a realistic distribution of materials, including the target windows, the beam pipes, target collimator etc. The setup was filled with air. The thickness of a coordinate detector plane was 0.7% of R.L., as the thickness of GEM detectors. For the calorimeter material, a lead-plastic sandwich was taken, with the average radiation length of 1.32 cm. The calorimeter was split into a preshower detector 8 cm thick and a shower detector 22 cm thick at both large angle and forward angle. The light gas Čerenkov threshold detector was about 2.1 m long, filled with CO^2. The thickness of the upstream and downstream windows were 0.2 and 0.5 mm of Al. The heavy Gas Čerenkov is about 1 m long filled with 1.5 atm C4F10 gas. The thickness of the upstream and downstream windows were 2 mm of Al. The MRPC is simulated as a combination of two layers of 2.5 mm thick glass in the front of and at the back of a standard tracking detector. A layer of plastic scintillator with 1/8 inch (3.1 mm) thickness is added between the light gas Čerenkov and heavy gas Čerenkov at forward angle. The layout of the detector system are shown in Fig. 6.

In the background estimation of the GEM tracking detector (Sec. 5.2) and calorimeter (Sec. 5.3), we include all the standard GEANT3 reaction process [14]. The same simulation is also used to estimate the soft photons (see Sec. 10). The soft photon, with energy larger than 200 MeV, rates are estimated to be about 170 MHz. [15] The background rates in the MRPC is shown to be about below 1 kHz/mm^2. The total rate on entire scintillator plane is below 300 MHz.

In this part, we focus on the discussion of simulation of Moller electron. Only Moller scattering was included in the event generator. The azimuthal angle of generated Moller scattered electron is from 0 to 360 degrees. The polar angle is from 4 degrees to 175 degrees in the center of mass frame. We require that every event generated is from Moller scattering. The distribution follows the cross section of Moller scattering within the simulated range. The effects of Moller scattering can be found in Fig. 42. It is clear that the Moller electrons will be constrained inside a cone around beam pipe, and will not reach the tracking detectors. The fringe field will bend the very low momentum electrons. The effect is confirmed by reversing the solenoid magnetic field direction. In this simulation, we turned off all the physics interaction for clarity purpose.

In this part, we focus on the discussion of the momentum cut-off at the forward angle. The acceptance are presented against the momentum and polar angle in Fig. 7. The momentum cut-off for forward angle detection is about 0.9 GeV/c. Fig. 43 give the detailed demonstration of this point. In this simulation, all physics GEANT interactions are turned off for clarity purpose. The particles are generated with a flat distribution within the polar angle range between 0.06 rad and 0.46 rad and 2π azimuthal angle. The generated momentum are generated for two situations: less than 0.8 GeV/c and 0.8-1.0 GeV/c.

The Background in the Čerenkov detectors were also simulated through the GEANT3 simulation. For the light gas Čerenkov, we used three sets of mirrors (about 1 cm thick)

[14] All the forward processes, including Moller, Mott etc, are included in the simulation.

[15] The hard photon is estimated by the π^o production. And its rate is shown to be less than 30 MHz, which is much smaller than the soft photon rates.

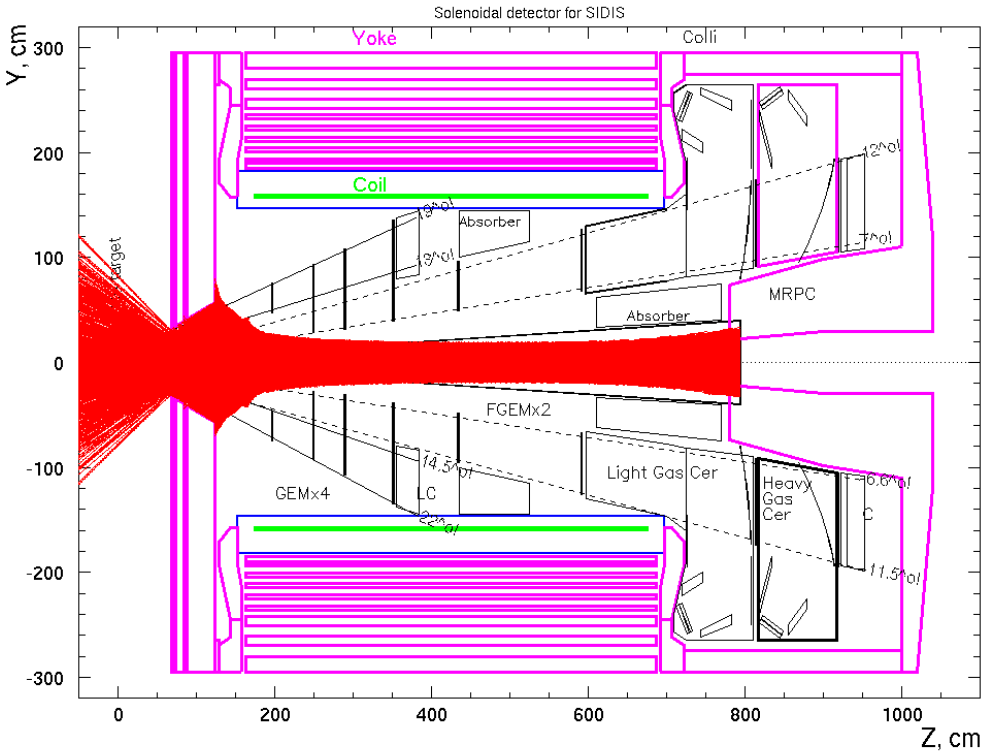

Figure 42: The effect of Moller scattering are shown. The magnetic field calculated by Superfish [44] was used (See. Sec. 5.1). The azimuthal angle of generated Moller scattered electron is from 0 to 360 degrees. The polar angle is from 4 degrees to 175 degrees in the center of mass frame. It is clear that the Moller electrons will be constrained inside a cone around beam pipe, and will not reach the tracking detectors. The fringe field will bend the large low momentum electrons.

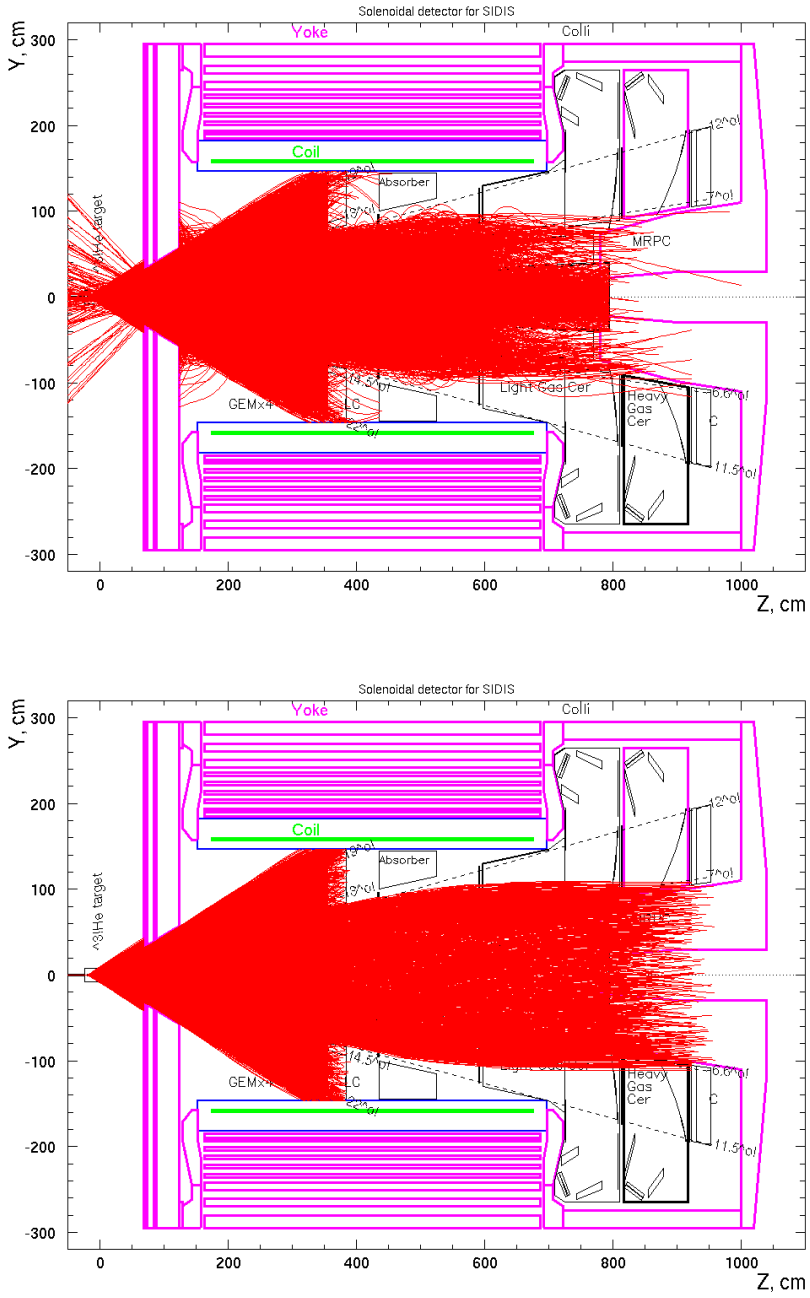

Figure 43: The top figure shows the bending of particles with momentum below 0.88 GeV/c. They can not reach the forward angle calorimeter. The bottom figure shows the bending of particles with momentum between 0.8 and 1.0 GeV/c. Some of the particles can reach the forward angle calorimeter.

to reflect the lights. For the heavy gas Čerenkov, we used one set of mirror (1 cm thick) to reflect the lights. All mirrors are assumed to be perfect in estimating the background. In reality, the physics charged particle will be bended inside the magnetic field. Thus, the mirror should be bended accordingly to have a better focus of the Čerenkov light generated by physics particle in the momentum region we are interested in. This bending can further suppressed the low energy backgrounds, which are generated in all possible angles. We assume the suppression factor is about 2 in the gas Čerenkov counters. In addition, the light collecting detectors were assumed to cover the entire 2π azimuthal angle for simplification of the geometry. In reality, the Čerenkov will be segmented into 30 smaller detectors. The low energy background simulation (same as the one used in simulating the background rates on the tracking detectors and calorimeters) yields about a total of 40 MHz rates in the light Gas Čerenkov. The rates on the heavy gas Čerenkov is about 60 MHz. The high energy background are simulated by generating electron, charged pions, proton, charged kaons and π^o in the acceptance for the momentum between 0.3 GeV/c and 8 GeV/c. Each event is weighed by the cross sectioned calculated with whitlow (electron) and updated wiser code (hadrons). For the π^o production, we assume the cross-section is twice of the sum of π^+ and π^- production cross-section. In addition, we also simulating the events from the target windows. Each of the target window has the similar thickness as the 40 cm long 10 atm ^{3}He. The high energy backgrounds from the sum of the processes mentioned above is ranging from 1 to 3 MHz, which are much smaller than the low energy background. The final background rates on the light (heavy) gas Čerenkov are 40 (60) MHz with both 11 and 8.8 GeV beam.

19 Appendix V: Discussion on different options of PID detectors

19.1 Gas Čerenkov Detector

There are other methods to collect Čerenkov light which are less sensitive to the magnetic field and background are being considered as well. One is the "hadro-blind" detector which is based on the GEM technology as described in PVDIS proposal [2]. The other one is the silicon photomultiplier (SiPM) which will be used in Hall-D gluon-X experiment [58] may be a good choice as well. Another possibility is to use Avalanche photon detector (APD) with Winston cone ..

19.2 Aerogel Čerenkov Detector

For the low momentum range, other than the TOF, the silion aerogel detector with n = 1.015 can also fill the hole. Its thresholds for π and K are 0.8 and 2.8 GeV/c, respectively, which give enough overlap with the heavy gas Čerenkov detector. With a 10 cm aerogel radiator, assuming 50% light collection efficiency and 20% quantum efficiency, the N_{pe} for high energy pion is about 14. Once again, the light collection should be treated properly.

References

[1] JLab proposal PR-12-09-014, PAC34
http://www.jlab.org/exp_prog/proposals/09/PR-09-014.pdf.

[2] JLab proposal PR-12-09-12 PAC34, PVDIS proposal.

[3] K. Hidaka, E. Monsay and D. Sivers, Phys. Rev. **D19**, 1503 (1979).

[4] J.P. Ralston and D.E. Soper, Nucl. Phys. **B152**, 109 (1979).

[5] R.L. Jaffe and X. Ji, Phys. Rev. Lett. **67**, 552 (1991).

[6] C. Bourrely, J. Soffer and O. V. Teryaev, Phys. Lett. **B420** (1998) 375, hep-ph/9710224.

[7] J. Soffer, Phys. Rev. Lett. **74**, 1292 1995.

[8] J. Ralston, *private communications*.

[9] M. Gockeler *et al.*, Phys. Lett. **B627**, 113 (2005).

[10] I. C. Cloet, W. Bentz and A. W. Thomas, Phys. Lett. **B659**, 214 (2008).

[11] M. Wakamatsu, Phys. Lett. **B653**, 398 (2007).

[12] H.-X. He and X. Ji, Phys. Rev. **D52**, 2960 (1995).

[13] B. Pasquini, M. Pincetti, and S. Boffi, Phys. Rev. **D72**, 094029 (2005).

[14] P. J. Mulders and R. D. Tangerman, *Nucl. Phys.* **B461** 197 (1996).

[15] D. Boer, P.J. Mulders, Phys. Rev. **D57**, 5780 (1998).

[16] J.C. Collins, Nucl. Phys. **B396**, 61 (1993).

[17] T. Meng, J. Pan, Q. Xie and W. Zhu, Phys. Rev. **D40**, 769 (1989).

[18] D.W. Sivers, Phys. Rev. **D41**, 83 (1990).

[19] M. Anselmino, M. Boglione, and F. Murgia, Phys. Rev. **D60**, 054027 (1999).

[20] S.J. Brodsky, D.S. Hwang, I. Schmidt, Phys. Lett. **B530**, 99 (2002).

[21] M. Burkardt, Phys. Rev. **D69**, 057501 (2004).

[22] A. Airapetian *et al.* (HERMES), Phys. Rev. Lett. **94**, 012002 (2005).

[23] The COMPASS Collaboration, Phys. Rev. Lett. **94**, 202002 (2005).

[24] A. Bravar *et al.*, Phys. Rev. Lett. **77**, 2626 (1996).

[25] J. Qiu and G. Sterman, Phys. Rev. D **42**, 83 (1990).

[26] J. Kodaira and K. Tanaka, Prog. Theor. Phys. **101**, 191 (1999).

[27] I. Arsene *et al.* (BRAHMS Collaboration), Phys. Rev. Lett. **101**, 042001 (2008).

[28] A. Airapetian *et al.* (The HERMES Collaboration), Phys. Rev. Lett. **103**, 152002 (2009).

[29] E.S. Ageev *et al.* (The COMPASS Collaboration) Nucl. Phys. **B765**, 31 (2007), hep-exp/0610068.

[30] M. Alekseev *et al.* (The COMPASS Collaboration), Phys. Lett. B **673**, 127 (2009).

[31] S. Levorato, for the COMPASS Collaboration, proceedings of Transversity 2008 Workshop, 2008, Ferrara, arXiv:0808.0086.

[32] M. Anselmino *et al.*, proceedings of the XVI International Workshop on Deep Inelastic Scattering and Related Subjects, DIS 2008, London, U.K. 2009. e-Print: arXiv:0807.0173.

[33] M. Anselmino *et al.*, Nucl. Phys. **A808**, 192 (2008), arXiv:0805.2677.

[34] H. Avakian *et al.*, for the CLAS Collaboration, Phys. Rev. **D69**, 112004 (2004), hep-ex/0301005.

[35] JLab Experiment E06-010, Spokespersons: X. Jiang, J. P. Chen, E. Cisbani, H. Gao and J. C. Peng.

[36] W. Vogelsang and F. Yuan, *private communications*.

[37] B.-Q. Ma, I. Schmidt and J.-J. Yang, Phys. Rev. **D66**, 094001 (2002).

[38] M. Anselmino and A. Prokudin, *private communications*. Predictions are based on the extractions of Ref. [32].

[39] W. Vogelsang and F. Yuan, Phy. Rev. **D72**, 054028 (2005), hep-ph/0507266.

[40] M. Anselmino *et al.*, Phys. Rev. **D71**, 074006 (2005), hep-ph/0501196.

[41] M. Anselmino *et al.*, Phys. Rev. **D72**, 094007, hep-ph/0507181.

[42] R. Seidl *et al.* (Belle Collaboration), Phys. Rev. Lett. **96**, 232002 (2006).

[43] M. Anselmino, M. Boglione, U. D'Alesio, and F. Murgia, Phys. Rev. **D71**, 014002 (2005).

[44] `http://poisson-superfish.software.informer.com/`.

[45] Y. Wang, *et al.*, Chinese Physics **C33** (5), 374 (2009).

[46] L. W. Whitlow, SLAC-Report-357 (1990).

[47] Developed J. W. Lightbody and J. S. O'Connell in 1988.

[48] D. E. Wiser, Ph.D. thesis, Univ. of Wisconsin (1977).

[49] `http://www.jlab.org/~xqian/SoLID/index.html`
username: "12transversity"; password: "SoLID"

[50] B. Pasquini, *private commuication.*
S. Boffi, A. V. Efremov, B. Pasquini and P. Schweitzer, Phys. Rev. **D79**, 094012 (2009) arXiv:0903.1271.

[51] Lai, H.L. *et al.*, *Eur. Phys. J.* **C12**, 375 (2000).

[52] J. Binnewies, B. A. Kniehl, G. Kramer, Zeit. Phys. **C65**, 471, (1995).

[53] A. Afanasev *et al.*, JLAB-PHY-07-620, Mar 2007, hep-ph/0703288 (2007).

[54] B. Anderson, G. Gustafson, G. Ingelmann, and T. Sjöstrand, Phys. Rev. **97**, 31 (1983).

[55] H. Avakian and E. Aschenauer *private communication.*

[56] J.-M. Laget *private communication.*

[57] R. Brun *et al.*, "GEANT Detector Description and Simulation Tool, CERN Program Library (1993)," GEANT version 3.21.
E. Chudakov, COMGEANT `http://www.jlab.org/~gen/simul/comgeant/`.

[58] HAll D Gluon-X experiment `http://www.jlab.org/Hall-D/`.